Proceedings of 38th Annual Condensed Matter and Materials Meeting

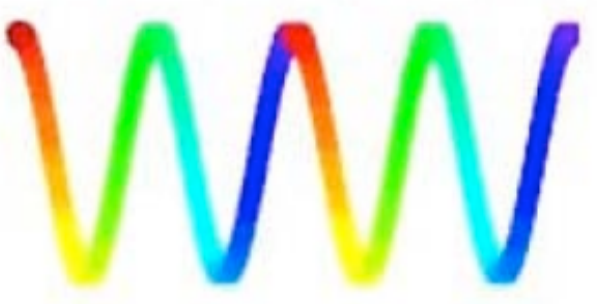

2014

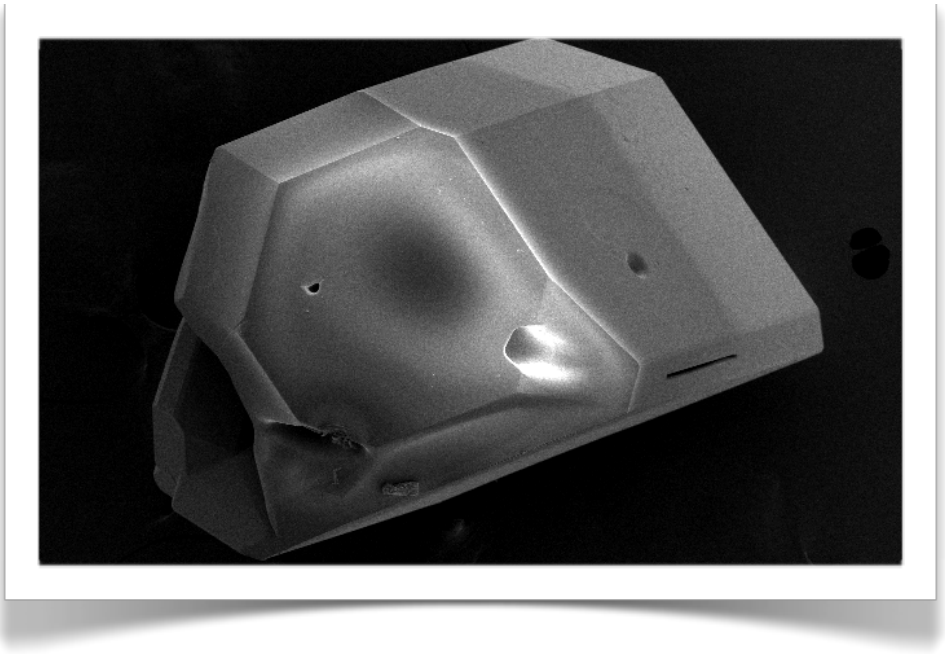

Waiheke Island Resort, Waiheke, Auckland, New Zealand

4th February - 7th February, 2014

ISBN: 978-0-646-93339-9

Australian Institute of Physics

Editorial Note

'Proceedings of Wagga 2014'

The 38th Annual Condensed Matter and Materials Meeting

ISBN: 978-0-646-93339-9

Editor: Tilo Söhnel

The 38th Annual Condensed Matter and Materials Meeting was held at Waiheke Island, Auckland, New Zealand, from 4-7 February, 2014. There were 87 attendees, including international visitors [France, Germany, USA, Taiwan]. A total of 11 invited and 28 contributed oral papers were presented during the two and one half days of scientific sessions. There were also two sessions with a total of 42 poster presentations. All presenters were invited to submit a manuscript (six pages for invited papers and four for contributed papers) for publication in the conference proceedings. Each manuscript was refereed by at least two anonymous reviewers who worked to a set of guidelines made available by the editor. Each accepted publication therefore satisfies the requirements for classification as a refereed conference publication (E1). The organizers would like to thank the reviewers for their time and effort in reviewing manuscripts, which resulted in 8 papers being accepted for publication. The accepted manuscripts are available at the on-line publication section of the Australian Institute of Physics national web site (http://www.aip.org.au/).

Organising committee: Tilo Söhnel (chair), Graham Bowmaker, Morgan Allison, Daniel Wilson (all University of Auckland), Dr Ben Ruck (Victoria University of Wellington), Dr Mark Waterland, (Massey University)

Correspondence: t.soehnel@auckland.ac.nz

Date: December 2014

Contents

http://www.iycr2014.org

PARTICIPANTS

Participant		E-mail	Affiliation
Abu Bakar	Faridah	faridah.abubakar@pg.canterbury.ac.nz	MacDiarmid Institute/The University of Canterbury
Al-Azri	Zakiya	zala006@aucklanduni.ac.nz	The University of Auckland
Allison	Morgan	mall632@aucklanduni.ac.nz	The University of Auckland
Andrae	Dirk	dirk.andrae@fu-berlin.de	Freie Universität Berlin, Germany
Anton	Eva-Maria	eva.anton@vuw.ac.nz	Victoria University of Wellington
Appadoo	Dominique	Dominique.Appadoo@synchrotron.org.au	Australian Synchrotron
Ashcroft	Neil	ashcroftnw@gmail.com	Cornell University, USA
Auckett	Josie	jauc3270@uni.sydney.edu.au	The University of Sydney
Binns	Jack	j.binns@sms.ed.ac.uk	The University of Edinburgh/The Bragg Institute
Bowmaker	Graham	g.bowmaker@auckland.ac.nz	The University of Auckland
Cadogan	Sean	s.cadogan@adfa.edu.au	The University of New South Wales, Canberra/ADFA
Callori	Sara	sara.callori@ansto.gov.au	The Bragg Institute/ANSTO/The University of New South Wales
Cashion	John	john.cashion@monash.edu	Monash University
Chahal	Harpreet	hcha203@aucklanduni.ac.nz	The University of Auckland
Chan	Andrew	acha343@aucklanduni.ac.nz	The University of Auckland
Chan	Ming	mcha281@aucklanduni.ac.nz	The University of Auckland
Chen	Wan-Ting	wche214@aucklanduni.ac.nz	The University of Auckland
Chong	Shen	shen.chong@callaghaninnovation.govt.nz	Callaghan Innovation/ Victoria University of Wellington
Culcer	Dimitrie	d.culcer@unsw.edu.au	The University of New South Wales, Sydney

Donaldson	Jethro	jethro.donaldson@gmail.com	Victoria University of Wellington
Edgar	Andy	andy.edgar@vuw.ac.nz	Victoria University of Wellington
Edwards	Alison	alisonedwar@gmail.com	The Bragg Insititute/ANSTO
Finlayson	Trevor	trevorf@unimelb.edu.au	The University of Melbourne
Golovko	Vladimir	vladimir.golovko@canterbury.ac.nz	The University of Canterbury/The MacDiarmid Institute
Hamilton	Alex	alex.hamilton@unsw.edu.au	The University of New South Wales, Sydney
Hutchison	Wayne	w.hutchison@adfa.edu.au	The University of New South Wales, Canberra
Hsieh	Pei-Huan	phsi013@aucklanduni.ac.nz	The University of Auckland
Jin	Jianyong	j.jin@auckland.ac.nz	The University of Auckland
Kang	Scott	hkan026@aucklanduni.ac.nz	The University of Auckland
Kharkov	Yaroslav	y.kharkov@gmail.com	The University of New South Wales, Sydney
Kinnersley	Tim	tim.kinnersley@cleveland.co.nz	Cleveland Process Automation Ltd
Lewis	Roger	roger@uow.edu.au	The University of Wollongong
Lee	Wai Tung (Hal)	wtl@ansto.gov.au	Australian Nuclear Science & Technology Organisation
Leveneur	Jerome	j.leveneur@gns.cri.nz	GNS Science
Li	Tommy	z3185754@zmail.unsw.edu.au	The University of New South Wales, Sydney
Liang	Chao	clia493@aucklanduni.ac.nz	The University of Auckland
Liu	Samuel	liu_s@chem.usyd.edu.au	The University of Sydney
Loewenhaupt	Michael	loewenhaupt@physik.tu-dresden.de	Technical University Dresden, Germany
Maity	Tanmay	Tanmay.Maity@vuw.ac.nz	MacDiarmid Institute/Victoria University of Wellington

Mayard-Casely	Helen	helenmc@ansto.gov.au	The Bragg Insititute/ANSTO
McCree-Grey	Jonathan	jonathan.mccree-grey@ansto.gov.au	The Bragg Insititute/ANSTO
McIntyre	Garry	garry.mcintyre@ansto.gov.au	Australian Nuclear Science & Technology Organisation
Mohamed	Zakiah	mohame_z@chem.usyd.edu.au	The University of Sydney
Narayanan	Narendirakumar	n.narayanan@adfa.edu.au	The University of New South Wales, Canberra
Narayanaswamy	Suresh	suresh.narayanaswamy@callaghaninnovation.govt.nz	MacDiarmid Institute/Victoria University of Wellington
Pahl	Elke	e.pahl@massey.ac.nz	Massey University, Auckland
Park	Sy Eun	park.syeun@gmail.com	The University of Auckland
Pavan	Adriano	apav0788@uni.sydney.edu.au	The University of Sydney
Prakash	Tushara	tusharap@gmail.com	MacDiarmid Institute/Victoria University of Wellington
Riley	Daniel	dry@ansto.gov.au	Australian Nuclear Science & Technology Organisation
Ruck	Ben	ben.ruck@vuw.ac.nz	Victoria University of Wellington
Qin	Meng	mqi@ansto.gov.au	Australian Nuclear Science & Technology Organisation
Sambale	Sebastian	sebastian.sambale@vuw.ac.nz	Victoria University of Wellington
Schwerdtfeger	Peter	peter.schwerdtfeger@gmail.com	Massey University, Auckland
Shahlori	Rayomand	RSHA206@aucklanduni.ac.nz	The University of Auckland
Smith	Kevin	kevin.smith@auckland.ac.nz	The University of Auckland
Söhnel	Tilo	t.soehnel@auckland.ac.nz	The University of Auckland
Srinivasan	Ashwin	ashwin@phys.unsw.edu.au	The University of New South Wales, Sydney
Stewart	Glen	g.stewart@adfa.edu.au	The University of New South Wales, Canberra

Storey	James	james.storey@callaghaninnovation.govt.nz	Callaghan Innovation
Sushkov	Oleg	sushkov@phys.unsw.edu.au	The University of New South Wales, Sydney
Tallon	Jeffery	j.tallon@irl.cri.nz	Callaghan Innovation
Timmers	Heiko	h.timmers@adfa.edu.au	The University of New South Wales, Canberra
Trodahl	Joe	joe.trodahl@vuw.ac.nz	MacDiarmid Institute/Victoria University of Wellington
Ulrich	Clemens	c.ulrich@unsw.edu.au	The University of New South Wales, Sydney
von Seggern	Heinz	seggern@e-mat.tu-darmstadt.de	Technical University Darmstadt, Germany
Wang	Xianglei	xianglei.wang@student.adfa.edu.au	The University of New South Wales, Canberra
Waterland	Mark	M.Waterland@massey.ac.nz	Massey University
Whittle	Thomas	thomas.whittle@chem.usyd.edu.au	The University of Sydney
Wildes	Andrew	wildes@ill.fr	Institute Laue-Langevin, Grenoble, France
Willmott	Geoff	g.willmott@auckland.ac.nz	The University of Auckland
Wilson	Daniel	dwil259@aucklanduni.ac.nz	The University of Auckland
Winch	Nicola	nicola.winch@vuw.ac.nz	Victoria University of Wellington
Wu	Chun-Ming	muconic@gmail.com	National Synchrotron Radiation Research Center, Taiwan
Xu	Guangyuan	gxu331@aucklanduni.ac.nz	The University of Auckland
Yeoh	Lareine	lareine.yeoh@phys.unsw.edu.au	The University of New South Wales, Sydney

Overall Timetable

Tuesday, 4th February

16:00 – 18:00	Registration
17:30 – 18:30	**Welcome Drinks at "The Lookout"**
18:30	**Dinner at "The Lookout"**

Wednesday, 5th February

08:50 – 09:00	Opening
09:00 – 10:40	Presentations
10:40 – 11:00	**Morning tea**
11:00 – 12:50	Presentations
12:50 – 13:50	**Lunch**
14:00 – 15:50	Presentations
15:50 – 16:10	**Afternoon Tea**
16:10 – 16:40	Presentation
16:45 – 17:00	Business Meeting
17:00 – 18:30	Poster Session & **Drinks from bar**
19:00	**Dinner – *BBQ Buffet***
20:30	Quiz night - 'Wagga Trivia'

Thursday, 6th February

09:00 – 10:30	Presentations
10:30 – 10:50	**Morning tea**
10:50 – 12:40	Presentations
12:50 – 13:50	**Lunch**
14:00 – 15:30	Presentations
15:30 – 15:50	**Afternoon Tea**
15:50 – 17:00	Presentations
17:00 – 18:30	Poster Session & **Drinks from bar**
19:00	**Departure to 'The Bay'**
19:30	**Conference Dinner at 'The Bay'**

Friday, 7th February

09:00 – 10:30	Presentations
10:30 – 10:50	**Morning Tea**
10:50 – 12:20	Presentations
12:20 – 12:30	Closing
12:30 – 13:30	**Lunch**

2014 Program

Tuesday, 4th February

16:00 – 18:00 **Registration**

17:30 **Welcome Drinks** at "The Lookout"

18:30 **Dinner** at "The Lookout"

Wednesday, 5th February

08:50 – 09:00 **Opening**: Tilo Söhnel, The University of Auckland

Chairperson: Glen Stewart

09:00 – 09:30 wo1 **Adventures in Reciprocal Space – From Laue to Bragg and Back Again**

Allison Edwards, ANSTO, Sydney, Australia ***INVITED***

09:30 – 09:50 wo2 Enhanced Ferroelectric Response in Strained Perovskites

Joe Trodahl, Victoria University of Wellington, New Zealand

09:50 – 10:10 wo3 Weak antilocalisation in topological insulators

Dimitrie Culcer, University of New South Wales, Sydney, Australia

10:10 – 10:40 wo4 **The dynamics and critical properties of $FePS_3$, an Ising-like two- dimensional magnet on a honeycomb lattice**

Andrew Wildes, Institut Laue-Langevin, Grenoble, France ***INVITED***

10:40 – 11:00 **Morning tea**

11:00 – 12:50 **Chairperson**: Sean Cadogan

11:00 – 11:30 wo5 **Colour Tunable Light Emission from Organic Field-Effect Transistors**
Heinz von Seggern, Technical University Darmstadt, Germany ***INVITED***

11:30 – 11:50 wo6 Organic luminescent solar concentrators for solar cells
Nicola Winch, Victoria University of Wellington, New Zealand

11:50 – 12:10 wo7 Structural Studies of Phase Transitions in Hybrid Organic-Inorganic Salts with Temperature and Pressure
Jack Binns, The University of Edinburgh, Scotland

12:10 – 12:30 wo8 Optically and Electrically Detected Electron Spin Resonance in OLEDs
Andy Edgar, Victoria University of Wellington, New Zealand

12:30 – 12:50 wo9 Characterization of a Fluoroperovskite Based Fibre Coupled Optical Dosimeter for Radiotherapy
Jethro Donaldson, Wellington Regional Hospital, New Zealand

12:50 – 13:50 Lunch

14:00 – 15:50 Chairperson: Mark Waterland

14:00 – 14:30 wo10 **Towards better understanding of atomically precise gold clusters and titania made using surface modifying agents**
Vladimir Golovko, University of Canterbury, New Zealand ***INVITED***

14:30 – 14:50 wo11 Low Cost Refractive Index Sensing Using Zirconia Inverse Opal Thin Films
Andrew Chan, The University of Auckland, New Zealand

14:50 – 15:10 wo12 Enhanced photocatalytic activity in F-TiO_2: effect of solvent and fluorine modifier towards the morphology of TiO_2
Fariah Abu Bakar, University of Canterbury, Christchurch, New Zealand

15:10 – 15:30 wo13 Induced few-electron GaAs Quantum Dots
Lareine Yeoh, University of New South Wales, Sydney, Australia

15:30 – 15:50 wo14 SDW and AFM order in single crystal $EuFe_2As_2$ system under high-pressue using a new ceramic anvil high-pressure cell
Narayanaswamy Suresh, Callaghan Innovation, Wellington, New Zealand

15:50 – 16:10 **Afternoon Tea**

16:10 – 16:40 **Chairperson**: John Cashion

16:10 – 16:40 wo15 **Tribute to CSIRO Scientists**
Trevor Finlayson, Melbourne University, Australia
INVITED

16:45 – 17:00 **Business Meeting**
Chairperson: Tilo Söhnel

17:00 – 18:30 **Poster Session**

19:00 **Dinner - BBQ Buffet**

20:30 **Wagga Trivia**

Thursday, 6th February

09:00 – 10:30 **Chairperson**: Roger Lewis

09:00 – 09:30 to1 **Toward an Accurate Description of Rare Gas Phases**
Peter Schwerdtfeger, Massey University, Auckland, New Zealand ***INVITED***

09:30 – 09:50 to2 Total State Designation for Electronic States of Periodic Systems
Dirk Andrae, Freie Universität Berlin, Germany

09:50 – 10:10 to3 Influence of Relativistic Effects on the Melting of Mercury
Elke Pahl, Massey University, Auckland, New Zealand

10:10 – 10:30 to4 Transport Models in Nanofluids
Geoff Willmott, The University of Auckland, New Zealand

10:30 – 10:50 **Morning tea**

10:50 – 12:40 **Chairperson**: Vladimir Golovko

10:50 – 11:20 to5 **Magnetic properties of rare-earth nitride heterostructures for MRAM devices**
Eva-Maria Anton, Victoria University of Wellington, New Zealand ***INVITED***

11:20 – 11:40 to6 Magnetically driven electric polarization in frustrated magnetic oxide multiferroics
Narendirakumar Narayanan, University of New South Wales, Canberra, Australia

11:40 – 12:00 to7 Exploring the Properties of Complex Layered Tin Cluster Compounds
Morgan Allison, The University of Auckland

12:00 – 12:20 to8 Low-temperature magnetic structure of $Ca_2Fe_2O_5$ determined by single-crystal neutron diffraction
Josie Auckett, The University of Sydney

12:20 – 12:40 to9 Magnetoelectric coupling in isotopically subtituted $TbMn^{16/18}O_3$ and RMn_2O_5 (R = Tb, Ho, and Y) explored by Raman light scattering
Clemens Ulrich, University of New South Wales, Sydney, Australia

12:50 – 13:50 Lunch

14:00 – 15:30 Chairperson: Peter Schwerdtfeger

14:00 – 14:30 to10 **Stress Controlled Metal-to-Insulator Transitions in Thin Film Vanadium Oxides**
Kevin Smith, The University of Auckland ***INVITED***

14:30 – 14:50 to11 Freudenbergite – a New Example of Electron Hopping
John Cashion, Monash University, Melbourne, Australia

14:50 – 15:10 to12 Crystal and magnetic structure of Li_2MnSiO_4 and Li_2CoSiO_4 characterized by neutron diffraction measurement
Zakiah Mohamed, The University of Sydney, Australia

15:10 – 15:30 to13 Exotic Physics in Neutron Laue Diffraction
Garry McIntyre, ANSTO, Sydney, Australia

15:30 – 15:50 Afternoon Tea

15:50 – 17:00 **Chairperson**: Graham Bowmaker

15:50 – 16:20 to14 **Condensed phase studies at the THz/Far-IR Beamline at the Australian Synchrotron**
Dominique Appadoo, Australian Synchrotron, Melbourne, Australia ***INVITED***

16:20 – 16:40 to15 Status Report on SIKA – Taiwan's Cold Neutron Triple-Axis Spectrometer at OPAL
Chun-Ming Wu, National Synchrotron Radiation Research Center, Taiwan

16:40 – 17:00 to16 Polarised Neutrons for Materials Sciences Research at the Australian Nuclear Science and Technology Organisation (ANSTO)
Wai Tung Hal Lee, ANSTO, Sydney, Australia

17:00 – 18:30 **Poster Session**

19:00 Departure to 'The Bay'

19:30 Conference Dinner at 'The Bay'

Friday 7th February

09:00 – 10:30 **Chairperson**: Ben Ruck

09:00 – 09:30 fo1 **Approaching Metallic Hydrogen by Stealth: Via the High-Hydrides**
Neil Ashcroft, Cornell University, USA ***INVITED***

09:30 – 09:50 fo2 Exploring Jupiter's icy moons with old techniques and big facilities – new insights on sulfuric acid hydrates
Helen Maynard-Casely, ANSTO, Sydney, Australia

09:50 – 10:10 fo3 Large room temperature magnetoresistance in nanogranular materials
Jérôme Leveneur, National Isotope Centre, GNS Science, Wellington, New Zealand

10:10 – 10:30 fo4 Magnetic order in gadolinium manganite probed by ^{155}Gd-Mössbauer spectroscopy
Glen Stewart, UNSW Canberra, Australia

10:30 – 10:50 **Morning Tea**

10:50 – 12:20 **Chairperson**: Clemens Ulrich

10:50 – 11:20 fo5 **Enigma of Resonant Inelastic X-ray Scattering (RIXS) data for cuprates**
Oleg Sushkov, University of New South Wales, Sydney, Australia ***INVITED***

11:20 – 11:40 fo6 Upper critical and irreversible fields of polycrystalline $CeFeAsO_{1-x}F_x$ superconductors
Shen Chong, Callaghan Innovation, Wellington, New Zealand

11:40 – 12:00 fo7 Phonons in a highly-correlated electron system: the heavy-fermion superconductor $CeCu_2Si_2$
Michael Loewenhaupt, Technical University, Dresden, Germany

12:00 – 12:20 fo8 The thermodynamics of high-T_c superconductors
Jeff Tallon, Victoria University of Wellington, New Zealand

12:20 – 12:30 **Awards and Closing**: Tilo Söhnel, University of Auckland

12:30 – 13:30 **Lunch**

from 12:30 onwards **Shuttle bus departures to Waiheke Wharf**

Poster Presentations

Wednesday, 5th February

wp1 First–principle study of palladium-defect pairing in doped Si
A.A. Abiona and H. Timmers

wp2 M/TiO_2 Photocatalysts (M=Au, Pd, Pt and Au-Pt) for H_2 Production from Ethanol-Water Mixtures
Z.H.N. Al-Azri and G.I.N. Waterhouse

wp3 Spin-reorientation in DyGa
R.A. Susilo, J.M. Cadogan, R. Cobas, S. Muñoz-Pérez and M. Avdeev

wp4 90° Magnetic Coupling in a NiFe/FeMn/biased NiFe Spin Valve Investigated by Polarised Neutron Reflectometry
S.J. Callori, T. Zhu and F. Klose

wp5 Synthesis and Characterisation of 3DOM ZIF-8 Thin-Films for Optical Gas Sensing Applications
H.K. Chahal, G.M. Miskelly and G.I.N. Waterhouse

wp6 Novel M-Pt/C (M = Ru, Sn, RuSn) Electrodes for Direct Alcohol Fuel Cells
M. H. Chan and G.I.N. Waterhouse

wp7 Ni/TiO_2 – A low cost photocatalyst system for H_2 Production from Biofuels
W.-T. Chen and G.I.N. Waterhouse

wp8 Enriching the properties of Mo-oxide layered hybrids with electron-rich zigzag fused aromatic spacer molecules
I. u-din, S.V. Chong, S.G. Telfer, G.B. Jameson, M.R. Waterland and J.L. Tallon

wp9 Inorganic/Organic Composites for X-ray Imaging
N. Winch and A. Edgar

wp10 Mechanical Properties of Tungsten Copper Composites: Direct Measurement by Neutron Diffraction
P.J. Mignone, T.R. Finlayson, S. Kabra, S-Y. Zhang, G.V. Franks and D.P. Riley

wp11 Novel SERS substrates for the Identification of Adulterants in Milk
P.-H. Hsieh, D. Sun-Waterhouse and G.I.N. Waterhouse

wp12 ESR studies of Magnetocaloric $PrMn_{2-x}Fe_xGe_2$
Q.Y. Ren, W.D. Hutchison, J.L. Wang and S.J. Campbell

wp13 Investigation of the order parameter of Pr in the filled skutterudite $PrRu_4P_{12}$ by soft resonant x-ray diffraction
F. Li, A.M. Mulders, W.D. Hutchison, M. Garganourakis, Y. Tanaka, K. Nishimura and H. Sato

wp14 The magnetic properties of $Nd_2Sn_2O_7$
P. Imperia, R.J. Aldus, K.C. Rule and A. Studer

wp15 Structure and Magnetism Studies of $Cu_{1-x}Co_xSb_2O_6$ Solid Solution
H.-B. Kang, C. Ling and T. Söhnel

wp16 Magnon mediated superconducting pairing in the vicinity of magnetic quantum critical point
Y. Kharkov and O.P. Sushkov

wp17 Ferromagnetism of Co,Eu Co-doped ZnO and 5%-Co doped TiO_2 Magnetic Semiconductors
O.J. Lee, X. Luo, W.T. Lee, V. Lauter, G. Triani, S. Li and J.B. Yi

wp18 Temperature dependence of structural parameters of the layered magnetic glass $Fe_{0.5}Ni_{0.5}PS_3$
D.J. Goossens, W.T. Lee and A.J. Studer

wp19 Generalization of the Onsager quantization condition for spin-orbit coupled systems
T. Li and O.P. Sushkov

wp20 Characterization of the carboxyl groups in graphene oxide
C. Liang, G. Xu and J. Jin

wp21 Designing new n = 2 Sillen-Aurivillius phases by lattice-matched substitutions in the halide and $[Bi_2O_2]^{2+}$ layer
S. Liu, P.E.R Blanchard, M. Avdeev, B.J. Kennedy and C.D. Ling

Thursday, 6th February

tp1 Thermoelectric Properties of Polycrystalline Gadolinium Nitride
T. Maity, H.J. Trodahl, B.J. Ruck, H. Warring and F. Natali

tp2 Reflectometry as a tool for studying dye molecule orientation in dye-sensitised solar cells (DSCs)
J. McCree-Grey and J.M. Cole

tp3 Fabrication, Optical and Photocatalytic Properties of TiO_2 Colloidal Crystals
S.E. Park and G.I.N. Waterhouse

tp4 Alkali metal and alkaline earth metal oxide materials for high temperature CO_2 absorption and desorption studies
A.F. Pavan and C.D. Ling

tp5 Characterisation of permalloy and magnetite nanopowders
T. Prakash, G.V.M. Williams, J. Kennedy, P.P. Murmu, J. Leveneur, S.V. Chong, P. Couture and S. Rubanov

tp6 Molecular Dynamics Simulations of Thermal Condutivity of UO_2, $PuCrO_3$ and $PuAlO_3$
M.J. Qin, E.Y. Kuo, M. Robinson, N.A. Marks, G.R. Lumpkin and S.C. Middleburgh

tp7 Influence of Plasma Impurities on the Effective Performance of Fusion Relevant Materials
D.P. Riley[a], M. Guenette[a], A. Deslandes[a], S. C. Middleburgh, G. Lumpkin[a], L. Thomsen[b] and C. Corr

tp8 Novel Magnetic Properties of Rare-Earth Nitrides
B.J. Ruck

tp9 ^{75}As NMR of underdoped $CeFeAsO_{0.93}F_{0.07}$
S. Sambale, D. Rybicki, G.V.M. Williams and S.V. Chong

tp10 Influence of Oxygen on the Performance of Organic Field Effect Transistors
L. Kehrer, A. Gassmann, C. Melzer and H. von Seggern

tp11 Solar Hydrogen Production using Au/TiO_2 Photocatalysts
R. Shahlori and G.I.N. Waterhouse

tp12 Electrical tuning of the hole Zeeman spin splitting in (100) Quantum wells
A. Srinivasan, I. Farrer, D.A. Ritchie and A.R. Hamilton

tp13 Identifying further inelastic neutron crystal field transitions in $ErNiAl_4$
G.A. Stewart, W.D. Hutchison, Z. Yamani, J.M. Cadogan and D.H. Ryan

tp14 Thin-Film Thermopower Measurement System Open for Business
J.G. Storey and N. Suresh

tp15 Phase transition enhanced thermoelectric performance in Cu_2Se
H. Liu, X. Shi, W. Zhang, L. Chen and S. Danilkin

tp16 Characterisation of self-supporting submicron-thick graphitic carbon foils with reflection spectroscopy
H. Timmers, C. Jansing, M. Tesch, M. Gilbert, A.G. Muirhead, A. Gaupp[d] and H.-Ch. Mertins

tp17 X-ray Dose Dependence and Spectral Hole-Burning Properties of Ball Milled Nanocrystalline $Ba_{0.5}Sr_{0.5}FCl_{0.5}Br_{0.5}:Sm^{3+}$
X.Wang and H. Riesen

tp18 Characterising Graphene Nanoribbons using Raman Microscopy
M.R. Waterland, H. Dykstra and A.J. Way

tp19 Structural Investigation of Tungsten Bronze Type Relaxor Ferroelectrics
T.A. Whittle and S. Schmid

tp20 Neutron powder diffraction and Synchrotron PD and XAS studies of $Cu_{5-x}Mn_xSbO_6$ and $Cu_5Sb_{1-x}Mo_xO_6$
D.J. Wilson and T. Söhnel

tp21 A novel approach to synthesis of highly reduced graphene oxide
G. Xu, C. Liang, J. Zhang, H. Kang and J. Jin

Refereed conference publications

Total State Designation for Electronic States of Periodic Systems

D. Andrae

Institute of Chemistry and Biochemistry, Physical and Theoretical Chemistry, Freie Universität Berlin, Takustr. 3, D-14195 Berlin, Germany.

The role of a complete set of commuting operators (CSCO) is first recalled with the discussion of the electronic states of two finite systems as illustrative examples. It is then shown that its role is very well transferable to sequences of finite systems that approach a real periodic system in the limit where the number of monomers becomes huge. In addition, the concept of the density of states (DOS) of total energy E, $n(E-E_0)$ (E_0 is the energy of the electronic ground state), is introduced as a system's characteristic.

1. Introduction

The state of a quantum mechanical system is completely specified by its eigenvalues associated with a complete set of commuting operators (CSCO) [1]. Consider bound states of the hydrogen atom as simple, but illustrative examples. The Hamiltonian $\boldsymbol{H}$, the squared orbital angular momentum operator $\boldsymbol{L}^2$ and its z-component $\boldsymbol{L}_z$ form part of the CSCO for this case (inclusion of the Runge-Lenz vector operator and of spin operators completes the CSCO). The well-known eigenvalue equations for this case can be written as (in atomic units)

$$\boldsymbol{H}\,|nlm\ ^2\mathrm{L}\rangle = -(2n^2)^{-1}\,|nlm\ ^2\mathrm{L}\rangle,\ \ \boldsymbol{L}^2\,|nlm\ ^2\mathrm{L}\rangle = l(l+1)\,|nlm\ ^2\mathrm{L}\rangle,\ \ \boldsymbol{L}_z\,|nlm\ ^2\mathrm{L}\rangle = m\,|nlm\ ^2\mathrm{L}\rangle, \quad (1)$$

where $|nlm\ ^2\mathrm{L}\rangle$ denotes a state under consideration. A given set of quantum numbers $\{n, l, m\}$ ($n > 0$, $0 \le l < n$, $-l \le m \le l$) identifies both the eigenvalues and the state (except for the spin part, which is, however, trivial in this case). Therefore, a state's quantum numbers can be used as labels to designate it, as has already been done in eq. (1).

Our example illustrates that "*group-theoretical deductions are usually quite easy to perform and the information so obtained concerning the solutions* [of the system's Schrödinger equation (D. A.)]*, although not complete, often contains the essential physics*" [2]. Only the eigenvalue associated with the Hamiltonian, i.e. the energy, cannot be deduced from group theory alone. The principle just stated, and illustrated above for the hydrogen atom, holds true for periodic systems (polymers, surfaces, crystals) as well, but it is not fully exploited there. In this context, one may ask to which extent we really master the problem of electronic structure in periodic systems with the currently available software tools. Or, more provoking, to which extent are we being mastered by the limitations still present in the theories that form the basis for existing software?

In the next section, two finite systems and their low-lying electronic states are briefly discussed, as a reminder of the type of information that is contained in the symmetry labels of total electronic states and in order to introduce the density of states (DOS) of total energy E, $n(E-E_0)$ (E_0 is the energy of the electronic ground state). The subsequent section extends the discussion then to electronic states of periodic systems, in order to show how the principle stated above is applicable there.

2. Electronic states of finite systems: two examples

The first example is the oxygen atom, O, with electron configuration $1s^2\ 2s^2\ 2p^4$ (point group K_h in Schönflies notation). Three LS terms exist in Russell-Saunders coupling [2]: ^{3}P

($L = S = 1$), ^{1}S ($L = S = 0$), ^{1}D ($L = 2$, $S = 0$). Each term has a weight $g = (2L+1)(2S+1)$, according to the number of degenerate states $|p^4\ LM_LSM_S\rangle$ differing only by M_L and M_S for given L and S. It is instructive to consider the situation also under reduced symmetry, because the full rotation-reflection group K_h cannot be used with standard software tools designed for the study of electronic structure of molecules. An overview of the situation, including the cases of the finite point groups D_{2h}, C_{2v} and C_1, is given in Table 1. It is important to remark that all properties of the states (like, e.g., degrees of degeneracy of orbital and state energies, orbital occupation numbers, orbital radial parts) are independent of the point group actually used. The density of states (DOS) of total energy E, $n(E-E_0)$, for this case is shown in Fig. 1 (up to $E-E_0 \approx 4.5$ eV, E_0 is the ground state energy).

Table 1. Low-lying electronic terms of the oxygen atom, O, and of a trinuclear transition metal complex ion, $[(\mu_3\text{-L})M_3]^{q+}$ (assuming one unpaired electron per M ion), labeled under different point groups. See Fig. 1 for corresponding densities of states (DOS) of total energy E.

Electron configuration and point group	List of resulting electronic terms[a]
O $2p^4$:	
$(p_{+1}, p_0, p_{-1})^4$ in K_h	^{3}P / ^{1}S / ^{1}D
$(p_x, p_y, p_z)^4$ in D_{2h}	$^3B_{1g}$, $^3B_{2g}$, $^3B_{3g}$ / ^1A_g / $^1A_g(2)$, $^1B_{1g}$, $^1B_{2g}$, $^1B_{3g}$
$(p_x, p_y, p_z)^4$ in C_{2v}	$^3A_2$, $^3B_1$, $^3B_2$ / $^1A_1$ / $^1A_1(2)$, $^1A_2$, $^1B_1$, $^1B_2$
$(p_x, p_y, p_z)^4$ in C_1	$^3A(3)$ / ^1A / $^1A(5)$
$[(\mu_3\text{-L})M_3]^{q+}$ $(a,e)^3$:	
$a^2\ e^1 - a^1\ e^2 - e^3$ in C_3	$^2E - {}^4A$ / ^2A, ^2A, $^2E - {}^2E$
$a^2\ (a,a)^1 - a^1\ (a,a)^2 - (a,a)^3$ in C_1	$^2A(2) - {}^4A$ / ^2A, ^2A, $^2A(2) - {}^2A(2)$

[a] Number of degenerate terms of same symmetry in parentheses.

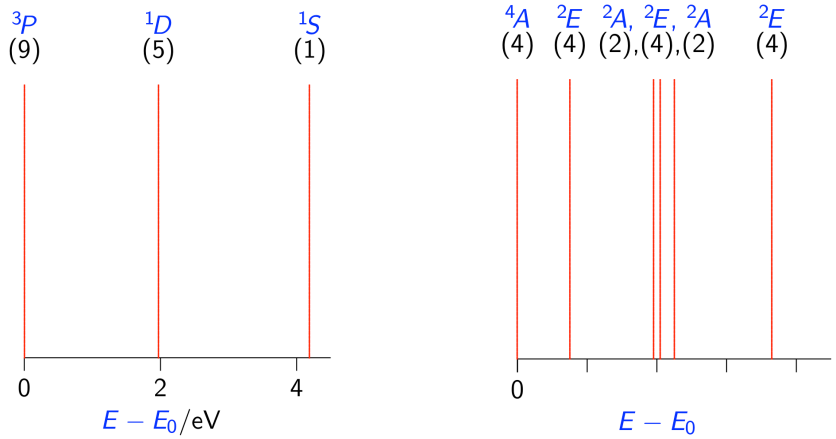

Fig. 1. Density of low-lying states (DOS) of total energy E, $n(E-E_0)$, for finite systems, being a sequence of Dirac delta "peaks" with weights (indicated in parentheses at the top of each panel). Left panel: O atom (point group K_h), DOS for LS terms [3] from electron configuration $1s^2\ 2s^2\ 2p^4$. Right panel: A trinuclear transition metal complex ion $[(\mu_3\text{-L})M_3]^{q+}$ (point group C_3), DOS for electronic terms from electron configuration $(a,e)^3$.

Our second example is a trinuclear transition metal complex ion with a triply bridging ligand L, $[(\mu_3\text{-L})M_3]^{q+}$ (point group C_3). We assume that each M ion contributes just a single unpaired electron, such that low-lying electronic states in ΓS coupling, $|\alpha\Gamma\gamma SM_S\rangle$, originate from an electron configuration $(a,e)^3$. The resulting sets of electronic terms, both in C_3 and in C_1, are listed in Table 1, and a density of states (DOS) of total energy E, $n(E-E_0)$, associated

with this case is schematically shown in Fig. 1 (details of energy spacings and sequence of states are case-dependent, but unimportant for the present discussion).

The designation of a state $| I \rangle$ of a quantum mechanical system properly combines spin and space symmetry information (here denoted by a composite index I). If the state's wave-function is constructed from single-electron functions (orbitals), then the eigenvalue associated with the Hamiltonian, the energy E_I, reduces to a linear combination of one- and two-electron integrals. For a normalized state function ($\langle I | I \rangle = 1$),

$$E_I = \langle I | \boldsymbol{H} | I \rangle = \Sigma_{ij} \gamma^I_{ij} h_{ij} + \Sigma_{ijkl} \Gamma^I_{ijkl} g_{ijkl}. \quad (2)$$

All summations run over orbital indices, the state-specific coefficients γ^I_{ij} and Γ^I_{ijkl} are known as structure factors or density matrix elements (for further details see [2] or any other good textbook on electronic structure theory for atoms and molecules).

3. Electronic states of periodic systems

An ideal infinite periodic system (polymer, slab, crystal) built from monomers A has an infinite number of electronic states. An important quantity of interest, irrespective of the actual electronic state of the system, is the energy per unit cell $\lim_{N\to\infty} E(A_N)/N$, which is finite (a single monomer A per unit cell was assumed). However, the limit process just indicated always ends abruptly because only finite pieces of periodic systems exist in the real world. But this implies that the tools discussed in the previous section become applicable, sometimes without great difficulties. For example, the designation $^1A_{1g}$ (point group O_h) can be given for the electronic ground state of both halite (rock salt, space group *Fm*-3*m*, no. 225) and diamond (space group *Fd*-3*m*, no. 227) crystals, if we idealize and assume cube-shaped crystals in the former case and octahedron-shaped crystals in the latter. In the case of diamond, dangling bonds at the crystal surface must have been saturated somehow (e. g. by H atoms) to make our designation valid. The situation is much more complicated for the simple metal lithium. Several polymorphs of lithium are known to exist up to moderate pressure [4], including bcc (under ambient conditions), fcc, hcp, and a low-temperature phase with samarium structure (hR9). What is the electronic ground state for each of these polymorphs, and how large are the energy differences between them at $T = 0$ K? How does the density of states (DOS) of total energy E per Li atom differ between these polymorphs? These questions cannot be answered yet.

An approach to the electronic structure of periodic systems via finite-sized structures requires again the consideration of the spin and space parts of the electronic states of these structures. The problem of designation of these states is addressed in the following.

3.1 The spin part

A set of N spins, each characterized by the same spin quantum number s ($2s = 1, 2, 3, \ldots$), leads to a Hilbert space of spin functions of dimension $d = (2s + 1)^N$. The resulting total spin quantum number S can take any value from the set $\{0 \le S_{min}, S_{min} + 1, \ldots, S_{max} - 1, S_{max} = Ns\}$, and for each value of S, the associated spin projection quantum number M is restricted to $2S + 1$ values obeying the condition $-S \le M \le S$. Total spin states $|\alpha SM\rangle$ can then be constructed as eigenfunctions of the total spin operators $\boldsymbol{S}^2$ and $\boldsymbol{S}_z$, such that

$$\boldsymbol{S}^2 |\alpha SM\rangle = S(S + 1) |\alpha SM\rangle, \qquad \boldsymbol{S}_z |\alpha SM\rangle = M |\alpha SM\rangle \quad (3)$$

(the label α distinguishes between eigenfunctions that do not differ in S and M). It is now of great interest to determine for given N the dimension of Hilbert subspaces with given M, $d(N,M)$, and with given S, $f(N,S)$. The calculation of these numbers for arbitrary s has been

solved, in principle: The dimensions $d(N,M)$ can be either read off from the expansion of their generating function $(1 + x + \ldots + x^{2s})^N = \Sigma_k\, a_k\, x^k$ ($a_{2Ns-k} = a_k$, $d(N,M) = a_{M+Ns}$) [5] or calculated from binomial coefficients [6]. And then for $S < S_{max}$: $f(N,S) = d(N,M = S) - d(N,M = S + 1)$ ($f(N,S_{max}) = 1$). The numbers $f(N,S)$ satisfy an invariance condition with respect to the dimension d of the complete Hilbert space: $\Sigma_S\, (2S + 1)\, f(N,S) = (2s + 1)^N = d$. It is remarkable that a recursive scheme for the calculation of $d(N,M)$ has been devised already around 1800, long before the discovery of quantum mechanics and spin degrees of freedom, by L. Euler [7]. The recursive scheme for the calculation of $f(N,S)$ generalizes the well-known branching diagram for the case $s = 1/2$ [8]. For arbitrary s and given N, the maximum value of $d(N,M)$ is obtained for $|M| = S_{min}$. The value of S for which $f(N,S)$ takes its maximum value is not known in general. But for s = 1/2 and given N, the maximum value of $f(N,S)$ occurs at $S_{peak} = (S_{max}/2)^{1/2}$ (see Fig. 2), and the maximum of the weighted dimensions $(2S + 1)\, f(N,S)$ is at $S'_{peak} = 2^{1/2}\, S_{peak} = (S_{max})^{1/2}$.

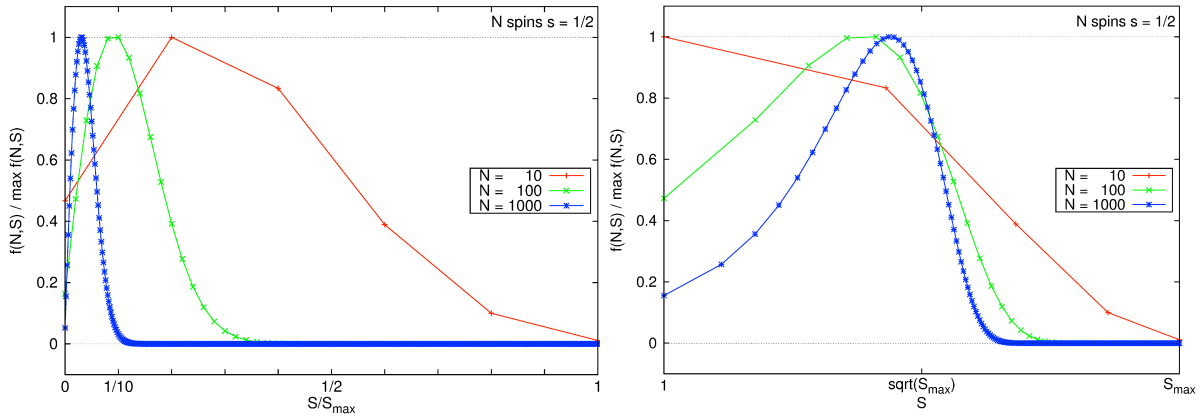

Fig. 2. Renormalized distributions of the number $f(N,S)$ of spin states with total spin S for N spins $s = 1/2$ ($0 \le S \le S_{max} = N/2$, $N = 10, 100, 1000$). The maximum of $f(N,S)$ is at $S_{peak} = N^{1/2}/2 = (S_{max}/2)^{1/2}$ for sufficiently large N. Left panel: Horizontal axis with linear scale for S/S_{max}. Right panel: Horizontal axis with logarithmic scale for S.

3.2 Combining the spin and space parts

The combination of spin and space parts has to be done individually for every system of interest (see the examples in Sect. 2). However, a list of the possible types of electronic terms that can occur for a given sequence of systems can be straightforwardly derived from group-theoretical considerations. The following examples illustrate the situation for Li oligomers:

Li_N linear chain: Point group $D_{\infty h}$, N times $(s\sigma, p\sigma)^1$, possible electronic terms:

N even: $^{1,3,\ldots}(\Sigma_g^+, \Sigma_g^-, \Sigma_u^+, \Sigma_u^-)$

N odd: $^{2,4,\ldots}(\Sigma_g^+, \Sigma_g^-, \Sigma_u^+, \Sigma_u^-)$

Li_N ring: Point group D_{nh}, N times $(s, p_t)^1$, possible electronic terms:

$N = 2k + 1 \ge 3$: $^{2,4,\ldots}(A'_1, A'_2, E'_1, \ldots, E'_k)$

$N = 2k \ge 4$ ($k = 2l$): $^{1,3,\ldots}(A_{1g}, A_{2g}, B_{1g}, B_{2g}, E_{1u}, E_{2g}, \ldots, E_{(k-1)u})$

$N = 2k \ge 6$ ($k = 2l + 1$): $^{1,3,\ldots}(A_{1g}, A_{2g}, B_{1u}, B_{2u}, E_{1u}, E_{2g}, \ldots, E_{(k-1)g})$

Li_N planar (lozenge-shaped cutout from close-packed layer): Point group D_{2h}, N times $(s, p_x, p_y)^1$, possible electronic terms:

N even: $^{1,3,\ldots}(A_g, B_{1g}, B_{2u}, B_{3u})$

N odd: $^{2,4,\ldots}(A_g, B_{1g}, B_{2u}, B_{3u})$

For given N and S, the number of terms transforming according to a given irreducible representation Γ of the point group G of the system can be denoted as $f(N,S,\Gamma)$. These numbers can be calculated recursively for a given sequence of systems (e.g. linear Li_N chains, $N = 2, 3, 4,$

…). It seems to be possible to obtain recursively also all the energies E_I, eq. (2), for all possible electronic terms of given N, from the energies E_J for all possible electronic terms seen for $N-1$. In this way, a sequence of densities of states of total energy E per monomer is generated that is likely to approach the one for the periodic system in the limit $N \to \infty$.

Acknowledgments

Fruitful discussions with J. Schnack (Bielefeld University) are gratefully acknowledged.

References

[1] Dirac P A M 1930 *The Principles of Quantum Mechanics* (Oxford : Clarendon) § 14.
[2] Weissbluth M 1974 *Atoms and Molecules* (New York : Academic) p 204.
[3] Kramida A, Ralchenko Yu, Reader J and NIST ASD Team 2013 *NIST Atomic Spectra Database* (version 5.0), see http://physics.nist.gov/asd [2014, January 19].
[4] Guillaume C L, Gregoryanz E, Degtyareva O, McMahon M I, Hanfland M, Evans S, Guthrie M, Sinogeikin S V, Mao H-K 2011 *Nature Physics* **7** 211.
[5] The coefficients b_k in $(x^{-s} + x^{-s+1} + \ldots + x^{s-1} + x^{s})^N = \Sigma_k\, b_k\, x^k$ generate the numbers $d(N,M)$ more directly ($d(N,M) = b_M$), but this approach requires consideration of Puiseux or Laurent polynomials (polynomials with fractional and/or negative powers), instead of just ordinary polynomials in x.
[6] Bärwinkel K, Schmidt H-J and Schnack J 2000 *J. Magn. Magn. Mater.* **212** 240.
[7] Euler L 1801 *Nova Acta Acad. Sci. Imper. Petropol.* **12** 47 (paper no. 709 in the Eneström index), also in Euler L (1992) *Opera Omnia* Ser 1, Vol 16 (Basel : Birkhäuser) p 28, see arXiv:math/0505425 for an English translation.
[8] McWeeny R and Sutcliffe B T 1969 *Methods of Molecular Quantum Mechanics* (New York : Kluwer) p 67.

Exploring the Properties of Complex Layered Tin Cluster Compounds

M. Allison[a, b], S. Liu[b], G. Stewart[c], C. Ling[b] and T. Söhnel [a]

[a] *School of Chemical Sciences, University of Auckland, Auckland, New Zealand.*
[b] *School of Chemistry, University of Sydney, NSW, Australia.*
[c] *School of PEMS, UNSW@AFDA, Canberra, Australia.*

Solid oxide sintering reactions were used to prepare three new phases with the formula: $Fe_{1+x}Mn_{3-x}Si_2Sn_7O_{16}$ (x = 0.82, 1.65, 2.52). High resolution neutron and synchrotron powder diffraction investigations determined these to be isostructural to the iron rich $Fe_4Si_2Sn_7O_{16}$ phase; space group *P*-3*m*1 (164). Surprisingly, these phases show non-linear changes in unit cell parameters and magnetic behaviour depending on the specific transition metal content, which may indicate that each type of transition metal exhibits a unique set of behaviours that compete rather than cooperate with each other.

1. Introduction

X-ray powder and neutron powder diffraction experiments have shown that all of the $Fe_{1+x}Mn_{3-x}Si_2Sn_7O_{16}$ (x = 0.82, 1.65, 2.52) phases form trigonal layered materials isostructural to the iron rich phase $Fe_4Si_2Sn_7O_{16}$ described by *Söhnel et. al.*[1]. All members of this solid state series form layered structures that can be viewed as a combination of a pseudo two dimensional layer of oxygen bridged $FeSn_6$ clusters linked by SiO_4 tetrahedra to a second two dimensional layer analogous to a tin substituted fayalite-like layer of MO_6 octahedra with a transition metal to tin ratio of 3:1 through the SnO_6 octahedra (Fig. 1). Ionically it can be broken down as $[(Fe^{2+})_1(Sn^{2+})_6](Fe^{2+})_1(Sn^{4+})_1(Si^{4+})_2(O^{2-})_{16}]$ with the solution of the 18 valence-electron rule for the Fe^{2+} cluster being: $6e^- + 6\times2e^- = 18e^-$ (octahedra). The predicted valence state of the Fe and Sn nuclei was confirmed with ^{57}Fe and ^{119}Sn Mössbauer spectroscopy [1]. The ^{57}Fe Mössbauer measurements also showed the presence of both high spin and low spin Fe^{2+} in a ratio of 3:1, indicating the oxide layer sites are all high spin Fe^{2+}. Magnetic measurements confirmed the predicted paramagnetic nature of this material dominating and there was no suggestion of magnetic ordering above 4.2 K. The novel structure of $Fe_4Si_2Sn_7O_{16}$ could however allow for substitution of other high spin nuclei into both of the transition metal crystallographic sites (the MSn_6 cluster and the three transition metal sites in the oxide layer) and presents us a unique opportunity to investigate the engineering of magnetic effects into semiconducting materials by substituting each of the sites by different transition metals. These results will help us to develop a model for synthesis of complex multiferroic stannides to be used in devices with molecular level electronic applications..

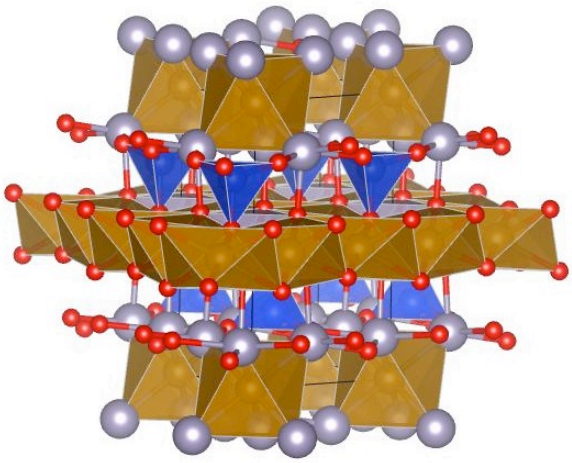

Fig. 1. Crystal structure of $Fe_{1+x}Mn_{3-x}Si_2Sn_7O_{16}$.

2. Experimental Details

Highly crystalline powders and single crystals were prepared by solid state sintering by combining the required metal oxide powders together with an excess of tin metal. The samples were places in corundum tubes and sealed under an air atmosphere in quartz tubes. The tubes were heated to 900 ºC over 48 hours followed by a controlled cooling to 750 ºC over a period of 200 hours.

Synchrotron X-ray powder diffraction (SXRD) measurements were conducted on the powder diffraction beamline, 10-BM, at the Australian Synchrotron over a 6 to 86° 2θ range with a step size of 0.00375° 2θ, using the MYTHEN detector and the double crystal monochromator of Si(111) flat crystal pair. High resolution neutron powder diffraction measurements (NPD) were carried out using the Echidna instrument located at the OPAL reactor in Sydney, Australia, over a range of 2.75° to 162° 2θ with a step size of 0.125° 2θ at room temperature. Low temperature NPD measurements were carried out using the same parameters with an Oxford Instruments 12T cryomagnet at 5 K at 0 T and 1.8 K between 0 and 10 T using 2 hours per scan. All powder diffraction measurement data sets were refined with the Reitveld method using the FullProf suite software package [2].

^{57}Fe Mössbauer spectra were recorded with transmission geometry in a constant acceleration mode using a ^{57}Co(Rh) source at room temperature in order to determine the valence and spin states of the iron nuclei. Magnetic susceptibility measurements were carried out using a Quantum Design Physical Properties Measurement System (PPMS) under a 1 T magnetic field from room temperature down to 2 K.

3. Results and Discussion

3.1 X-ray Powder Diffraction

High-resolution synchrotron X-ray powder diffraction patterns were collected at the Australian Synchrotron between 6 and 86° 2θ at room temperature to determine the structure of the solid solution $Fe_{1+x}Mn_{3-x}Si_2Sn_7O_{16}$. These measurements confirmed the presence of new phases with a pattern near identical to that of the iron rich phase. However, all mixed Fe/Mn phases showed the presence of a significant amount of SnO_2 contamination indicating an incomplete reaction and/or the oxidation of some of the final products and tin flux during the reaction cooling phase. Rietveld refinements show that as the transition metal ratio trends towards the Mn rich end of the series, there is an increase in the unit cell volume consistent with increasing replacement of Fe^{2+} with Mn^{2+} in line with Vegard's law [3]. However, a more detailed look at the cell parameters show that they increase slightly asymmetrically with the *a/b* parameters increasing more rapidly than that of the *c* parameter. This indicates that the oxide layer transition metal positions rather than the cluster positions were being preferentially substituted. That is be explained by the oxide layer transition metal positions being substituted with Mn as there are three potential transition metal crystallographic positions that lie in that plane rather than two positions which lie in the *c* plane.

Synchrotron measurements from 303 to 823 K were also carried out which allowed us to determine the coefficient of thermal expansion for each of our phases (Fig. 2 and Table 1). These results show a decreasing coefficient of thermal expansion as the phases became richer in Mn, however, the most surprising results showed that the thermal expansion seen is asymmetric in the *a/b* plane with a value of almost double that of the *c* coefficient. Whilst this is commonly seen in most non-cubic materials, the large difference between the *a/b* plane and the *c* plane indicates that this behaviour is related to the layering that we have described in the crystal structure.

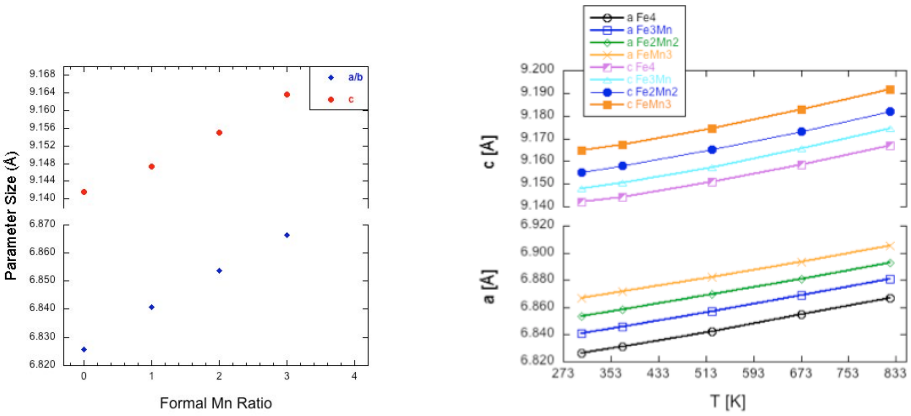

Fig. 2. Cell parameter of $Fe_{1+x}Mn_{3-x}Si_2Sn_7O_{16}$ as a function of composition at room temperature (left) and temperature between 303 K and 823 K (right).

Table 1. Calculated coefficients of thermal expansion.

Formal Phase Composition	αL (a) [Å.K^{-1}]	αL (c) [Å.K^{-1}]	αV [Å^3.K^{-1}]
$Fe_4Si_2Sn_7O_{16}$	1.176x10^{-5}	5.500x10^{-6}	2.912x10^{-5}
$Fe_3MnSi_2Sn_7O_{16}$	1.147x10^{-5}	5.831x10^{-6}	2.888x10^{-5}
$Fe_2Mn_2Si_2Sn_7O_{16}$	1.111x10^{-5}	5.841x10^{-6}	2.820x10^{-5}
$FeMn_3Si_2Sn_7O_{16}$	1.094x10^{-5}	5.837x10^{-6}	2.783x10^{-5}

3.2. Neutron Powder Diffraction

Neutron powder diffraction (NPD) measurements were carried out between 2.75° and 162° 2θ at room temperature in order to refine the occupation of the transition metal positions, the results of these measurements are shown in Table 2. Refinements of all samples were solved for the space group *P-3m1*. Except for the iron rich end member of the solid solution the calculated change in unit cell parameters were within agreement with those obtained from the synchrotron powder diffraction measurements. The elemental occupation refinement of the oxide layer and cluster layer transition metal positions revealed that there was no measurable amount of Mn contained in the Sn_6 clusters. The occupational refinements did however show that the iron rich end member phase was iron and oxygen deficient but this has yet to be explained satisfactorily. For the mixed Fe/Mn phases refinements showed that a significantly lower than expected amount of Mn had been substituted into the oxide layer positions resulting in the phase formulas needing to be recalculated to: $Fe_{1+x}Mn_{3-x}Si_2Sn_7O_{16}$ (x = 0.82, 1.65, 2.52).

Table 2. Unit cell parameter changes for formal and actual fractional change in Mn elemental composition.

Formal Composition	Fe% (refined)	Mn% (refined)	*a/b* [Å]	*c* [Å]	Vol. [Å^3]
$Fe_4Si_2Sn_7O_{16}$	100.00	0	6.8322(2)	9.1385(3)	369.42(2)
$Fe_3MnSi_2Sn_7O_{16}$	79.50	20.50	6.8278(2)	9.1331(2)	368.73(2)
$Fe_2Mn_2Si_2Sn_7O_{16}$	58.75	41.25	6.8399(2)	9.1395(2)	370.28(2)
$FeMn_3Si_2Sn_7O_{16}$	37.00	63.00	6.8550(2)	9.1477(3)	372.26(2)

3.3 ^{57}Fe Mössbauer Spectroscopy

^{57}Fe Mössbauer spectra (Fig. 3) were recorded in order to determine the valence state and amount of Fe in each environment for the new phases. The measurements for all phases were resolved using MOSFIT and are resolved into two sets of doublets each phase that show two chemical environments of the iron nuclei present - the cluster and oxide layer positions. No sextets were observed indicating a lack of room temperature magnetic ordering and so these results are typical for paramagnetic Fe^{2+} nuclei [4].

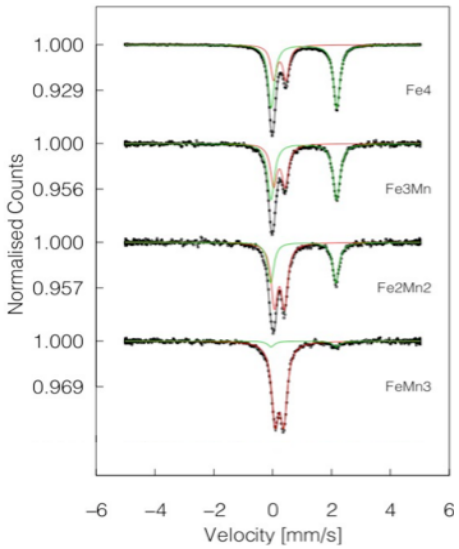

Fig. 3. ^{57}Fe Mössbauer spectra of $Fe_{1+x}Mn_{3-x}Si_2Sn_7O_{16}$

3.4. Magnetic Properties

Magnetic susceptibility measurements were carried out down to 2 K to explore magnetic behaviours of the phases. These measurements show that the Mn richest member $Fe_{1.48}Mn_{2.52}Si_2Sn_7O_{16}$ showed a transition to antiferromagnetic (AFM) ordering at 2.5 K, whilst all other phases remained paramagnetic above 2 °K. These low Curie temperatures are likely due to strong spin-orbit of the Fe^{2+} that prevents the Mn from ordering within the layer. Low temperature (1.8 K) neutron powder diffraction measurements were then carried out under magnetic fields on $Fe_{1.48}Mn_{2.52}Si_2Sn_7O_{16}$ in order to determine the magnetic structures. These powder patterns showed new peaks at low angles – indicating the AFM transition, at low magnetic fields up to about 1 T. These magnetic peaks disappeared at fields above 2 T and the nuclear peaks increased in intensity, which could be a sign of a spin flip transition. However, work is still currently ongoing to explain these results.

Acknowledgements

We would like to thank Maxim Avdeev and the Bragg Institute (ANSTO) for the opportunity to carry out neutron experiments and AINSE for financially supporting this work. We also thank the Australian synchrotron for support with synchrotron experiments. Finally we also thank the University of Auckland for financial and academic support with this research.

References

[1] Söhnel T, Böttcher P, Reichelt W, Wagner F E 1998 *Z. Anorg. Allg. Chem.* **624**, 708
[2] Rodriguez-Carvajal, J 1993 *Physica B.* **192**, 55
[3] Vegard, L. 1921 *Z. Phys.* **5** 17
[4] Recham N, Casas-Cabanas M, Cabana J, Grey C P, Jumas J-C, Dupont L, Armand M and Tarascon J-M 2008 *Chem. Mater.* **20** 6798

Freudenbergite – a New Example of Electron Hopping

J. D. Cashion[a], A. Lashtabeg[b*], E. R. Vance[c], D.H.Ryan[d] and J. Solano[e]

[a] *School of Physics, Monash University, Melbourne, Victoria 3800, Australia,*
[b] *Nanolytical, PO Box 21, The Gap, Brisbane, Qld 4061, Australia,*
[c] *Australian Nuclear Science and Technology Organisation, Menai, NSW 2234, Australia,*
[d] *Physics Department, McGill University, Montreal, Québec H3A 2T8, Canada,*
[e] *School of Chemistry, Monash University, Melbourne, Victoria 3800, Australia.*

Mössbauer spectra of freudenbergite samples with different composition have showed that although the Fe and Ti populate the octahedra randomly, Fe prefers the M(1) site over the M(2) site by approximately 1.3:1. Ti was able to accommodate mixed valence more easily than Fe, but some samples showed dynamic electron hopping in the Fe ions, which also affected the diffuse reflectance in the 400-800 nm region.

1. Introduction

The monoclinic freudenbergite structure of $Na_2Fe^{3+}{}_2Ti_6O_{16}$ is composed of double sheets of edge sharing $(Fe,Ti)O_6$ octahedra parallel to (001), with corner sharing along [100] to make a 3D structure [1]. The charge compensating Na^+ ions are in the channels between the octahedra. We have recently [2] examined several samples of ferric and ferrous freudenbergite and showed that some samples of freudenbergite with mixed valence can undergo electron hopping, as evidenced by temperature dependence of the quadrupole splitting in their Mössbauer spectra.

2. Sample preparation

Several samples of freudenbergite were prepared. Most were prepared from aqueous mixtures of $NaNO_3$, $Fe(NO_3)_3.9H_2O$, and Ti isopropoxide as previously described [2, 3]. The compositions were chosen to correspond to ferric freudenbergite, $Na_2Fe^{3+}{}_2Ti_6O_{16}$ **(1),** to ferrous freudenbergite, $Na_2Fe^{2+}Ti_7O_{16}$, **(2)**, with additional samples containing aluminium to try and achieve mixed valence. These had the composition $Na_2Al_{2-2x}Fe_xTi_{6+x}O_{16}$, with x = 0.50, **(3),** and 0.25, **(4)**, and were heated in argon. Both used 10% excess of Na and 10% excess of Ti to try to keep all the Fe in the freudenbergite. A further sample, **(5),** was prepared from the oxides of iron, titanium and aluminium in sodium hydroxide, with several sequences of sintering, pressing and grinding. This method produces a slightly reduced freudenbergite.

SEM studies of the samples showed that those from the aqueous mixture method were all homogeneous. However, the solid state reaction sample was two-phase with the second phase being an iron-free alumina-based composition.

All the samples were checked by XRD and SEM. The XRD showed that sample **1** had a few percent of the ferric brownmillerite Fe_2TiO_5, which has Mössbauer parameters very similar to those expected for freudenbergite [6]. Samples **2** and **3** had freudenbergite as the only iron-containing phase. These results were all confirmed by SEM.

We note that in the previous report of our experiments on some of these samples [2], the sample labels **2** and **3** were reversed between the description of the preparation, which is correct, and the description of the spectra. Samples **2** and **3** in the preparation description in [1] correspond to the same samples in this report.

3. Results

3.1 Colour, composition and diffuse reflectance spectra

We have made ten samples of freudenbergite with different compositions of Fe, Ti and Al in the octahedral sites to try and achieve ferric, ferrous and mixed ferric-ferrous systems. Heating was carried out in both air and argon. However, only two of the samples gave mixed valence and these two also exhibited electron hopping. The remainder were either pure ferric or pure ferrous. The cation charges in the octahedra should sum to 30, assuming a stoichiometric Na concentration, and even when compositions were chosen to try and force mixed valence, e.g. $Na_2Al_{2-2x}Fe_xTi_{6+x}O_{16}$, which was all ferrous, or $Na_2AlFeTi_{6+x}O_{16}$, which was all ferric, the mixed valence was accommodated by the Ti and not by the Fe.

It was noticeable that the two samples with electron hopping were black (**2**) or blue-black (**5**) and the remainder were coloured through the gold-green-grey hues, except for the two ferrous samples of $Na_2Al_{2-2x}Fe_xTi_{6+x}O_{16}$, with x = 0.50 and 0.25 (**3** and **4**), which were also black. As Coey [4] points out, materials which host spontaneous charge transfer are usually black, with a metallic lustre, but the converse, strong broadband absorption in the visible is not a guarantee of thermally-activated electron hopping. However, the colour of these last two samples raises the possibility that they are close to an electron hopping regime. We note that the Fe^{2+} - Ti^{4+} charge band absorbs in the red, so the crystals are usually blue.

Diffuse reflectance spectra of powders is made up of light which has been reflected from the surface, and hence resembles the inverted specular reflectance spectrum, and light which has penetrated the sample before being scattered and hence contains the transmission spectrum. For a strong absorber, the former effect dominates. Diffuse reflectance spectra were taken of samples **1**, **2** and **3** over the range 200-800 nm, using a Carey 1e spectrophotometer. Sample **1** showed a very rapid drop-off in reflected intensity between 500-600 nm (Fig. 1a), very similar to the spectra of the ferric α-, β- and γ-FeOOH polymorphs [5]. In contrast, the spectra of the other two samples (Fig. 1b, 1c) showed a continuous increase from 400 nm up to 800 nm, very similar to wüstite [5]. Wüstite is non-stoichiometric $Fe_{1-x}O$, where the charge balance is maintained by a small percentage of the iron ions being ferric, so that it is mixed valence.

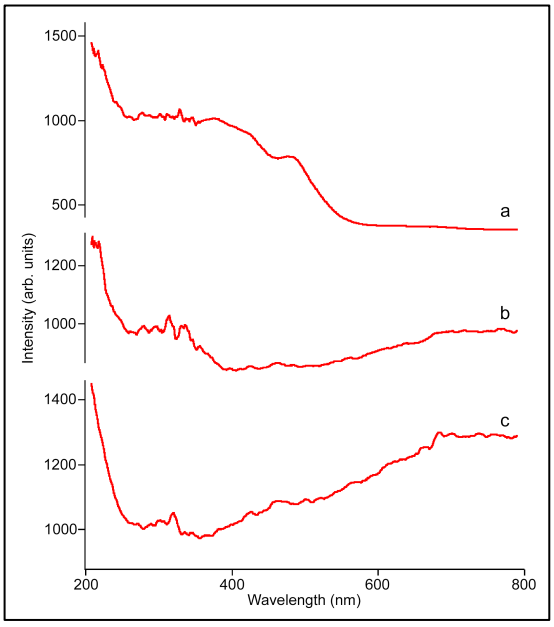

Fig 1. Diffuse reflectance spectra of (a) **1**, (b) **2** and (c) **3**

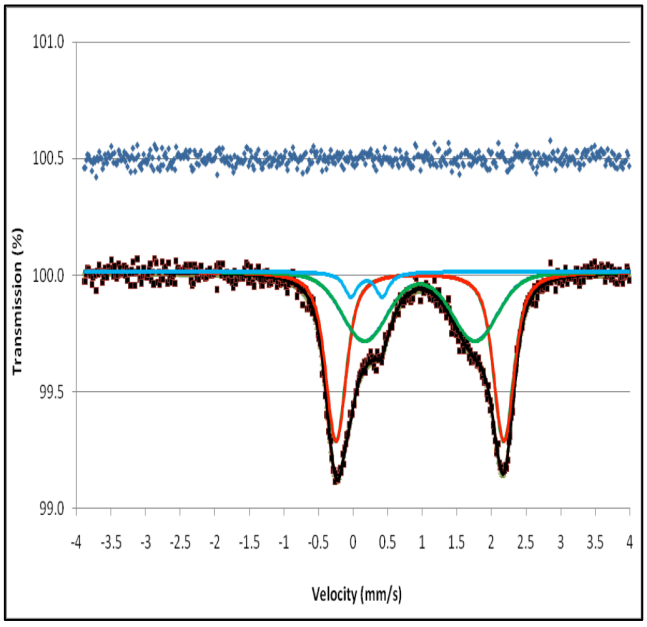

Fig. 2. Room temperature Mössbauer spectrum of **4**.

Absorption features in Fe-Ti materials are typically in the 400-2000 nm region, but assigning their origin is notoriously difficult [6]. This is particularly true when there are multiple possibilities, such as the homonuclear inter-valence transitions, $Fe^{2+} \leftrightarrow Fe^{3+}$, $Ti^{3+} \leftrightarrow Ti^{4+}$, or the heteronuclear $Fe^{2+} + Ti^{4+} \leftrightarrow Fe^{3+} + Ti^{3+}$, and will not be attempted here.

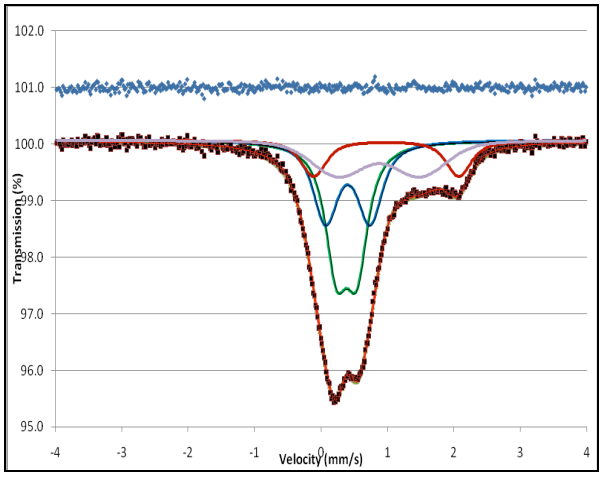

Fig. 3a. Mössbauer spectrum of **5** showing broadening due to electron hopping.

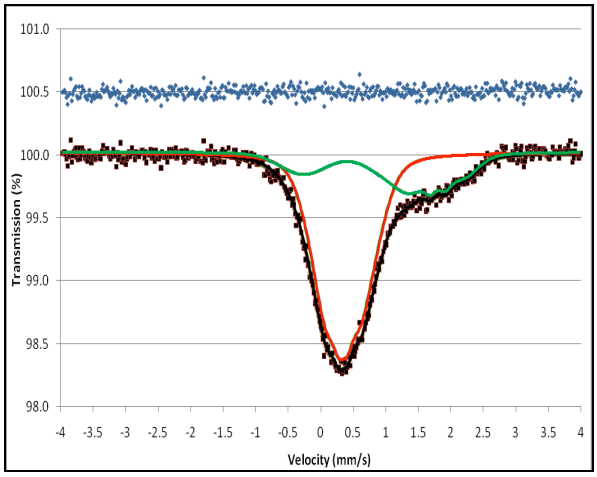

Fig. 3b. Mössbauer spectrum of **5** in an applied field of 1.6 T showing modification of the electron hopping.

3.2 Mössbauer spectra

The Mössbauer spectrum of **4** at room temperature is shown in Fig. 2. It has been fitted, similarly to that of **3** [1], to two ferrous doublets and a weak ferric doublet, all with Voigtian lineshapes, and the parameters for both samples are given in Table 1. The top blue line is the difference between the data and the fit in all the spectra. It is notable that the width of the inner doublet is approximately 2.5 times larger than that of the outer one.

The Mössbauer spectrum of **5** at room temperature is shown in Fig. 3a, with the effect of the electron hopping in the ferrous component evident in the broadened right hand region. Each of the ferrous and ferric components have been fitted to two doublets with the inner ferrous doublet being noticeably broadened. The fit to the ferric doublets was very unstable, depending critically on the allowed width of the lines as characterised by the standard deviation, $\sigma(\Delta)$, of the Gaussian spread in the quadrupole splitting, Δ. However, the total ferric area remained quite constant at 66%. Fig. 3b shows **5** in a transverse applied field of 1.6 T. This modified the electron hopping so that each valence state was now able to be fitted to one unresolved sextet with a Gaussian spread of hyperfine fields. The mean hyperfine fields of 2.6 T for the ferric sites and 4.2 T for the ferrous sites are both significantly larger than the applied field, due to enhancement by the magnetization of the paramagnetic iron ions.

Table 1. Fitted parameters to the room temperature Mössbauer spectra.

Sample	B	Ferric sites					Ferrrous sites				
	T	δ mm/s	Δ, ε mm/s	σ(Δ) mm/s	B T	Area %	δ mm/s	Δ, ε mm/s	σ(Δ) mm/s	B T	Area %
3	0	0.23(3)	0.48(5)	0	0	3.2	0.99(1)	2.43(1)	0.21	0	55.3
							1.00(1)	1.55(7)	0.50	0	41.5
4	0	0.19(2)	0.45(4)	0.02	0	5.5	0.96(1)	2.43(1)	0.18	0	53.1
							0.96(1)	1.60(9)	0.55	0	41.4
5	0	0.39(1)	0.30(1)	0.10	0	37.7	0.97(1)	2.18(3)	0.17	0	12.8
		0.40(1)	0.67(3)	0.16	0	27.6	0.87(3)	1.23(9)	0.63	0	21.9
5	1.6	0.35(1)	0.01(1)		2.4	73.1	1.10(4)	-0.69(3)		4.2	26.9

4. Discussion and Conclusions

In the fitting of **3** [1] and **4** (Fig 2), the isomer shifts of the weak ferric doublet in the two mainly ferrous samples were consistently lower than would be expected for an Fe^{3+} ion in an octahedral environment. Attempts to force them to a value in the region 0.35-0.38 mm/s produced a noticeably poorer fit. It was tentatively suggested in [1] that although the subspectrum could be due to an impurity, it was also possible that the parameters appropriate for a pure ferric freudenbergite had been altered by a change in lattice parameter. We now believe that the most likely explanation for the observed values is that the Fe^{3+} is in a tetrahedral environment, which does not exist in the freudenbergite structure. The samples were made with an excess of Na and a small amount of $NaAl_{11}O_{17}$ impurity was found in sample **3.** All the compounds $NaAlO_2$, $Na_7Al_3O_8$, $Na_{17}Al_5O_{16}$ and Na_5AlO_4 have Al in a tetrahedral coordination, with Fe^{3+} being able to substitute for Al^{3+} in all of them. Hence, we attribute the location of the Fe^{3+} to such a tetrahedral site and with only a few percent of the total iron being incorporated, it would be undetectable by XRD.

It would thus seem that the ferric doublet in the spectra of **3** and **4** is not associated with the freudenbergite so we can accept the areas of the two ferrous doublets without needing any modification. Following Stähle *et al*. [7], we will assign the outer doublet to the more distorted M(1) site. We then get the ratio of the populations of the two sites, M(1)/M(2), to be 1.28 for **3** and 1.33 for **4**, showing that although the filling of the octahedral sites by Fe^{2+} and Ti^{4+} appears to be random, in the sense that there is no clustering, there is a preference by the Fe^{2+} as the larger ion, for the larger M(1) site. Stähle *et al*. obtained a ratio of 1.22 for the M(1)/M(2) ratio for Fe^{3+} even though the ionic radius of Fe^{3+} of 0.064 nm is slightly smaller than that of Ti^{4+} at 0.068 nm.

We noted before that **3** and **4** were the only two of the non-electron hopping Mössbauer samples which were black. However, their spectra showed that the inner doublet was very much broader than the outer one, as was the case in **5** and the diffuse reflectance of **3** showed an increase in the 400-800 nm region, similar that of the electron hopping **5**. The raises the suggestion that electron hopping is close to occurring in **3** and **4** and furthermore that it is easier to achieve on the M(2) site, which is the less favoured site for Fe occupation. We must remember that the Fe concentration in the octahedra has dropped from 25% in ferric freudenbergite, to 6% in **3** and 3% in **4**, with the Al substitution inhibiting electron movement. Our results also show that mixed valence is easier to achieve for the Ti ions than for the Fe ions, but it is not clear whether the Ti mixed valence states are static or dynamic.

Acknowledgments

We are pleased to acknowledge the support of Monash University for this work. We are grateful to Joel Davis for carrying out the SEM analysis.

References

[1] Ishiguru T, Tanaka K, Marumo F, Ismail M G M U, Hirano S and Somiya S 1978 *Acta Crystallogr*. **B34** 255
[2] Cashion J D, Lashtabeg A, Vance E R and Ryan D H 2013 *Hyperfine Interact.* **226** 579
[3] Vance E R. Angel P J, Cassidy D J, Stewart M W A, Blackford M G and McGlinn P A 1994 *J. Amer. Ceram. Soc.* **77** 1576
[4] Coey J M D 1984 *Mössbauer Spectroscopy Applied to Inorganic Chemistry, Vol. 1* ed G J Long (New York: Plenum) p443
[5] Strens R G J and Wood B J 1979 *Mineral. Mag.* **43** 347
[6] Burns R G 1981 *Ann. Rev. Earth Planet. Sci.* **9** 345
[7] Stähle V, Koch M, McCammon C A, Mann U and Markl G 2002 *Can. Mineral.* **40** 1609

Tribute to CSIRO Scientists

T.R. Finlayson[a]

[a] *School of Physics, University of Melbourne, Victoria 3010, Australia.*

In this invited presentation we pay tribute to the four CSIRO colleagues, Drs. John Dunlop, Tony Farmer, Gerry Haddad and Don Price, who lost their lives in the horrific crash of a Robinson R44 helicopter in March, 2013. The presentation briefly summarises the scientific careers of all four colleagues. Two of these scientists, Dunlop and Price, had been most enthusiastic supporters of and regular contruibutors to this Annual Condensed Matter and Materials Conference, since its inception in 1977, and their respective contributions are also included.

1. Introduction

A couple of months ago, I received a call from Dr. Stephen Collocott, CSIRO, Lindfield, who had been invited by the Organising Committee for this Conference, to prepare and present a tribute to his four colleagues, Drs. Tony Farmer, Gerry Haddad, Don Price and John Dunlop, who lost their lives in the horrific crash of a Robinson R44 helicopter, near Panorama House, Bulli Tops, Wollongong, on 21st March, 2013. While Stephen shared the view of the Organising Committee that it would be most appropriate for such a tribute to be presented at the 2014 "Wagga" Conference, he knew at the time that he could not attend, so before accepting the invitation, he telephoned me to ask if I would present such an invited tribute. As I too felt it was a good idea on the part of the Organising Committee, I agreed and while I cannot claim to have known all four of Stephen's CSIRO colleagues as well as he did, I am grateful to the Organising Committee for the opportunity to make this presentation on Stephen's behalf.

2. Tony Farmer, 1944 - 2013

Anthony John Douglas Farmer was brought up in Adelaide and following a BSc (Hons) from the University of Adelaide, he completed a PhD in physics at that same university in 1970. "Post-doccing" followed, firstly overseas at York University in Toronto, Canada, and then a year at the University of Newcastle, NSW.

Tony Farmer (1944 – 2013)

Farmer started with the CSIRO in 1973 as a Research Scientist with the Division of Applied Physics, then based in the grounds of Sydney University. His research had already been in spectroscopy at very short wavelengths (in the vacuum ultraviolet range) and his initial project with the CSIRO was the development of a new method to make precise measurements of the spectral characteristics of light sources and detectors. He also collaborated with the US National Bureau of Standards on a successful project that eventually improved the accuracy of silicon photodiodes.

From 1981, Farmer was involved in a new research area, thermal plasmas, in keeping with the increased emphasis on industrial physics of what was then the Division of Applied Physics. With Gerry Haddad, he published a series of benchmark papers on temperature measurements of electric arcs. Initially the measurements used spectroscopic techniques, which made use of the light emitted by the arc.

After that, to avoid some of the problems inherent in this approach, Farmer and Haddad were pioneers in the use of laser scattering - a more accurate approach, but one that presented extreme experimental difficulties, as the strength of the scattered signal is minuscule compared to that of the intense arc radiation. It was a tribute to Farmer's skill and persistence that this work was successful.

He led many industrial projects in the arc-physics area in the 1990s, two of which were outstanding successes. One was the development of a process to coat artificial hip joints with hydroxyapatite using plasma spraying, for Portland Square Pty Ltd. The second, in collaboration with the CSIRO's Division of Manufacturing Technology and SRL Plasma, was on the development of the PLASCON waste treatment process to allow destruction of ozone-depleting substances. Twelve PLASCON plants, most of which are still operating, have been constructed around the world. For this work, Farmer was awarded, together with two CSIRO colleagues, the 2008 Alan Walsh Medal for Service to Industry, by the Australian Institute of Physics (AIP). Shortly before his untimely death, he had taken on the position of Editor of the "house journal" of the AIP, *Australian Physics*, but unfortunately only two issues of the journal (Jan-Feb and Mar-Apr, 2013) resulted from this voluntary involvement with the Institute.

Farmer was promoted to Senior Principal Research Scientist (Level 8) in 1998. In 2000, he took on the leadership of the sub-surface radar project. This team made significant advances in the understanding of the interaction of electromagnetic waves and the geophysical environment, and they developed borehole electromagnetic probes for geophysical measurements while drilling, in coal mines. This technology was adapted for environmental applications including measuring moisture, salinity and soil quality. This team also developed SiroPulse, a sub-surface radar system designed for security counter-measures applications, which received wide acceptance within Australia, New Zealand and US government agencies.

In 2005, Farmer became a Theme Leader in CSIRO's Industrial Physics Division, and from 2008 was Deputy Chief of Operations at CSIRO's Materials Science and Engineering Division. He retired in 2010, but continued as an Honorary Fellow, working in the area of high-power ultrasonic processing.

3. Gerry Haddad, 1941 - 2013

Gerry Haddad (1941 – 2013)

Gerald Neil Haddad hailed from Mount Gambier in South Australia but completed his secondary schooling at Adelaide High School after winning a bursary to attend that institution. There followed a BSc (Hons) and a PhD in the Physical Sciences from the University of Adelaide in 1968. He then worked at the University of Adelaide, Culham Laboratory in the UK, the University of Nebraska and the University of Oklahoma and he returned to Australia as a Research Fellow at the Australian National University.

His CSIRO career began in 1982 when he was recruited as a Senior Research Scientist with the Division of Applied Physics at Lindfield. He was an outstanding experimentalist, with a real talent for the engineering and technical development of new systems. Less than a year after starting at the CSIRO, his group leader described him as being "the best experimentalist I have ever worked with." Haddad led a number of projects in the gas-discharge field, ranging from fundamental studies of the interactions of electrons with molecules, through spectroscopic measurements of welding arcs to the design of high-power

arc plasma reactors for mineral processing for Australian companies, including a facility for the dissociation of zircon sands to produce zirconia for ICI.

The success of his work contributed strongly to the rapid development of the CSIRO plasma group's international reputation. The landmark papers of Haddad and Tony Farmer on the temperature measurements of electric arcs, which are cited in leading textbooks on arc welding, showed that the approximate properties of welding arcs can be predicted theoretically assuming "local thermal equilibrium." This made the development of sophisticated computer codes for the prediction of weld properties possible for almost any industrial configuration, and these have been adopted worldwide by companies and universities. Haddad earned rapid promotion as a scientist, reaching Senior Principal Research Scientist (Level 8) in 1989.

In 1988, Haddad decided to pursue a career in research management and took a position as Program Manager in plasmas, thin films and thermometry in the Division of Applied Physics. Nevertheless, for many years he remained strongly involved in the research and development of the plasma group, often taking the opportunity to "get his hands dirty" in the lab. The plasma researchers who followed, remained indebted to him for the experimental facilities he had developed.

Haddad's success as a research manager and leader echoed that of his research career. Following the formation of CSIRO Telecommunications and Industrial Physics, he was appointed as a Portfolio Manager in 1996, Deputy Chief in 1999 and Chief in 2003. He was also Chief of CSIRO Industrial Physics from its formation in 2004 until he retired in 2007. After retiring he took a position at Standards Australia and was there until his second retirement in 2012.

4. Don Price, 1945 - 2013

Donald Carruthers Price was born in Dumfries, Scotland, where his parents had been taking part in the British war effort. After the war, the family returned to Australia and settled in Melbourne. Don's first degree was at the "new" (at least then) Monash University and this was followed by a PhD in which he applied Mössbauer spectroscopy to the measurement of hyperfine field distributions at the ^{119}Sn nuclei in ferromagnetic, transition-metal alloys, under the supervision of the late Professor Bob Street. There followed a series of post-doctoral fellowships at the University of Manitoba, Canada, the University of Liverpool, UK, the Research School of Physical Sciences at the Australian National University and the Royal Military College, Duntroon, where his prime research interest was again focussed on the Mössbauer effect. He then worked on the detection of breast cancer using ultrasound at the Queensland Institute of Technology.

Don Price (1945 – 2013)

It was in the field of ultrasonics that in 1982, he was appointed to the CSIRO, Division of Applied Physics in Lindfield, as a Research Scientist, and where he expanded his research to include both measurement techniques and materials properties. He went on to become Discipline Leader (equivalent to a Research Group Leader) for Acoustics and Ultrasonics, and held leadership positions, including as a member of Divisional Management teams. He was promoted to Senior Principal Research Scientist in 1993.

Price's work on modelling the behaviour of ultrasonic waves in composite materials led to the development of instrumentation for the non-destructive testing of aerospace structures. Modern aeroplanes are no longer just made of metal riveted together, but rather materials such as carbon fibres glued together, and Price worked out how to test the joins ultrasonically

without destroying them. He performed outstanding research in this area in collaboration with Boeing for many years.

He was instrumental in the development of a collaboration with NASA that resulted in the Ageless Aerospace Vehicle (AAV) project, for which he was project leader. The project focused on intelligent active sensing systems for structural health management in aerospace vehicles, though the principles had much broader applicability.

Price also led the tube eccentricity measurement project, which developed an online system to measure the wall thickness and eccentricity of extruded copper tube using high-frequency ultrasound. The system was installed in the production line at Metal Manufactures Ltd., Port Kembla Tube and Fittings Mill, where it is used to sort tubes for subsequent processing, and continues to provide valuable results.

Beyond science, Price contributed greatly to the Division. As a member of the management teams of CSIRO Telecommunication and Industrial Physics, he was instrumental in setting research directions and increasing the awareness of the Division's science achievements in the broader community. He played a major role in internal Divisional review processes, and in managing the Division's contribution to external reviews of its science. He was responsible for coordinating and leading the work of various research teams, and managed and developed valuable external collaborations. He was also a great mentor to students, regularly hosting students from both Australia and overseas. He was very active in the Australian physics community, being a regular attendee at AIP events. In addition, for a number of the issues of *Australian Physics*, prior to Don's untimely death, he had been preparing a column for the journal, reporting on topical issues of physics research and development, internationally, that had "caught his eye" in the literature.

Don was conscientious and generous, frequently making sacrifices for the benefit of his colleagues. He was quietly spoken, with a wry sense of humour. He was never comfortable with self-promotion, preferring the quality of his work to speak for itself. Following his retirement in 2009, Price continued with the Division at Lindfield as an Honorary Fellow.

My personal friendship with Don Price began in his early years as a PhD student at Monash University where he was also an active sportsman, and particularly excelled at baseball. In his later years he took to long-distance running and could boast a best time for the marathon of 2 hrs 36 mins. He has been an active contributor to this conference throughout its history and from the records, I have counted a total of 21 "Wagga" papers which he authored or co-authored and 17 attendances at "Wagga" conferences.

5. John Dunlop, 1946 - 2013

John Burton Dunlop's life began in Wigan, England and following an English Grammar School education, he graduated with a Bachelor of Science with Honours and a PhD in Physics in 1972, from Imperial College, London. His research was concerned with the magnetic properties of hard magnetic materials. John had research fellowships at the University of Sheffield in England and at the University of Genoa, Italy, prior to joining the CSIRO in 1976 as a Research Scientist with the National Measurement Laboratory, then in the grounds of Sydney University. Subsequent changes within CSIRO meant that he worked in CSIRO Applied Physics, CSIRO Telecommunications and Industrial Physics and, later, CSIRO Materials Science and Engineering. He was promoted to Principal Research Scientist (Level 7) in 1987 and retired in 2008.

John Dunlop (1946 – 2013)

In his early years at the CSIRO, Dunlop's research focused on the magnetic properties of transition metal alloys and glassy metals. With the latter he developed techniques for their fabrication, which involved rapid solidification from the molten phase. However, the greater part of Dunlop's career was devoted to the study of the rare-earth permanent magnets and their application in devices, in particular, electrical nachines. He was part of the team that developed a pilot plant for the production of the rare-earth magnet neodymium-iron-boron. This was as an extremely successful project, and resulted in the formation of a spin-out company, Australian Magnet Technology.

John was always keen to see his science translated into real-world applications, and this was achieved many times with projects conducted through the Sydney Electrical Machines, Controls and Applied Magnetics (or SEMCAM) consortium and with industrial partners that included, for example, General Motors Holden and Electrolux. These more commercial activities were balanced by a fundamental interest in the magnetism of rare-earth metals, and related alloys, and Dunlop and his fellow team members were credited with the discovery of the so-called ''Fifth Family of Permanent Magnets'', the 3:29 alloys. He also contributed to the development of novel methods for producing titanium-based alloys.

However, he was not comfortable seeking rewards for himself, he preferred instead to perform useful work for his colleagues and collaborators and for Australian companies. He was highly respected for his deep scientific knowledge, his cheerful willingness to assist and provide practical advice to other researchers, and his friendly and generous nature.

Dunlop was also very active in the Australian solid-state physics community. His efforts, with close colleagues, saw the establishment, in 1977, of the Australian Institute of Physics Solid State Physics Meeting which, on account of its residential location in Wagga Wagga, NSW, became known simply as "Wagga." A later name change to ANZIP Solid State Physics Meeting evolved from the participation in and hosting of this annual conference by New Zealand groups and later still, further name changes to "Condensed Matter Physics" and "Condensed Matter and Materials" reflected changes in fashion of the day. But it remains the "Wagga Meeting" and the records show that of the 37 "Wagga" conferences up to and including "Wagga 2013", John Dunlop had attended 29 of them and had authored or co-authored 33 "Wagga" papers.

(L→R): Stephen Collocott, John Dunlop, Charles Johnson and Don Price, at "Wagga 2012."

6. Conclusion

In conclusion, may I say that at a personal level I must pay tribute to both John Dunlop and Don Price for their active involvement in what has become an aspect of "Wagga" conferences, the Trivia Night. John, in particular, was a master at setting Trivia Quiz questions and recently both John and Don served as Trivia judges on the night itself. They will be sadly missed from this year's quiz night.

May I invite you all to stand and observe a minute's silence, to enable those of you who knew any of Tony Farmer, Gerry Haddad, Don Price or

(L→R): John Dunlop, Don Price and Trevor Finlayson running the Trivia Night at "Wagga 2013."

John Dunlop, to reflect on your own personal experiences in interacting with them professionally and/or socially.

Acknowledgments

The assistance, particularly of Dr. Stephen Collocott, and also that of Dr. Tony Murphy, both of CSIRO, Lindfield, in providing most of the information concerning their colleagues, presented in this invited tribute is gratefully acknowledged.

Exploring the Structural and Magnetic Phase Transition of $Cu_{1-x}Co_xSb_2O_6$

H.-B. Kang[a] C.D. Ling[b] and T. Söhnel[a]

[a] *School of Chemical Sciences, University of Auckland, Auckland, New Zealand.*
[b] *School of Chemistry, University of Sydney, Sydney, Australia.*

The system $Cu_{1-x}Co_xSb_2O_6$ has been investigated using sealed-tube and synchrotron X-ray powder diffraction, neutron powder diffraction and single crystal neutron diffraction. An orthorhombic phase is proposed between the previously established tetragonal and monoclinic phases for $x < 1$. In addition, evidence is presented for a possible ferroelastic phase transition in $Cu_{0.3}Co_{0.7}Sb_2O_6$ single crystals at low temperatures. Magnetic susceptibility measurements confirm antiferromagnetic ordering across the complete solid solution series.

1. Introduction

$CuSb_2O_6$ has been the most intensively studied compound in the ternary Cu-Sb-O system since the high transition temperature (T_c) superconducting materials based on copper oxides were found by Bednorz and Müller in 1986 [1]. It is reported to undergo a second-order phase transition from a tetragonal to a monoclinic distorted trirutile structure between 100 and 130 °C [2]. The transition is thought to be driven by a Jahn-Teller distortion on Cu^{2+} (a d^9 ion, stabilising square-planar geometry). This square lattice cupric oxide layer is similar to that found in the two-dimensional Heisenberg antiferromagnet (HAF) La_2CuO_4, [3, 4]; however, the magnetic behaviour of $CuSb_2O_6$ is considered to be an S=½ one-dimensional Heisenberg antiferromagnet with strong anisotropy above 20 K [2]. The difference between these two compounds can be understood by applying and combining the total energy and tight-binding model calculation results [5]. A sudden decrease in magnetic susceptibility at 8.6 K indicates antiferromagnetic long-range ordering due to inter-chain interactions [2], and has recently been revealed as a crossover behavior from S = ½ one-dimensional HAF to a three-dimensional HAF [8]. $CuSb_2O_6$ also exhibits a spin-flop transition at 2.2 T and 5 K, leading to greatly enhanced magnetic moments [6].

$CoSb_2O_6$ also crystallizes in the tetragonal trirutile structure (Fig. 1) and exhibits two-dimensional HAF behaviour with a broad transition at about 35 K [7]. The magnetic structure of $CoSb_2O_6$ has only been refined against neutron powder diffraction (NPD) data. Two alternative models for antiferromagnetic ordering have been proposed, which are indistinguishable by NPD [7].

This study concerns the doping of divalent Co onto the A site of $CuSb_2O_6$, which is of interest for two reasons. Firstly, a direct second-order phase transition from a tetragonal to a monoclinic trirutile ought not to be possible. A systematic reduction in symmetry, as shown in Bärnighausen trees, would require the existence of an orthorhombic

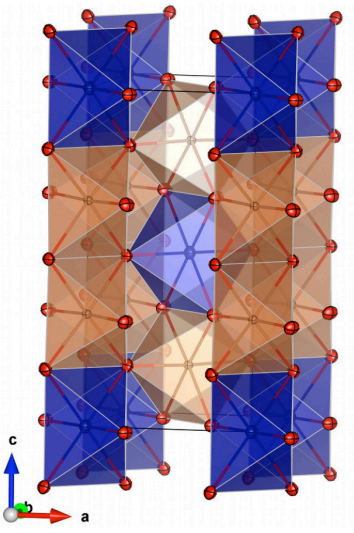

Fig. 1. The structure of $CoSb_2O_6$ as refined against single crystal neutron Laue diffraction data (Co: blue, Sb: brown, O: red).

intermediate phase. Secondly, this doping changes the magnetic behaviour from a S=½ one-dimensional Heisenberg antiferromagnet to a two-dimensional Heisenberg antiferromagnet. The main aim of this study is thus to investigate the structural and magnetic behaviour of the solid solutions $(Cu_{1-x}Co_x)Sb_2O_6$ in combination with very detailed investigations of the phase transition of $CuSb_2O_6$.

2. Sample preparation

Stoichiometric mixtures of CuO, Co_3O_4 and Sb_2O_3 powders were placed in corundum crucibles and heated to 960 °C for 36-48 hours in a muffle furnace prior to quenching in air yielding in phase pure powders. Powder samples were initially characterized by X-ray powder diffraction (XRD) using a sealed-tube source (Panalytical Empyrean, monochromated Cu K_α radiation, 10 - 80° 2θ range). Synchrotron X-ray powder diffraction (SXRD) data were subsequently collected on the Powder Diffraction beamline (10-BM) at the Australian Synchrotron over a 6 to 86° 2θ range with a step size of 0.00375° 2θ, using the MYTHEN detector and the double crystal monochromator of Si(111) flat crystal pair (λ = 0.774235 Å, calibrated with LaB_6). Single crystal neutron Laue diffraction data were collected on the instrument Koala at the OPAL research reactor, Lucas Heights, Australia. Complete single crystal data sets were collected at 100 K, 25 K and 5 K (well above, close to, and below the magnetic ordering temperature respectively) for each crystal, comprised of 0.5 h measurements taken at 15 different orientations. Magnetic susceptibility data from room temperature to 2 K were collected on a Quantum Design Physical Properties Measurement System (PPMS) in zero-field-cooled mode using a 1 T magnetic field.

3. Results

3.1 X-ray Powder Diffraction Analysis

Sealed-tube XRD data were collected from samples prepared at 960 °C and quenched in water. Preparations using slower cooling rates from high temperatures down to room temperature could not preserve the 960 °C structure, the sample composition was identical in all cases independent of cooling rate. At room temperature, a wide two-phase region was observed from x = 0.2–0.5, involving a Cu-rich monoclinic phase and a Co-rich tetragonal phase. For the monoclinic Cu-rich component, all the lattice constants increase from x = 0–0.15 (Fig. 2). Between 0.2 and 0.5, the lattice constants *a* and *b* are relatively constant, while *c* decreases slightly. The tetragonal phase could be Rietveld-refined starting from x = 0.2, with the lattice constant *a* increasing and *c* decreasing from x = 0.2–1. Despite the observed doping trend and two-phase region, it was not possible to fully interpret the phase behaviour of the system based on these XRD data, due to difficulties in refining two phases distinguished only by a small monoclinic distortion (~1 °).

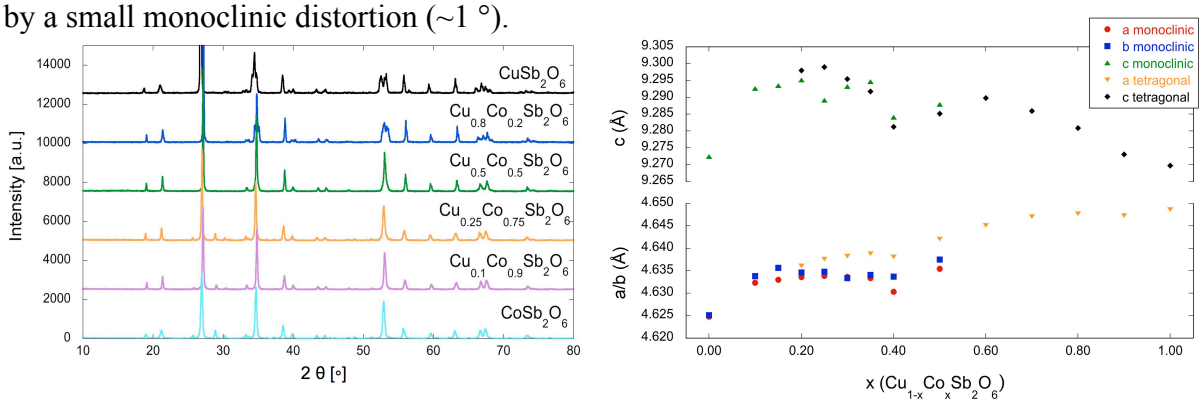

Fig. 2. Lab X-ray powder diffraction patterns of $Cu_{1-x}Co_xSb_2O_6$ solid solutions (left) and lattice constants distribution of $Cu_{1-x}Co_xSb_2O_6$ solid solutions (right).

3.2 High Resolution Synchrotron Powder Diffraction Analysis

SXRD data were used to analyse the two-phase region in more detail. These data confirmed the existence of a two-phase region at room temperature. At 200 °C, we had expected to observe a complete solid-solution in the tetragonal phase, as the tetrgonal-monoclinic phase transition of $CuSb_2O_6$ is observed around 100 °C to 130 °C; however, the SXRD data indicate that this is not the case (Fig. 3). An orthorhombic phase is clearly identifiable on the Cu-rich side, including undoped $CuSb_2O_6$. The proposed space group is *Pnnm*, which is the only possible space group according to Bärnighausen trees. A second order transition from the tetragonal modification ($P4_2/mnm$) to the monoclinic modification ($P2_1/n$) can be related via *translationsgleiche* group-subgroup relations but only *via* an orthorhombic modification (*Pnnm*):

$$P4_2/mnm \xrightarrow{\text{-t2}} Pnnm \xrightarrow{\text{-t2}} P2_1/n$$

The structural distortion in *Pnnm* is very subtle, even using synchrotron radiation. Nevertheless, the diffraction peaks clearly show different behaviours on the Cu-rich and the Co-rich sides of the solid solution, indicating the presence of two different structural modifications (Fig. 3). No additional peaks were observed that could indicate a superstructure ordering of Cu and Co. The orthorhombic phase was observed at 200 °C for the entire $Cu_{1-x}Co_xSb_2O_6$ solid solution except $CoSb_2O_6$.

Even at 500 °C, we still observe different symmetries on the Cu-rich and Co-rich ends of the solid solution. The phase transition from tetragonal to lower symmetry can be observed for compositions of x = 0–0.3 (Fig. 3). All these transitions were fully reversible.

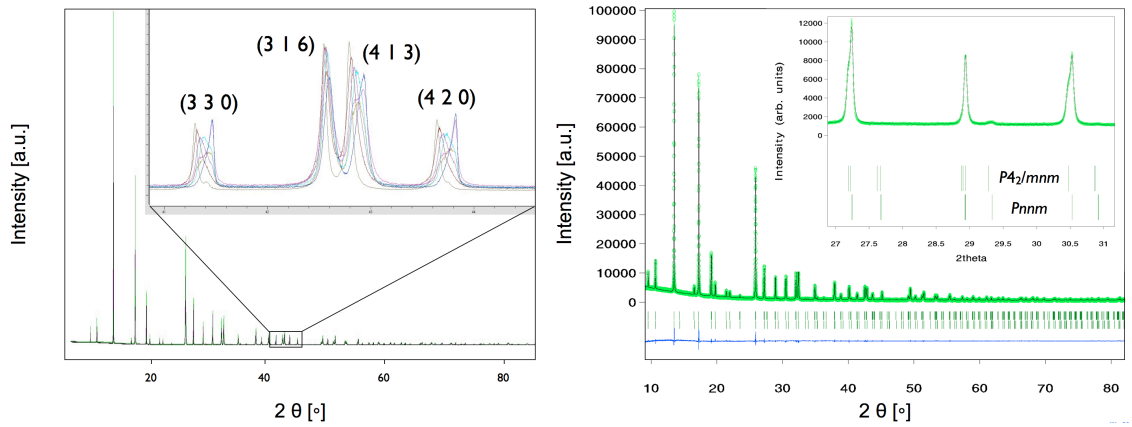

Fig. 3. SXRD patterns of $Cu_{1-x}Co_xSb_2O_6$ solid solutions at 200 °C (left) and Rietveld refinement of synchrotron powder diffraction data of $Cu_{0.3}Co_{0.7}Sb_2O_6$ at 500 °C (right).

3.3 Single Crystal Neutron Laue Diffraction

Single crystal Laue diffraction data were collected for $CuSb_2O_6$, $Cu_{0.3}Co_{0.7}Sb_2O_6$ and $CoSb_2O_6$ single crystals. The trirutile structure of $CoSb_2O_6$, which could be refined against these data, is shown in Fig. 1. All $CuSb_2O_6$ crystals were twinned and could not refined successfully. For $Cu_{0.3}Co_{0.7}Sb_2O_6$, after the initial appearance of diffuse scattering below room temperature, a peak splitting could be observed on decreasing the temperature from to 100 K and then 5 K (Fig. 4). This peak splitting was reversible on increasing the temperature, which suggests a ferroelastic phase transition.

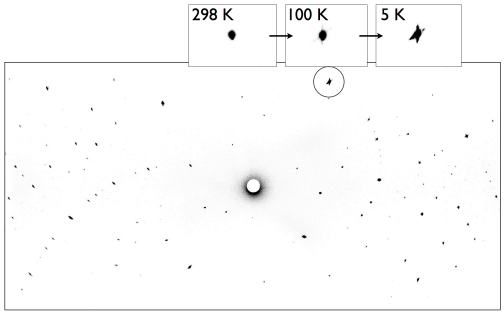

Fig. 4. Single-crystal neutron Laue diffraction pattern of $Cu_{0.3}Co_{0.7}Sb_2O_6$

3.4 Magnetic Measurements

The magnetic susceptibilty behaviour of $Cu_{1-x}Co_xSb_2O_6$ from x = 0.3 and 0.7 is similar to that of $CoSb_2O_6$ (Fig. 5), confirming antiferromagnetic ordering across the entire solid solution. The transition is broad, as reported for the pure Co sample (x = 1) [7]. The composition at x = 0.1 shows behaviour more akin to that of the pure Cu sample (x = 0). The change in Néel temperatures is small for x = 0–0.7 (13 K difference) but a significant jump is observed to x = 1 $CoSb_2O_6$ (13 K difference, Fig. 5 inset). It appears that all these compounds except the Cu-rich samples are likely to exhibit 2D HAF behavior, with magnetic susceptibility decreasing in accordance with the reduced moment of Cu(II) compared to Co(II).

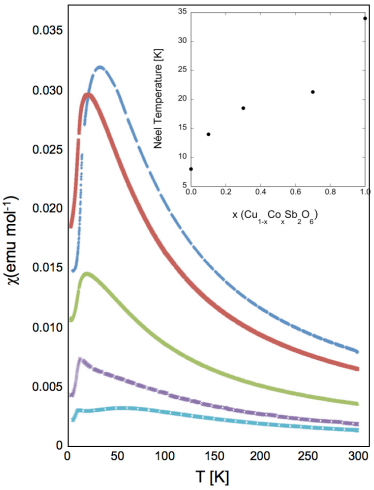

Fig. 5. Magnetic susceptibility data (x = 0, 0.1, 0.3, 0.7 and 1, from the bottom to top) and Néel temperatures for $Cu_{1-x}Co_xSb_2O_6$.

Acknowledgments

The authors thank Dr Justin Kimpton at the Australian Synchrotron and Drs Ross Piltz and Maxim Avdeev at the Australian Nuclear Science and Technology Organisation (ANSTO) for their advice and assistance in the collection of diffraction data. They also thank the Australian Institute of Nuclear Science and Engineering (AINSE), The University of Auckland and The University of Sydney for funding.

References

[1] Bednorz J G and Müller K A 1986 *Z. Phys.* **B64** 189

[2] Prokofiev A V, Ritter F, Assmus W, Gibson B J and Kremer R K 2003 *J. Cryst. Growth* **247** 457

[3] Nakua A, Yun H, Reimers J N, Greedan J E and Stager C V 1991 *J Solid State Chem.* **91**, 105

[4] Sandvik A W and Scalapino D J 1995 *Phys. Rev. B.* **51** 9403

[5] Kasinathan D, Koepernik K and Rosner H 2008 *Phys. Rev. Lett.* **100** 237202

[6] Nakua A M and Greedan J E 1995 *J. Solid State Chem.* **118** 199

[7] Reimers J N, Greedan J E, Stager C V, Kremer R 1989 *J. Solid State Chem*. **83** 20

[8] Rebello A, Smith M G, Neumeier J J, White B D and Yu Y-K. 2013, *Phys. Rev. B* **87** 224427.

Identifying Further Inelastic Neutron Crystal Field Transitions in $ErNiAl_4$

G.A. Stewart[a], W.D. Hutchison[a], Zahra Yamani[b], J.M. Cadogan[a] and D.H. Ryan[c]

[a] *School of Physical, Environmental and Mathematical Sciences, UNSW Canberra, Australian Defence Force Academy, PO Box 7916, ACT, BC 2610, Australia.*
[b] *Canadian Neutron Beam Centre, National Research Council, Chalk River, Ontario, ON K0J 1J0, Canada.*
[c] *Physics Department, McGill University, Montreal, Quebec, H3A 2T8, Canada.*

Interim results are presented for a thermal INS project seeking to identify further crystal field transitions for the J = 15/2 ground state of Er^{3+} in $ErNiAl_4$. Previously reported transitions at 3, 7.4 and 11.3 meV are confirmed and a possible two further transitions have been located at 14.4 and 18.2 meV.

1. Introduction

The orthorhombic, intermetallic series $RNiAl_4$ (R = rare earth) exhibits interesting magnetic behaviour [1-2], including the potential for low temperature, inverse, magnetic cooling [3]. Given that the $RNiAl_4$ magnetism is associated solely with the R sub-lattice and is influenced strongly by the local crystal field (CF) interaction at the R-site, it is important that the CF interaction is characterised. Thermal neutrons are used here to extend a previous cold neutron inelastic neutron scattering (INS) investigation [4] of the crystal field (CF) transitions at the single Er^{3+} site in $ErNiAl_4$.

2. Experimental details

Substantial amounts of $ErNiAl_4$ (34.8 g) and $YNiAl_4$ (26 g) were prepared as a set of smaller 1-2 g lots via repeated argon arc melting followed by vacuum annealing for 5-6 d at 1050 °C. X-ray powder diffraction was used to identify the acceptable single-phase lots. All neutron scattering measurements were performed on the C5 polarised triple-axis spectrometer at CNBC in Chalk River, Canada. The INS spectra were accumulated with a final scattering energy of $E_f = 14$ meV.

3. Results

Neutron scattering measurements were performed using both the elastic and inelastic modes of operation for the C5 spectrometer.

3.1 Elastic neutron scattering

Neutron diffraction patterns ($\lambda = 2.37051$ Å) were recorded for $ErNiAl_4$ at 290 K and 3.9 K (Fig. 1). Rietveld analysis of the 3.9 K pattern (well below $T_N = 5.8$ K) using *FullProf* software [5] yielded an incommensurate sinusoidal structure with a propagation vector of [0.191 1.0 0.038] and a local moment amplitude of $\mu(Er^{3+}) = 7.0\ \mu_B$ aligned with the c-axis (Fig. 2). The propagation vector is similar to that reported earlier [6] although the moment is about 16% smaller (cf 8.3 μ_B). Recent ^{166}Er-Mössbauer results [7] rule out a spread in the local Er moment so that a square wave modulation is more appropriate. However, in subsequent reconsideration of the Rietveld analysis, it has proved difficult to identify the weak higher harmonics.

In order to confirm the magnetic origin of the reflection at $Q = 2.3134$ Å^{-1} ($2\theta \approx 51.75°$) its intensity was monitored as a function of temperature using polarised neutrons ($\underline{p}$ // $\underline{Q}$) with both spin flip (SF) and non spin flip (NSF) detection. From Fig. 3, it is evident that the net

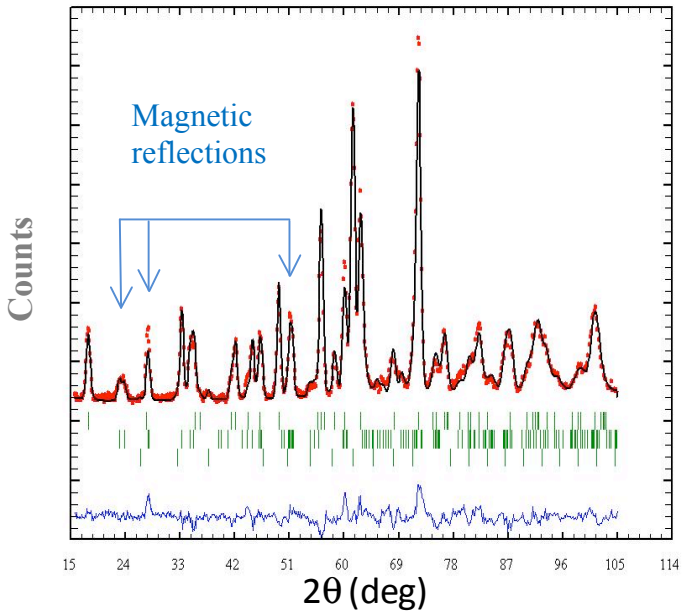

Fig. 1. Neutron diffraction pattern of $ErNiAl_4$ recorded at 3.9 K (λ = 2.37051 Å). The three rows of Bragg position markers are (top) nuclear, (middle) incommensurate magnetic, and (bottom) small component of Er_2O_3 impurity.

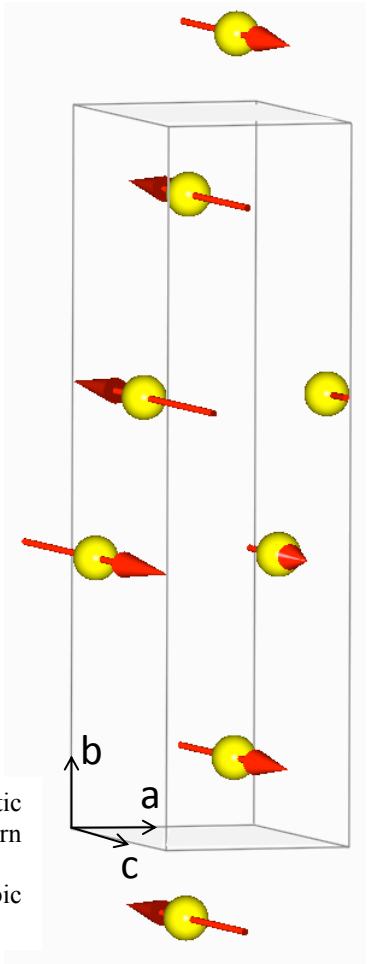

Fig. 2. Incommensurate sinusoidal magnetic structure fitted to the neutron diffraction pattern for $ErNiAl_4$ at 3.9 K. For simplicity, the Ni and Al atoms are ignored and just one orthorhombic crystallographic cell is shown.

magnetic intensity (SF - normalised NSF) drops to zero above the ordering temperature. The maximum of the differentiated net signal (upper inset in Fig. 3) yields an ordering temperature of 6.5 K, in close agreement with the bulk specific heat value of T_N = 5.8 K [6].

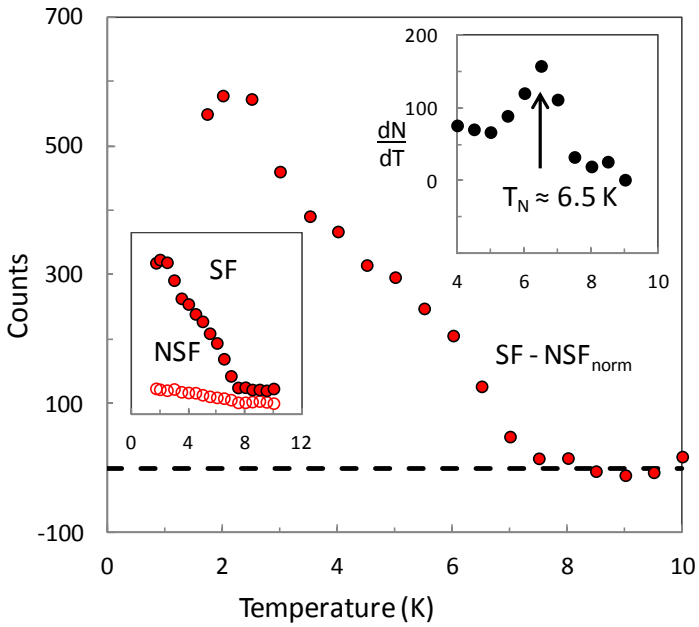

Fig. 3. Temperature dependent intensity of the $ErNiAl_4$ magnetic reflection at 2θ = 51.75° (λ = 2.37051 Å):
SF = spin flip, NSF = non spin flip, and NSF_{norm} indicates $\overline{NSF}$ normalised to $\overline{SF}$ in the temperature range 7.5 < T < 10 K.

3.1 Inelastic neutron scattering

Unpolarised INS spectra were recorded for $ErNiAl_4$ at 10 K with four different scattering vectors, Q, over the energy ranges of 0 - 25 meV (Q = 1.2 $Å^{-1}$), 0 - 41 meV (Q = 2.7 $Å^{-1}$), 0 - 50 meV (Q = 3.0 $Å^{-1}$), and 20 - 50 meV (Q = 5.2 $Å^{-1}$). As shown in Fig. 4, strong transitions were observed at 3.08(2), 7.53(2) and 11.6(1) meV. These energies are in excellent agreement with those observed previously using cold neutrons [4] and the evident Q-independence confirms that they are associated with "magnetic" CF transitions.

However, the objective of these new measurements was to identify additional CF transitions at higher energies. From Fig. 5 the INS spectra in the range of 15 - 50 meV are seen to be of relatively low intensity with broader features that are believed to be associated with phonon transitions. Because of this, additional INS spectra were recorded for non-magnetic $YNiAl_4$ whose Y^{3+} ion's ground S-state is not subjected to a CF interaction.

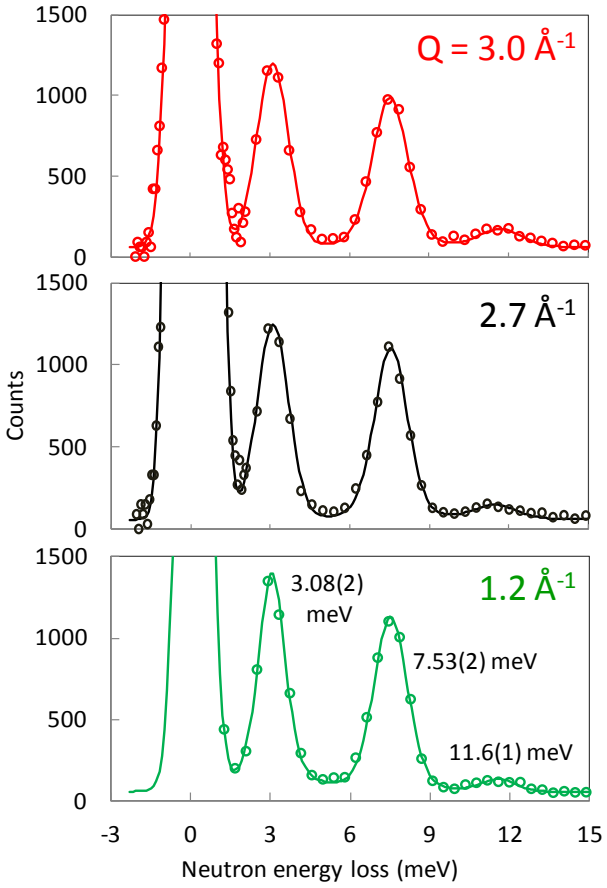

Fig. 4. The 0 < E < 15 meV region of the INS spectra recorded for $ErNiAl_4$ at 10 K with scattering vectors of Q = 1.2, 2.7 and 3.0 $Å^{-1}$. The solid lines are fitted Pseudo-Lorentzian peaks superimposed on a linear background.

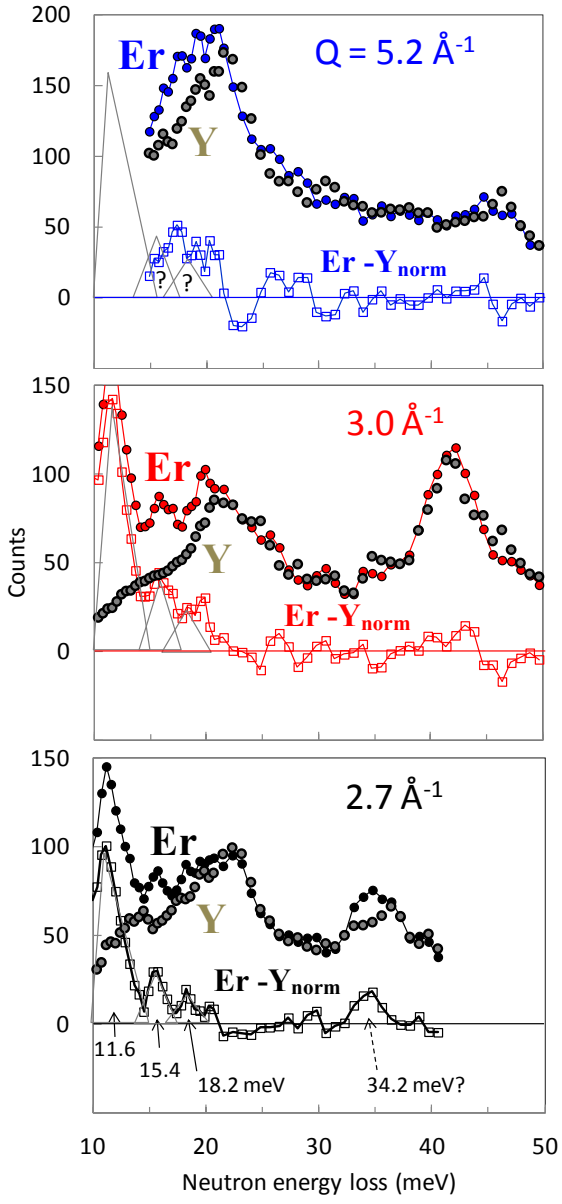

Fig. 5. The 10 < E < 50 meV region of INS spectra recorded at 10 K with scattering vectors of Q = 2.7, 3.0 and 5.2 $Å^{-1}$. The data for $ErNiAl_4$, the scaled up data for $YNiAl_4$, and their subtraction are indicated by the labels "Er", "Y" and "Er - Y", respectively. The scaling of the $YNiAl_4$ spectra employed a multiplying factor of the form A + B*E (where E is the neutron energy loss) and the spectra were smoothed prior to their subtraction.

The approach taken was to scale up the intensities of the$YNiAl_4$ spectra so that their broad features matched as closely as possible those of their $ErNiAl_4$ counterparts. To this end, it was found useful to employ a scaling factor that increased linearly across the spectra. The scaled $YNiAl_4$ spectra were then subtracted from the $ErNiAl_4$ spectra in an effort to identify the true CF transitions for $ErNiAl_4$. Based on this approach, possible additional CF transitions are located at 14.4 and 18.2 meV as indicated by the superimposed triangular peaks in Fig. 5. A further candidate is observed at 34.2 meV with Q = 2.7 $Å^{-1}$ but it is no longer evident for Q = 3.0 and 5.2 $Å^{-1}$.

Conclusions and on-going work

Valuable information has been gained regarding the incommensurate magnetic phase of $ErNiAl_4$ below T_N = 5.8 K and likely additional CF transitions have been located at 14.4 and 18.2 meV. It is hoped that further polarised neutron beam INS measurements currently being conducted on the C5 spectrometer at Chalk River will ultimately separate the remaining weak CF transitions out from the broad phonon signals via the comparison of SF and NSF spectra.

Acknowledgments

The CNBC is gratefully acknowledged for time allocated on the C5 spectrometer and Vernon Edge is thanked for his valuable assistance with the specimen preparation.

References

[1] Stewart G A, Hutchison W D, Edge A V J, Rupprecht K, Wortmann G, Nishimura K and Isikawa Y 2005 *J. Magn. Magn. Mater.* **292** 72.
[2] Hutchison W D, Goossens D J, Whitfield R E, Studer A J, Nishimura K and Mizushima T 2012 *Phys. Rev. B* **86** 014412/1-5.
[3] Li L, Nishimura K and Hutchison W D 2009 *Solid State Commun.* **149** 932.
[4] Saensunon B, Stewart G A, Gubbens P C M, Hutchison W D and Buchsteiner A 2009 *J. Phys.: Condens. Matter* **21** 124215; Corrigendum 2010 *J. Phys.: Cond. Matter* **22** 029801.
[5] Rodriguez-Carvajal J 1993 *Physica B* **192** 55.
[6] Hutchison W D, Goossens D J, Saensunon B, Stewart G A, Avdeev M and Nishimura K 2007 *Proceedings of the 31st Annual Condensed Matter and Materials Meeting, 6-9 Feb., Wagga Wagga*.
[7] Ryan D H**,** Lee-Hone N and Stewart G A 2013 *Solid State Phenom.* **194** 84.

Structural Investigation of Tungsten Bronze Type Compounds in the Relaxor Ferroelectric $Sr_3Ti_{1-y}Zr_yNb_4O_{15}$ System

T. A. Whittle[a] and S. Schmid[a]

[a] *School of Chemistry, The University of Sydney, NSW 2006, Australia.*

Compounds in the $Sr_3Ti_{1-y}Zr_yNb_4O_{15}$ system were investigated by synchrotron X-ray powder diffraction. New structural models are proposed for all compositions across the series. These models include a doubled unit cell and orthorhombic symmetry. A solid solution was found to persist across the composition range from y = 0 - 1. Variable temperature studies reveal phase transitions from orthorhombic to tetragonal symmetry on heating.

1. Introduction

Compounds of the general formula $A1A2_2B1B2_4O_{15}$ have been shown to form with a tungsten bronze type structure. The tungsten bronze structure consists of a network of corner sharing BO_6 octahedra with *A* cations located in interstitial sites. The *A1* site is a 12-coordinate site and the *A2* site is a larger 15-coordinate site. Combined with a smaller, unnocupied, 9-coordinate *C* site, these *A* and *C* sites form channels through the structure running along the c-direction. The compositional and structural flexibility of tungsten bronzes allows for a variety of *A* and *B* site cations as well as cation mixing in these sites. *A* site cations tend to be large alkali, alkaline earth or Pb^{2+} cations. The *B* sites are occupied by smaller transition metal cations such as Ti^{4+}, Zr^{4+}, Ta^{5+} and Nb^{5+}. Tungsten bronze type compounds have been shown to display technologically important properties, finding use in volatile memory, actuators, infrared radiation detection as well as in optical applications amongst others [1-4].

$Sr_3TiNb_4O_{15}$ and $Sr_3ZrNb_4O_{15}$ are compounds which form with tungsten bronze type structures. Both have been described in the literature. While a variety of different models have been reported for $Sr_3TiNb_4O_{15}$ [5-7], $Sr_3ZrNb_4O_{15}$ has only one mention in the literature [8] and no detailed structural analysis has been performed on it.

This report is on the the results of synchrotron X-ray powder diffraction investigations of the $Sr_3Ti_{1-y}Zr_yNb_4O_{15}$ system from, y = 0 - 1, at both room temperature and high temperatures.

2. Sample preparation

Polycrystalline powder samples were prepared using standard solid state synthesis techniques. Reagent oxides and carbonates: $SrCO_3$ (Sigma Aldrich, 99.9 %), TiO_2 (Aithaca, 99.999 %), ZrO_2 (Aithaca, 99.99 %) and Nb_2O_5 (Aithaca, 99.999 %) were weighed out in stoichiometric ratios with x values of: x = 0.0, 0.2, 0.4, 0.6, 0.8 and 1.0. Samples were ground either by hand using an agate mortar and pestle or by an agate ball mill. These samples were then pressed into dense pellets or rods using a pellet press at 8 tonnes for pellets or hydrostatic press at between 50-60 MPa for rods. The samples were calcined at 950 ºC for 36 h and then sintered with intermittent grinding at 1300 ºC for periods between 24 h to 96 h.

Synchrotron X-ray powder diffraction data were collected on the powder diffraction beamline, 10-BM, at the Australian synchrotron using the MYTHEN microstrip detector and a Si(111) monochromator that accepts the beam directly from a bending magnet source.

3. Results

3.1 Room Temperature

For $Sr_3TiNb_4O_{15}$ three models are reported in the literature with slight variations between them. The first proposed model for $Sr_3TiNb_4O_{15}$ was that it formed with a tetragonal tungsten bronze structure, with space group *P*4*bm* [5]. The second model in the literature was for a C-centred othrhombic structure with space group *Cmm*2 [6]. The final model proposed before this work was for a primitive orthorhombic structure with space group *Pba*2 [7]. All these models were refined against our synchrotron X-ray diffraction data and the *Pba*2 model gave by far the best fit to the data. However, the data provided evidence that there was an unreported doubling of the unit cell in the c-direction. Additionally, we found that a better fit to the data could be achieved with space group $Pna2_1$ [9]. The refinement profile for the $Sr_3TiNb_4O_{15}$ model against the data can be seen in Fig. 1.

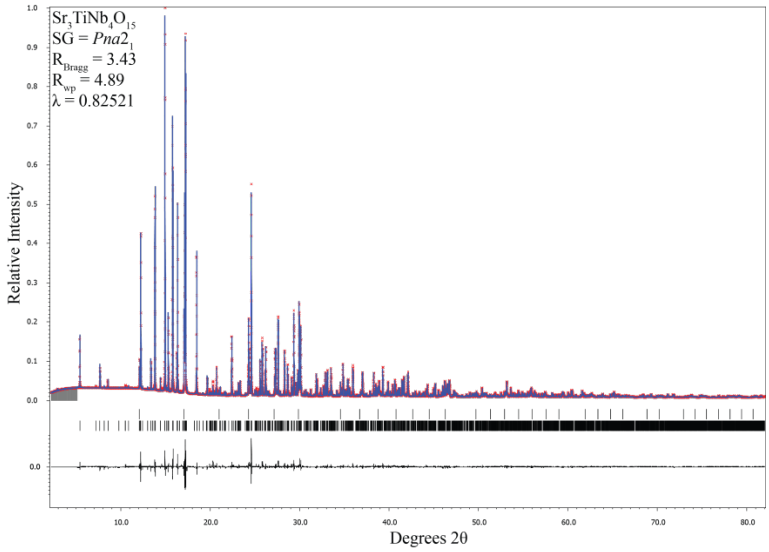

Fig. 1. Refinement profile for $Sr_3TiNb_4O_{15}$. Red crosses are observed data, blue lines are the calculated pattern and the black line is the difference between them. The grey region is excluded from the refinement.

As for the titanium analogue, $Sr_3ZrNb_4O_{15}$ was reported to form with a tetragonal structure [8]. Refinements against synchrotron X-ray diffraction data indicate that it is isostructural to $Sr_3TiNb_4O_{15}$. All diffraction patterns reveal peak splitting which is evidence of the orthorhombic symmetry. Reflections of the type hk1 are present in all patterns indicating a doubling of the unit cell along the c-direction (see Fig 2).

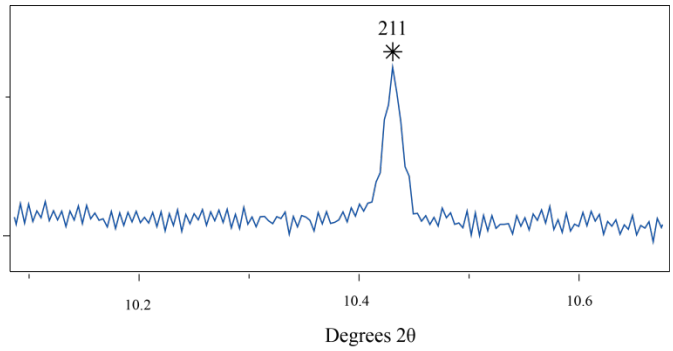

Fig. 2. Section of synchrotron X-ray powder diffraction pattern for $Sr_3ZrNb_4O_{15}$. Shown is the 211 reflection, the presence of which indicates a unit cell doubling along c.

The unit cell dimensions and volumes for each composition are seen to increase linearly across the composition range. This is consistent with a solid solution forming and is in agreement with Vegard's law (see Fig. 3).

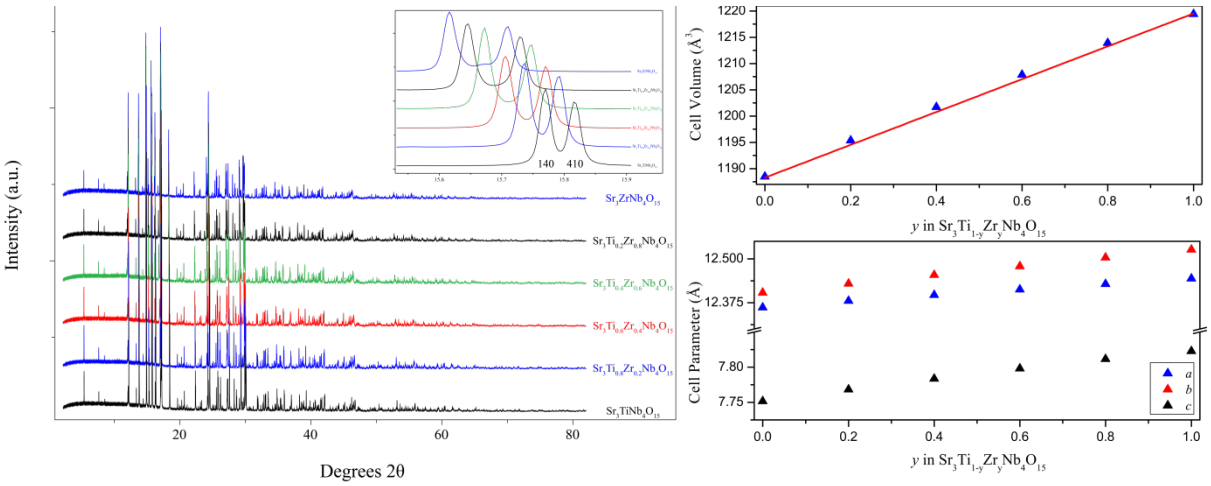

Fig. 3. Left, synchrotron X-ray diffraction patterns across $Sr_3Ti_{1-y}Zr_yNb_4O_{15}$ (from bottom to top: y = 0, 0.2, 0.4, 0.6, 0.8, 1). Top right, plot of cell volume as a function of composition. Bottom right, plot of cell parameters as a function of composition.

3.2 High Temperature

High temperature synchrotron X-ray diffraction data were collected for all members across the $Sr_3Ti_{1-y}Zr_yNb_4O_{15}$ composition range at 300 - 950 K. It was found that every composition underwent an orthrhombic, *Pna*2_1, to tetragonal, P4*bm*, phase transition on heating (Fig. 4). The transition to tetragonal conicided with disappearence of superlattice reflections, which indicated the doubled unit cell. The phase transition temperatures were found to be proportional to the zirconium content in the sample. Higher zirconium content samples underwent the transition at a higher temperature.

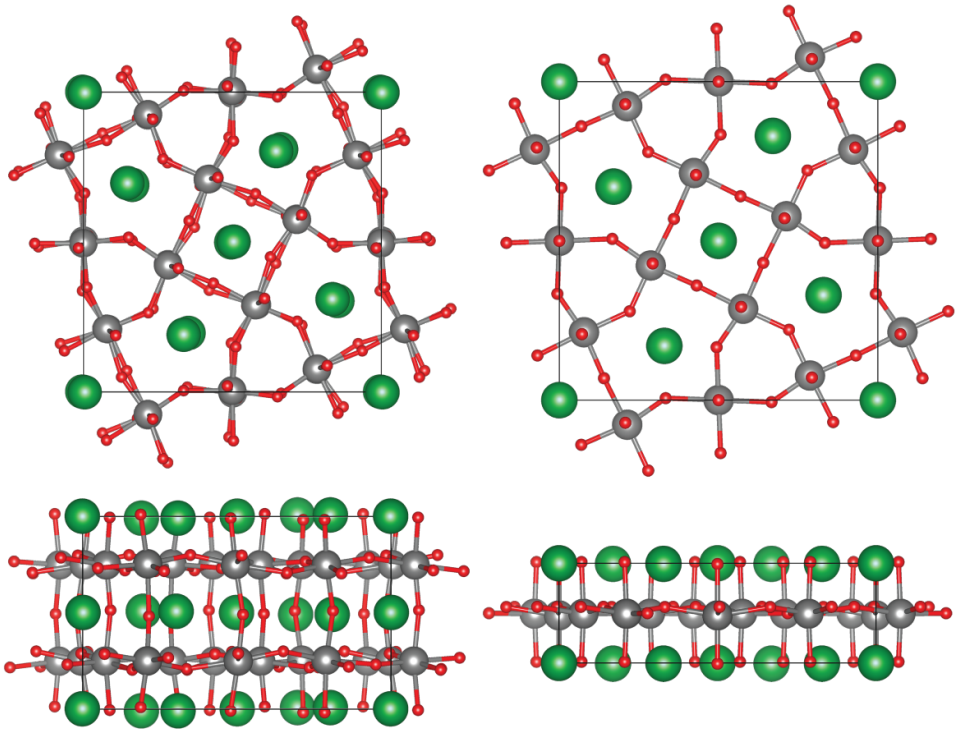

Fig. 4. Refined structure of $Sr_3ZrNb_4O_{15}$. Left, room temperature *Pna*2_1 structure. Right, high temperature *P*4*bm* structure. Top, looking down c axis, bottom, looking down the a axis.

The orthorhombic strain (b-a/b+a), as a function of temperature was determined for each composition in the series. Analysis of the strain showed that the structure continously evolved towards the higher symmetry tetragonal structure upon heating, but at the final stages the transition occurred abruptly (Fig. 5). For $Sr_3ZrNb_4O_{15}$ without the abrupt phase transition the strain would indicate a transition temperature of 990 K instead of the 800 K observed. This type of behaviour has been observed before in other compounds, *e.g.* spinel type $CuCrO_4$ [11] and perovskite type $LaMnO_3$ [12] both show a gradual change in lattice parameters and then an abrupt shift at the transition point.

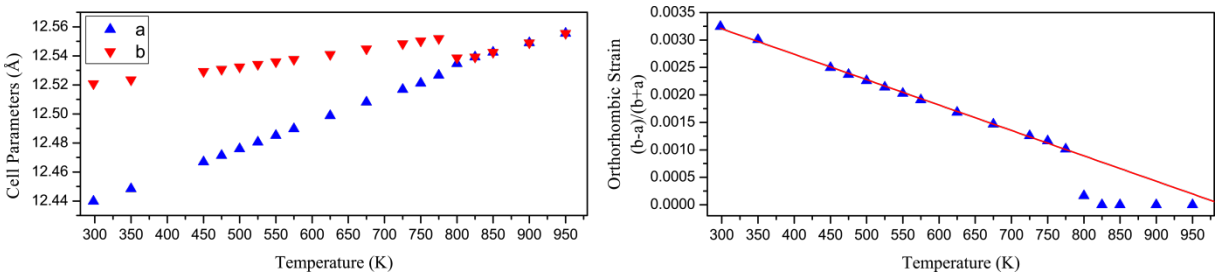

Fig. 5. Left, a and b cell parameters for $Sr_3ZrNb_4O_{15}$ as a function of temperature. Right, orthorhombic strain, (b-a)/(b+a) as a function of temperature.

Acknowledgments

This research was undertaken on the powder diffraction beamline at the Australian Synchrotron, Victoria, Australia and the authors thank Dr Q. Gu, Dr J. Kimpton and Dr H. Brand for their assistance. The authors also want to thank Prof. B. J. Kennedy for helpful discussions.

References

[1] Chang H Y, Sivakumar T, Ok K M, Halasyamani P S 2008 *Inorg. Chem* **47** 8511
[2] Stephenson N 1965 *Acta Crystallogr.* **18** 496
[3] Fang L, Zhang H, Yang J F, Hong X K, Meng F C 2004 *J. Mater. Sci. Mater. Electron.* **15** 355
[4] Massarotti V, Capsoni D, Bini M, Azzoni C B, Mozzati M C, Galinetto P, Chiodelli G 2006 *J. Phys. Chem. B* **110** 17798
[5] Ainger F W, Brickley W P, Smith G V 1970 *Proc. Br. Ceram. Soc.* **18** 221
[6] Neurgaonkar R R, Nelson J G, Oliver J R 1992 *Mater. Res. Bull.* **27** 677
[7] Chi E O, Gandini A, Ok K M, Zhang L, Halasyamani P S *Chem. Mater.* **16** 3616
[8] Kryshtop V G, Devlikanova R U, Fesenko E G 1979 *Inorg. Mater.* **15** 1777
[9] Whittle T A, Brant W R, Schmid S, in: Schmid S, Withers L R, Lifshitz R, (Eds.), 2013 *Aperiodic Crystals*, Springer Netherlands, pp. 179-185.
[11] Kennedy B J, Zhou Q 2008 *J. Solid State Chem.* **181** 2227
[12] Rodríguez-Carvajal J, Hennion M, Moussa F, Moudden A H, Pinsard L, Revcolevschi A 1998 *Phys. Rev. B* **57** R3189.

Synchrotron and Neutron Powder Diffraction and XANES Studies of $Cu_{5-x}Mn_xSbO_6$

D. J. Wilson[a] and T. Söhnel[a]

[a] *School of Chemical Sciences, University of Auckland, Auckland, New Zealand.*

Cu_5SbO_6 is a mixed copper compound that crystallises in a modified Delafossite structure type ($CuFeO_2$), with two distinct modifications. Compounds, like $CuFeO_2$, that crystallise in the Delafossite group are one of the few groups that showcase the rare property of multiferroic behaviour. The high temperature modification is of particular interest due to ferromagnetic-antiferromagnetic short range ordering of Cu^{2+} pairs in the structure. In order to influence the properties of Cu_5SbO_6, manganese were doped into the structure. This lead to an overall increase to the unit cell volume and distorted the copper to oxygen and antimony to oxygen bond lengths. Two oxidations states of manganese were found to be present within $Cu_{5-x}Mn_xSbO_6$, with a different ratio of oxidation states in the modifications.

1. Introduction

Low-dimensional transition metal compounds, especially copper based oxides with mixed Cu valence states, such as Cu_5SbO_6, seem to be very promising for strongly correlated electron systems. Cu_5SbO_6 forms two modifications. The high temperature modification shows a ferromagnetic-antiferromagnetic short range ordering of Cu^{2+} pairs. Doping of Cu_5SbO_6 with a magnetically active transition metals such as Mn, replacing either the magnetic Cu^{2+} or the non-magnetic Sb^{5+} ions, would significantly influence the electric and magnetic properties in this system. $Cu_5SbO_6 = [(Cu^{+}(Cu^{2+}_{2/3}Sb^{5+}_{1/3})O_2)]_3$ crystallises in a modified Delafossite structure type ($CuFeO_2$) [1-3]. Compounds like $CuFeO_2$ crystallising in the Delafossite structure are one of the few groups of compounds showing the rare property of multiferroic behaviour [4]. In Cu_5SbO_6 the magnetically active brucite-like CuO_2 layer is diluted in an ordered fashion with non-magnetic Sb^{5+}. Exploring and tuning the properties of compounds that crystallise in the Delafossite structure type could lead to interesting new developments. In particular, doping magnetically active transition metals could lead to changes of the short range ordering.

The main perspective of this study is to investigate the effects of doping manganese in to brucite-like layer of Cu_5SbO_6. By doping metals into the oxide layer, the properties of the material should change, such as magnetism or conductivity. Manganese should have interesting influences on Cu_5SbO_6, with the potential to affect the short-range magnetic ordering already present. Here, we describe the structural changes that occur due to the doping of manganese into Cu_5SbO_6 by using synchrotron and neutron powder diffraction. XANES measurements have been used to determine the oxidation state of Mn in the solid solution $Cu_5Sb_{1-x}Mn_xO_6$.

2. Experimental details

Powder samples of $Cu_{5-x}Mn_xSbO_6$ were prepared by mixing stoichiometry amount of starting oxides CuO, MnO_2 and Sb_2O_3; the mixtures were then place inside a furnace at 1100 °C and 900°C for the high and low temperature modification, respectively. After a nominal time, the samples were quenched in air proceed by grinding with a mortar and pestle.

Laboratory X-ray powder diffraction patterns were obtained on a Siemen D5000 X-ray Diffractometer, equipped with a copper anode X-ray tube (λ= 1.5418 Å). The diffraction patterns were collected at room temperature between 2θ range of 10°-80° with a step size of 0.02°. Synchrotron X-ray powder diffraction (SXRD) measurements were conducted on the powder diffraction beamline, 10-BM, at the Australian Synchrotron with approximate photon energy of 16 keV, using the MYTHEN dectector and the double crystal monochromator of Si(111) flat crystal pair. Complementary to the SXRD experiments, neutron powder diffraction (NPD) measurements were performed on the high-resolution powder diffractometer 'ECHIDNA' at the Australian Nuclear Science and Technology Organisation (ANSTO). The desired wavelength of 1.6220 λ was selected by Ge 355 monochromator. The powder diffraction patterns were obtained at room temperature under atmospheric pressure. For data analysis of the synchrotron and neutron powder data the software packages GSAS and FullProf were used [5-7]. The oxidation state of manganese was investigated by X-ray absorption near edge structure (XANES) spectroscopy on the X-ray absorption spectroscopy beamline, Australian Synchrotron. These measurements were carried out at the Mn K-edge (Mode 2, 6539 eV) at room temperature, with a 100 element Ge Fluoro detector. In addition to measurements performed on samples, a range of binary and ternary manganese oxides with known oxidation states were utilised as standards. Data analysis was done with software package IFEFFIT (data reduction (Athena) and data analysis (Artemis)) with Average2.0 used to calibrate against a metal foil standard (Mn) [8].

3. Results

3.1 Laboratory X-ray powder diffraction of $Cu_{5-x}Mn_xSbO_6$

Initially samples were prepared to the composition of $Cu_5Mn_xSb_{1-x}O_6$ in an attempt to replace Sb^{5+} with Mn^{4+} or Mn^{5+}. However, during quenching a green flame was observed. This was attributed to excess copper, which laboratory diffraction patterns of $Cu_5Mn_xSb_{1-x}O_6$ confirmed the presence of CuO. The excess of CuO suggested the nominal composition of $Cu_5Mn_xSb_{1-x}O_6$ required adjustment. Preparation of further samples was done with the adjusted composition $Cu_{5-x}Mn_xSbO_6$ to compensate for the excess CuO. The adjusted composition diffraction patterns did not contain the characteristic reflections expected from the presence of a CuO phase.

3.2 Synchrotron and neutron powder diffraction of $Cu_{5-x}Mn_xSbO_6$

SXRD was performed on both high temperature and low temperature modifications of $Cu_{5-x}Mn_xSbO_6$ in order to determine the structural changes with increasing fractional content of manganese. Comparing the diffraction patterns for the low temperature modification showed small shifts of reflections with manganese doping. However, in the high temperature modification diffraction patterns, there is a noticeable shift of the reflections as shown in Fig. 1. These shifts in reflections are indicative of a change in the lattice parameters with doping of manganese. According to the oxidation state of manganese obtained from XANES measurements, we expect the high temperature modification to incorporate more Mn^{2+}, with consideration of the ionic sizes of Cu^{2+}, Mn^{2+} and Mn^{3+} (0.65 Å, 0.83 Å and 0.645 Å, respectively) [9]. The Cu^{2+} and Mn^{3+} ions are similar in size, while Mn^{2+} is significantly larger. Thus the incorporation of Mn^{2+} into the Cu^{2+} sites results in an overall increase of the unit cell volume of 0.6% for $Cu_{4.7}Mn_{0.3}SbO_6$. The inclusion of manganese into the structure also lead to a linear expansion of *a*, a non-linear contraction of *b*, a non-linear expansion of *c* and increasing plane angle β. In addition to changes in the lattice parameters, there is a noticeable increase to reflections attributed to the low-temperature modification in the high-temperature modification samples with increasing manganese content (Fig. 1; reflections of the lt-modification are marked with italic indicies). The increase in these reflections is not

present in samples with longer preparation time. It is suggested that the presence of these reflections is due to the increase disorder by statistical nature of doping manganese into the structure and prompts that the two modifications differ by disordered and ordered nature, with reaction temperature affecting the oxidation state of manganese.

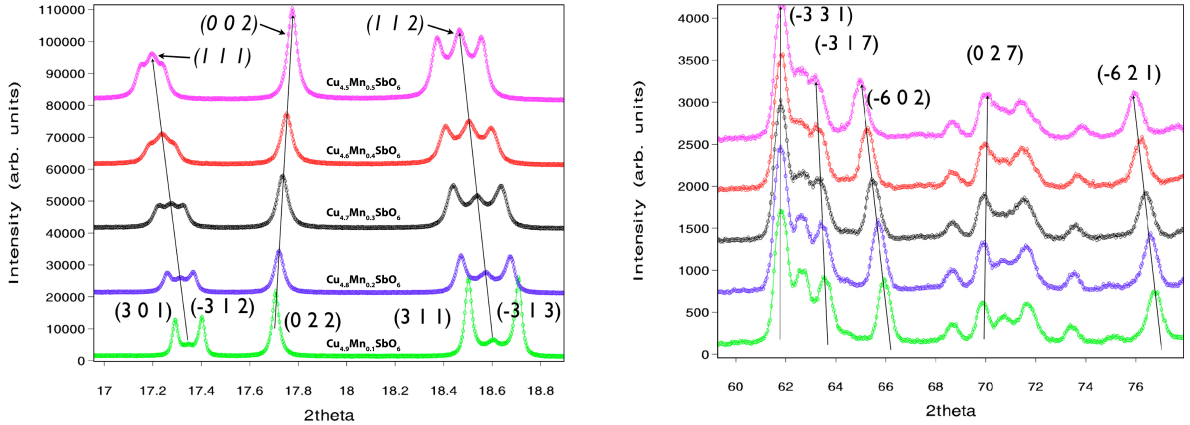

Fig.1. Left: Synchrotron X-ray powder patterns of $Cu_{5-x}Mn_xSbO_6$ normal indicies: high temperature modfaction, italic indicies low temperature modification. Right: Neutron powder diffraction patterns.

In addition to SXRD, NPD has been utilised to refine the atomic positions, in order to confirm where manganese is placed within the structure and the effect on the bonding environment. Rietveld refinements were attempted with different positions of manganese, manganese replacing Cu^{2+} or manganese replacing Sb^{5+} in order to confirm the results on manganese obtained during SXRD Rietveld refinement. Due to the difference in neutron scattering lengths of manganese and copper, Rietveld refinements of the NPD patterns were able to confirm that the doped manganese is in the copper positions. Thus it is expected that the replacement of the Cu^{2+} with the larger Mn^{2+}, the bond lengths of Cu-O and Sb-O will be distorted. Distortion of the bond lengths were observed in the NPD patterns, increasing the manganese content lead to the increase of 3% in the bond lengths of Sb-O in the antimony octahedral at a manganese content of 0.5. While, the copper octahedral shows an overall decrease in Cu-O length of 2% at the same manganese content.

	$Mn_{0.1}$	$Mn_{0.2}$	$Mn_{0.3}$	$Mn_{0.4}$	$Mn_{0.5}$
Sb-O average bond distance	1.965(7)	1.978(8)	1.983(9)	2.004(5)	2.028(9)
Cu-O average bond distance	2.135(1)	2.127(1)	2.123(1)	2.119(5)	2.113(1)

Table.1. The average metal to oxygen bond lengths in the antimony and copper octahedral for $Cu_{5-x}Mn_xSbO_6$ (x = 0.1 to 0.5), showing the increase of the Sb-O and the decrease Cu-O bond lengths.

3.3 Oxidation state analysis of $Cu_{5-x}Mn_xSbO_6$ by XANES

To determine the oxidation state of manganese in $Cu_{5-x}Mn_xSbO_6$, a series of XANES measurements were performed at the Mn K-edge. Comparing the energy position of the absorption edge for the variety of manganese oxidation state standards (oxidation state ranging between Mn^0 to Mn^{7+}), a linear relationship between energy position of the absorption edge and oxidation state of manganese was produced (Fig. 2). Comparing the energy position of the absorption edge for both modifications of $Cu_{5-x}Mn_xSbO_6$ against the manganese standards enabled us to determine the average oxidation state of manganese in these compounds. The high temperature modification was determined to have an average manganese oxidation state of 2.3, while the low temperature modification was found to be 2.7. This result suggested that manganese contained in both modifications is a mixture of

Mn^{2+} and Mn^{3+}, while the ratio of these two oxidation sates is different between the two modifications. Also there was no observance of a shift in energy position of the absorption edge with varying manganese content and thus no change in manganese oxidation state with varying manganese content. For $Cu_{5-x}Mn_xSbO_6$ to remain charge neutral without the inclusion of oxygen, the Mn^{2+} has to sit in the Cu^{2+} site, replacing the copper ion, while the Mn^{3+} must be replacing a unit of $Cu^{2+}_{2/3}\,Sb^{5+}_{1/3}$ to remain charge neutral.

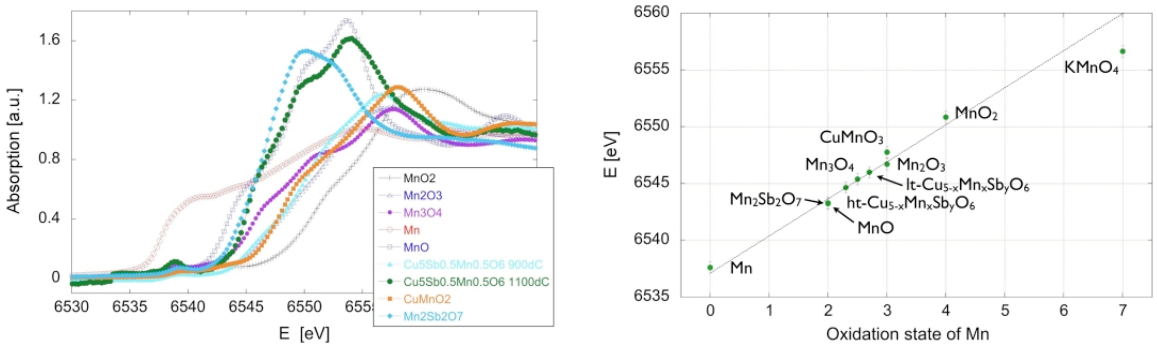

Fig.2. XANES spectra of various manganese containing tertiary and binary oxides (left). The relationship of oxidation state of manganese with the position of the absorption edge (right).

4 Conclusions

Powder samples of both high and low temperature of $Cu_{5-x}Mn_xSbO_6$ were prepared by tradition solid state reactions. The manganese in $Cu_{5-x}Mn_xSbO_6$ was found to be a mixture of Mn^{2+} and Mn^{3+}, with a higher 2+ to 3+ ratio for the high temperature modification than the low temperature modification. SXRD and NPD confirmed the replacement of copper in the structure by manganese, with distortions in the Cu-O and Sb-O bond lenths by 2% and 3% respectively in $Cu_{4.5}Mn_{0.5}SbO_6$. While an increase in low temperature modification with increasing manganese content in the high temperature modification was observed in SXRD.

Acknowledgments

The Authors would like to thank Dr. Bernt Johannessen and Dr. Justin Kimpton for the help they provide at the X-ray absorption beamline and the powder diffraction beamline, respectively, at the Australian Synchrotron and Dr. Maxim Avdeev for this help while preforming experiments on Echinda beamline at ANSTO. We would like to thank and acknowledge the financial support provided by the Australian Institute of Nuclear Science and Engineering Inc. (AINSE), the Australian Synchrotron and the University of Auckland.

References

[1] Rey E 2010 *BScHons Thesis* The University of Auckland
[2] Rey E, Si P Z and Söhnel T 2011 *Proceedings of the 35th Annual Condensed Matter and Materials Meeting,* Australia Australian Institute of Physics Publications, Canberra, Australian Institute of Physics 22. http://www.aip.org.au/wagga2011
[3] Climent-Pascual E, Norby P, Anderson N H, Stephens P W, Zandbergen H W, Larsen J and Cava R J 2012 *Inorg. Chem.* **51** 557
[4] Kimura T, Lashley J C, Ramirez A P 2006 *Phys. Rev.B.* **73** 220401
[5] Toby B H 2001 *J. Appl. Crystallog.* **34** 210
[6] Larson T C and Von Dreele R B 2000 *Los Alamos National Laboratory Report* **86** 748
[7] Rodriguez-Carvajal J 1993 *Physica B* **192** 55
[8] Ravel B and Newville M 2005 *J. Synch. Rad.* **12** 537
[9] Shannon R D 1976 *Acta Crystallog.* **A32** 751

ABSTRACTS

Oral Presentations

Adventures in Reciprocal Space – From Laue to Bragg and Back Again

A.J. Edwards[a]

[a] *Bragg Institute, Australian Nuclear Science and Technology Organization, Lucas Heights, N.S.W., Australia.*

The earliest X-ray diffraction experiments [1] employed radiation "as generated" without monochromation to produce the reciprocal space images we know as Laue patterns. The pioneering work of W.L. Bragg [2] using monochromated X-rays followed rapidly and provided the major simplification in the mathematics required to analyse X-ray diffraction patterns to derive data from which atomic resolution structural information can be deduced. In the following century, physicists, chemists and later biologists developed the Bragg methodology into a powerful tool which underpins the structure based paradigm at the core of modern chemistry and biology. Application of the Laue method to questions of structure determination at atomic resolution languished for many decades until the availability of fast computers and the technical challenges of Synchrotron sources led to a resurgence in this experimental approach [3]. With the cost of neutron beams being substantially more than that of X-ray beams, the applicability of this method to neutron diffraction studies was soon investigated [4] and today Laue neutron diffraction is the method of choice for the determination of structures where neutron diffraction is scientifically required to prove aspects of structure for which X-ray diffraction can only be "suggestive".

Chemists typically employ an array of physical methods to support their structural assertions, but a crystal structure is often presented as absolute proof and as justification of inferior characterization by other methods. This being the case it is of great concern that crystallographic studies be critically reviewed by both analyst and in the publication process. Checkcif is a fine tool but insufficient to ensure the integrity of the scientific literature – that is properly the role of the analyst and the reviewers.

[1] W. Friedrich, P. Knipping, M. Laue, Sitzungsberichte der (Kgl.) *Bayerische Akademie der Wissenschaften* 973 (1912).

[2] W.L. Bragg, *Proc. Camb. Philos. Soc.* **17**, 45 (1913).

[3] J.R. Helliwell, J. Habash, D.W.J. Cruickshank, M.M. Harding, T.J. Greenhough, J.W. Campbell, I.J. Clifton, M. Elder, P.A. Machin, M.Z. Papiz and S. Zurek, *J. Appl. Cryst.* **22,** 483 (1989).

[4] C. Wilkinson and M.S. Lehmann, *Nucl. Instrum. Methods A.* **310**, 411 (1991).

Enhanced Ferroelectric Response in Strained Perovskites

B. Wylie-van Eerd[a], T. Yamada[b], J. Wang[c,d], N. Setter[d] and J. Trodahl[a]

[a] *MacDiarmid Institute of Nanotechnology and Advanced Materials, School of Chemical and Physical Sciences, Vitoria University of Wellington, PO Box 600, Wellington, New Zealand.*

[b] *Department of Materials, Physics and Energy Engineering, Nagoya University, Furo-cho, Chikusa-ku, Nagoya 464-8603, Japan.*

[c] *Graduate School at Shenzhen, Tsinghua University, 518055, Shenzhen, China.*

[d] *Ceramics Laboratory, Swiss Federal Institute of Technology (EPFL), 1015 Lausanne, Switzerland.*

Ferroelectrics are ubiquitous in technology, based on their strong piezoelectric and pyroelectric responses, their nonlinear dielectric response and their multi-stable polarization states. The vast majority of applications make use of polycrystalline $PbZr_xTi_{1-x}O_3$ (PZT) ceramics, but there is an ongoing interest in a search for alternative ferroelectrics, both for avoiding Pb in their manufacture and to find stronger responses. Among the aveneus showing promise is a srearch for materials and structures in which the ferroelectric state and its responses are enhanced by built-in strain. Raman spectroscopy provides an especially convenient signature of structural phase transitions that has made it the measurement of choice for the delineation of phase transition lines in a stress-temperature diagram. This presentation will focus on Raman investigations of strong increases of the ferroelectric-phase transition temperatures in two strained systems: (1) core-shell PZT nanowires supporting tensile hydrostatic strain (i.e. negative pressure) and (2) strained $SrTiO^3$ (STO) films grown on sbstrates that impose biaxial compressive strain. The former showed a transition temperature enhanced from 500 to over 600 °C, while the latter led to a ferroelectric phase in normally nonferroelectric STO.

Weak antilocalisation in topological insulators

X. Bi[a], E.M. Hankiewicz[b] and D. Culcer[c]

[a] *ICQD, The University of Science and Technology of China, Hefei 230026, China.*

[b] *Universitaet Wuerzburg, Wuerzburg, Germany.*

[c] *School of Physics, The University of New South Wales, Sydney 2052, Australia.*

Topological insulators (TI) have revolutionised our understanding of insulating behaviour. They are insulators in the bulk but conducting along their surfaces, thanks to surface states in which the spin and the charge are strongly coupled by means of the spin-orbit interaction. Much of the recent research on TI focuses on overcoming the *transport bottleneck* [1], namely the fact that surface state transport is overwhelmed by bulk transport stemming from unintentional doping. The key to overcoming this bottleneck is identifying unambiguous signatures of surface state transport. This talk will discuss one such signature, which is manifest in the coherent backscattering of electrons in TI. Because of the strong spin-orbit coupling in TI one expects to observe weak antilocalisation rather than weak localisation, meaning that coherent backscattering increases the electrical conductivity [2]. The features of this effect, however, are rather subtle, because in TI the impurities have strong spin-orbit coupling as well, greatly increasing the complexity of the problem [3]. I will show that spin-orbit coupled impurities introduce an additional time scale, which is expected to be shorter than the dephasing time, and the resulting conductivity has a *logarithmic dependence* on the carrier number density, a behaviour hitherto unknown in 2D electron systems. The result we predict is directly observable experimentally and would provide a smoking gun test of surface transport. Furthermore, I will also discuss the effect of electron-electron interactions on transport in this regime.

[1] D. Culcer, *Physica E* **44**, 860 (2012).

[2] G. Tkachov and E.M. Hankiewicz, *Phys. Rev. B* **84**, 035444 (2011).

[3] X. Bi, E.M. Hankiewicz and D. Culcer, to be published.

The dynamics and critical properties of $FePS_3$, an Ising-like two-dimensional magnet on a honeycomb lattice

A. Wildes[a], K. Rule[b], D. Lançon[a,c] and T. Hicks[d]

[a] *Institut Laue-Langevin, Grenoble, France.*

[b] *Australian Nuclear Science and Technology Organisation, Lucas Heights NSW 2234, Australia.*

[c] *Ecole Polytechnique Fédérale de Lausanne, Lausanne, Switzerland.*

[d] *School of Physics, Monash University, Victoria 3800, Australia.*

The MPS_3 compounds (M = transition metal) are a family of materials where the M^{2+} ions lie in planes forming a honeycomb lattice. The planes are weakly bound by van der Waals forces and, when the M^{2+} carries a magnetic moment, the materials are good approximations of two-dimensional (2D) antiferromagnets.

The $FePS_3$ compound is of particular interest as it is a rare example of an Ising-like 2D magnet with honeycomb symmetry [1]. We have performed experiments with neutron scattering to investigate the magnon dynamics on both a powder [2] and, more recently, on a single crystal. We have further made extensive measurements of the critical dynamics of the compound. We will present our results, showing the magnon dispersion surface and the magnitudes of the exchange interactions along with the scaling behaviour of the magnetization and the anisotropy. The results will be contrasted with a sister compound, $MnPS_3$, which is a good example of a Heisenberg-like 2D magnet. We will also discuss the possibilities for tricritical points and quantum phase transitions in this compound.

[1] K.C. Rule, G. McIntyre, S.J. Kennedy and T.J. Hicks, *Phys. Rev. B* **76**, 134402 (2007).

[2] A.R. Wildes, K.C. Rule, R.I. Bewley, M. Enderle and T.J. Hicks, *J. Phys.: Condens. Matter* **24**, 416004 (2012).

Colour Tunable Light Emission from Organic Field-Effect Transistors

H. von Seggern[a]

[a] *Electronic Materials Division, Institute of Materials Science,*
Technische Universität Darmstadt, Alarich-Weiss-Straße 2, 64287 Darmstadt, Germany.

The unique property of ambipolar organic light emitting field-effect transistors (OLETs) is the ability to position the light emission zone within the transistor channel through the applied transistor biases. In this talk the basics of the ambipolar OLET will be discussed [1,2,3] and two examples for colour tuning will be demonstrated [4,5]. Both approaches take advantage of the ability of a controlled displacement of the recombination zone through the organic semiconductors. In the first approach two different acenes with different emission colours are employed in a parallel stack in a top-contact bottom-gate FET configuration [4]. It will be demonstrated that due to thermionic emission of electrons at the source, light of one colour can be generated near the source contact even in hole accumulation. Due to the electrically controllable positioning, the charge carrier recombination zone can be directed from the top acene layer to the bottom acene layer. Thereby the emitted light can be continuously shifted by about 50 nm from green to red emission. A second approach takes advantage of the horizontal displacement of the recombination zone within the channel of the transistor [5]. On top of the semi-transparent gate electrode of a F8BT transistor a colour conversion layer is deposited in a wedge-like shape partially covering the channel. In the ambipolar regime the charge carrier recombination takes place in the F8BT layer, and dependent on the position of the recombination zone either the emitted light of the F8BT layer or the partially absorbed and converted light from the colour conversion layer can be detected. The electroluminescence maximum of the emitted light can be shifted by about 30 nm. The physics and potential applications of such colour tuneable OLETs will be discussed.

[1] A. Hepp, H. Heil, W. Weise, M. Ahles, R. Schmechel and H. von Seggern, *Phys. Rev. Let.* **91**, 157406 (2003).

[2] J. Zaumseil, R.H. Friend and H. Sirringhaus, *Nat. Mater.* **5**, 1 (2006).

[3] M. Schidleja, C. Melzer and H. von Seggern, *Adv. Mater.* **21**, 1172 (2009).

[4] E.J. Feldmeier, M. Schidleja, C. Melzer and H. von Seggern, *Adv. Mater.* **22**, 3568 (2010).

[5] E.J. Feldmeier and C. Melzer, *Org. Electron.* **12**, 1166 (2011).

Organic luminescent solar concentrators for solar cells

N.M. Winch[a], G.J. Smith[a], D.H. Bhuiyan[b], R.D. Breukers[b] and A.J. Kay[b]

[a] *School of Chemical and Physical Sciences, Victoria University of Wellington, Wellington, New Zealand.*

[b] *Callaghan Innovation Research Limited, Lower Hutt, New Zealand.*

Current inorganic solar cells use silcon-based semiconductors to convert the incident sunlight into electricity. Solar cells are inherently expensive due to the high cost of the semiconductor, and because the light to energy efficiency is very low. The low efficiency arises from both the solar cell not absorbing across the whole solar spectrum, and their poor response to diffuse sunlight. An alternative to solar cells are luminescent solar concentrators (LSCs). A LSC is a device which absorbs sunlight over a large area of material, and then directs the energy, through luminescent emission, to solar cells mounted on the edges. Typically a LSC consists of a glass waveguide with organic luminescent molecules either embedded in the glass matrix, or as a thin film coating. Due to the small number of solar cells required, LSCs are more cost effective than straight silicon solar cells, and have the advantage that they work in diffuse sunlight.

Conjugated polymers based on polyphenylenevinylene (PPV) have been widely studied for use in organic light emitting diodes and solar devices [1]. An alternative based on oligo-fluorenevinylenes (OFV) has also been suggested [2] but not extensively investigated. We are investigating the use of these two chromophore families as luminescent molecules for LSCs. The luminescent properties of these molecules have been characterised (for example, quantum yield and fluorescent lifetimes) in a wide range of solvents and as a guest-host system in polymethyl methacrylate (PMMA) thin films.

[1] A.J. Tilley, S.M. Dancak, C. Browne, T. Young, T. Tan, K.P. Ghiggino, T.A. Smith and J. White, *J. Org. Chem.* **76**, 3372 (2011).

[2] Q. Liu, W. Liu, B. Yao, H. Tian, Z. Xie, Y. Geng and F. Wang, *Macromolecules* **40**, 1851 (2007).

Structural Studies of Phase Transitions in Hybrid Organic-Inorganic Salts with Temperature and Pressure

J. Binns[a,d], S. Parsons[a,d], S. Moggach[a,d], R. Valiente[b], G. McIntyre[c], K. Kamenev[d]

[a] *School of Chemistry, Joseph Black Building, West Mains Road, Edinburgh, Scotland.*

[b] *Applied Physics Department, Faculty of Science, University of Cantabria, 39005 Santander, Spain.*

[c] *Bragg Institute, ANSTO, Lucas Heights NSW 2234, Australia.*

[d] *Centre for Science at Extreme Conditions, The University of Edinburgh, Erskine Williamson Building, The King's Buildings, Mayfield Road, Edinburgh, Scotland, United Kingdom.*

The alkylammonium tetrachlorometallates have attracted significant attention for the numerous phase transitions observed in a relatively narrow range of temperatures and pressures as well as ferroelectric,-elastic and -magnetic behaviours. [1,2] Such simple organic salts could find possible applications as thin-film functional materials in low cost ferroelectric capacitors and RAM. With the exception of bis(tetramethylammonium) tetrachlorozincate(II) this class of materials has been subject to relatively little structural investigation, with a number of general phase sequences being determined from calorimetric and polarisation measurements. [3,4] While there are known to be ferroelectric phase transitions in many of these materials, the exact mechanism by which these simple organic salts exhibit such behaviour is unknown.

We report on the phase sequences observed in two related materials: tetramethylammonium tetrachloroferrate(III) (TCF), and the previously unknown tetramethylammonium tetrachlorogallate(III) (TCG) which display re-entrant as well as plastic crystalline phases.

[1] D. Wyrzykowski, R. Kruszynski, J. Klak, J. Mrozinski and Z. Warnke, *Inorg. Chim. Acta* **361**, 262 (2008).

[2] H. Shimizu, N. Abe, N. Kokubo, N. Yasuda, S. Fujimoto, T. Yamaguchi and S. Sawada, *Solid State Commun.* **34**, 363 (1980).

[3] Z. Czapla, O. Czupinski, Z. Galewski and L. Sobczyk, *Solid State Commun.* **56**, 741 (1985).

[4] I. Ruiz-Larrea, A. Lopez-Echarri and M.J. Tello, *Solid State Commun.* **64**, 1099 (1987).

Optically and Electrically Detected Electron Spin Resonance in OLEDs

R. Sutton[a] and A. Edgar[a]

[a] *School of Chemical and Physical Sciences, Victoria University,Wellington, New Zealand.*

Organic light-emitting diodes (OLEDs) bring the promise of efficient large area light emitting devices which can be manufactured by simple techniques such as spin coating [1]. Whilst technical progress has been rapid, such that OLED screens are now being introduced into television displays (and have been available for some time in cell phones), the basic mechanisms which underpin light emission and "killer" process of non-radiative recombination are as yet still poorly understood. One particular on-going problem with OLEDs is the question of ageing – a deterioration of emission efficiency with time and use. Since the process of electron-hole recombination is spin-dependent, one possible technique which may help unravel the details of the processes is electron spin resonance. However, there are too few spins in a thin OLED layer for the conventional microwave detection of ESR, but detection via a change in electrical conductivity and/or optical emission intensity has been shown to be effective in some cases [2].

We have customised a 9 GHz ESR spectrometer for electrical and optical detection, and present here results of an investigation of spin-dependent ageing processes in OLEDs based on ITO/PEDOT:PSS/emissive layer/metal layer with the emissive layer being PFO or PPV and the metal layer being aluminium, silver, or calcium. Spin-dependent signals are observed at room temperature and discussed in terms of spin dependent trapping, whilst significant zero-field magnetoresistance effects are also observed.

[1] J.W. Park, D.C. Shin and S.H. Park, *Semicond. Sci. Technol.* **26**, 034002 (2011).

[2] J.M. Lupton, D.R. McCarney and C. Boehme, *ChemPhysChem* **11**, 3040 (2010).

Characterization of a Fluoroperovskite Based Fibre Coupled Optical Dosimeter for Radiotherapy

J. Donaldson[a,b], G.V.M. Williams[b] and S.G. Raymond[c]

[a] *Blood & Cancer Centre, Wellington Regional Hospital, Wellington, New Zealand.*

[b] *MacDiarmid Institute, SCPS, Victoria University, Wellington, New Zealand.*

[c] *Callaghan Innovation, Lower Hutt, New Zealand.*

The increasing complexity of modern radiation treatment techniques demands comparable advances in clinical radiation dosimetry equipment, with emphasis on improving spatial resolution and further developing two and three-dimensional dosimetry systems [1]. Fibre coupled optical dosimeters can potentially deliver significant gains in miniaturization and sensitivity when compared to both ionisation chambers and established solid state detectors. For this reason we are developing a fibre optic dosimeter that uses inorganic fluoroperovskite crystals ($NaMgF_3$ and $RbMgF_3$, activated with either Eu^{2+} or Mn^{2+}) as the active radiation detection material for applications in medical radiation dosimetry [2].

In this report we discuss the requirements for radiation dosimeters specific to radiotherapy and the results of a selection of radioluminescence characterization measurements made with a prototype fibre optic dosimeter at Wellington Hospital. The results include a dose history dependence as low as 0.01% per Gy, a radioluminescence temperature dependence measured in both the prototype system and bulk crystal samples of less than 0.1% per °C, and independence from dose per pulse for $NaMgF_3$. The response was also compared to measurements made using a small field ionisation chamber. Of the materials studied, only those based on $NaMgF_3$ were found suitable for radiotherapy dosimetry. The primary difficulties arising from use in medical radiations are the stem signal due to Čerenkov photons and the residual dose history dependence. Potential solutions to these difficulties will be discussed, along with the possibilities offered by a wider range of luminescence activators.

[1] M.M. Aspradakis *et al.* Report Number **103**, Institute of Physics and Engineering in Medicine, York (2010).

[2] G.V.M. Williams and S. Raymond, *Radiation Measurem.* **46**, 1099 (2011).

Towards better understanding of atomically precise gold clusters and titania made using surface modifying agents

V.B. Golovko[a,b], J.Y. Ruzicka[a], F. Abu Bakar[a,c], D.P. Anderson[a], R. Adnan[a], B. Donoeva[a,b], D. Ovoshchnikov[a], G.F. Metha[d], G.G. Andersson[e], L. Thomsen[f], B. Cowie[f], C. McNicoll[a,b,g], B. Ingham[b,g], T. Kemmitt[b,g], V. Fang[h] and J. Kennedy[b,h]

[a] *Department of Chemistry, University of Canterbury, Christchurch 8140, New Zealand.*

[b] *The MacDiarmid Institute for Advanced Materials and Nanotechnology, New Zealand.*

[c] *University Tun Hussein Onn Malaysia, 86400 Parit Raja, Batu Pahat, Johor, Malaysia.*

[d] *Department of Chemistry, University of Adelaide, SA 5005, Australia.*

[e] *Flinders Centre for NanoScale Science and Technology, Flinders University, Adelaide, SA 5001, Australia.*

[f] *Australian Synchrotron, 800 Blackburn Road, Clayton Vic-3168, Australia.*

[g] *Callaghan Innovation, P.O. Box 31-310, Lower Hutt 5040, New Zealand.*

[h] *National Isotope Centre, GNS Science, P.O. Box 31312, Lower Hutt 5010, New Zealand.*

Controlled synthesis of titania nanoparticles using recently perfected sol-gel methodology [1,2], synthesis of atomically precise metal clusters, their deposition and activation on oxide supports and studies of properties of the resulting materials as promising catalysts and sensors will be briefly discussed [3-9].

Our work on synthesis of titania nanoparticles is focused on careful tuning of the reaction conditions and use of selected surface modifying agents capable of directing and controlling growth of nanoparticles with specific size, phase and even population of Ti^{+3} sites at the surface [2]. Promising performance of titania made using our methodology as near-IR reflective coating will be briefly highlighted.

From pre-historic times gold was known as a chemically inert, "noble" metal until, in 1987, Haruta *et al.* proved that gold nanoparticles can be catalytically active. Results of research focused on the use of size-controlled, chemically pre-synthesised nanoparticles (colloids and clusters) with core sizes ranging from classical 1.5 nm "Au_{55}" systems to atomically precise, uniquely small clusters (Au_9 *etc*.) including a range of mixed-metal clusters will be presented. Immobilization of such clusters on a variety of supports had been pursued in an attempt to fabricate a family of site-isolated

catalysts, where properties of the active site are defined by the nature of the precursor with great precision. Catalytic performance in selected reactions will be highlighted. New insights in the nature of our precisely defined precursors (pure and immobilised onto supports) obtained using relevant materials characterization techniques, such as Synchrotron X-ray Photoelectron Spectroscopy will be presented.

[1] T. Kemmitt *et al*., *Curr. Appl. Phys.* **13**, 142 (2013).
[2] J.Y. Ruzicka *et al*., *RSC Advances* (submitted).
[3] M. Turner, *et al.*, *Nature* **454**, 981 (2008).
[4] D. Anderson *et al.*, *Phys. Chem. Chem. Phys.* **15**, 3917 (2013).
[5] D. Anderson *et al.*, *Phys. Chem. Chem. Phys.* **15**, 14806 (2013).
[6] M.Z. Ahmad *et al.*, *Int. J. Hydrogen Energy* **38**, 12865 (2013).
[7] M.Z. Ahmad *et al.*, *Sensors and Actuators B* **179**, 125 (2013).
[8] B.G. Donoeva *et al*., *ACS Catal.* **3**, 2986 (2013).
[9] D. Ovoshchnikov *et al.*, *Catal. Sci. Technol.* DOI: 10.1039/C3CY01011B (2013).

Low Cost Refractive Index Sensing Using Zirconia Inverse Opal Thin Films

A. Chan[a], D. Sun-Waterhouse[a] and G.I.N. Waterhouse[a]

[a] *School of Chemical Sciences, The University of Auckland, Auckland, New Zealand.*

A series of zirconia (ZrO_2) inverse opal thin films and powders with pseudo photonic band gaps along the [111] direction at 465, 525 and 628 nm were successfully fabricated by the colloidal crystal template technique. SEM, TEM and XRD analyses revealed that the ZrO_2 inverse opals comprised a fcc array of spherical macropores (diameters 260, 287 and 342 nm, respectively) within a matrix of nanocrystalline tetragonal ZrO_2. The specific surface areas of all samples were 45-47 m^2 g^{-1}, and independent of the macropore size. The optical properties of the ZrO_2 inverse opal thin films were comprehensively characterised and were found to be in excellent accord with a modified Bragg's law expression that considers both refraction and diffraction of light in the inverse opal architectures [1]. The photonic band gap (PBG) position for the ZrO_2 inverse opals thin films red shifted on immersion in organic solvents, with the magnitude of the shift being directly proportional to the refractive index of the solvent. Solvent refractive index sensing with a precision of ~0.0005 is demonstrated.

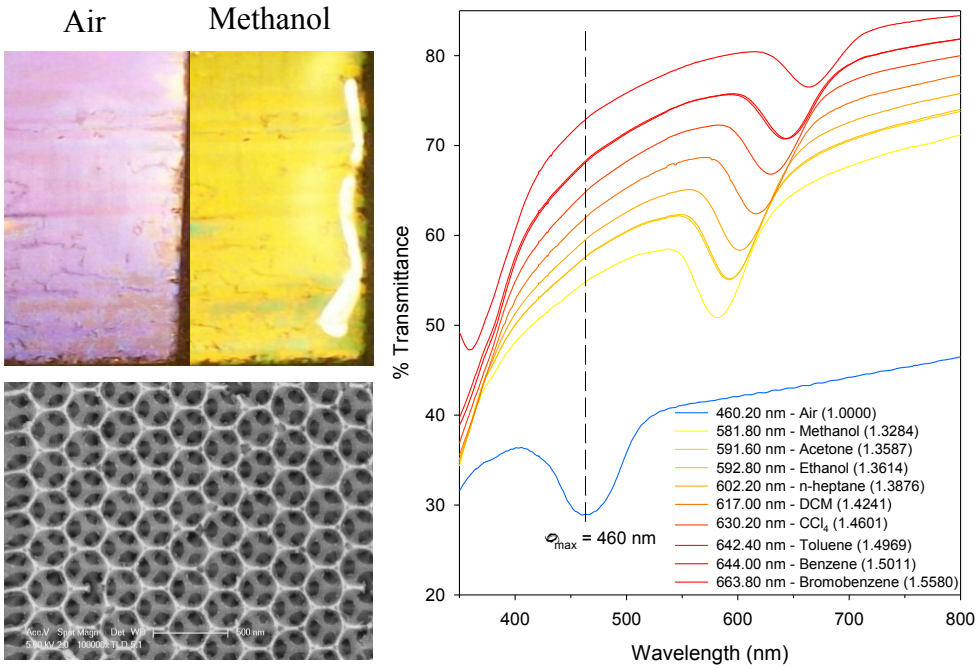

Figure 1. (above left) ZrO_2 inverse opal thin films in air and in methanol. (below left) SEM image of ZrO_2 inverse opal thin film. (right) UV-Vis transmittance data of a ZrO_2 inverse opal thin film in solvents of increasing refractive index.

[1] R. Schroden, M. Al-Daous, C.F. Blanford and A. Stein. *Chem. Mater.* **14**, 3305 (2002).

Enhanced photocatalytic activity in F-TiO_2: effect of solvent and fluorine modifier towards the morphology of TiO_2

F. Abu Bakar[a,b,c], J.-Y. Ruzicka[a,c], B.E. Williamson[a], C. McNicoll[a,c,d], B. Ingham[c,d], T. Kemmitt[c,d] and V.B. Golovko[a,c]

[a] *Department of Chemistry, University of Canterbury, Christchurch 8140, New Zealand.*

[b] *University Tun Hussein Onn Malaysia, 86400 Parit Raja, Batu Pahat, Johor, Malaysia.*

[c] *The MacDiarmid Institute for Advanced Materials and Nanotechnology, New Zealand.*

[d] *Callaghan Innovation, PO Box 31-310, Lower Hutt 5040, New Zealand.*

Unlike homogeneous radical chemistry, heterogeneous photocatalytic reactions strongly depend on the properties of titania (TiO_2), such as its surface chemistry, lattice defects, crystallinity and particle size. Surface properties are particularly critical: surface modification of TiO_2 changes not only the reaction rate [1,2] but also the mechanism of the product formation [3,4]. In this study, a range of fluorine-modified TiO_2 were synthesised by thermal degradation of peroxotitaic acid in the presence of three non-toxic (*cf*. HF) surface modifiers: NBu_4F, NBu_4BF_4 and NBu_4PF_6. Two solvents, ethanol and isopropanol, were used in the synthesis to elucidate the effect of the solvents on the morphology and photocatalytic activity of the resulting materials. The hydrolysis rate of titanium isopropoxide (TTIP) and thus the aggregation rate of primary particles may be affected when different types of solvents are used in the synthesis of TiO_2. As a result, primary and secondary particle sizes, morphology and phase composition may be altered. The morphology, crystal phase and specific surface area *etc*. of the catalyst were determined using FESEM, TEM, PXRD, ATR-FTIR, TGA and BET analysis methods. The photocatalytic activity of synthesised TiO_2 was evaluated in the photodegradation of popular, industrially used Reactive Blue 19 (RB19) under both broad spectrum and visible light only irradiation. Obtained results indicate that different anions in the surface-modifying agent and the type of solvent used significantly affect the morphology, particle size and crystal phase of the catalysts. The catalyst synthesised in the presence of EtOH as a solvent using NBu_4PF_6 as a surface modifier exhibits the highest degradation percentage under both broad spectrum and visible light irradiation compared with other surface-modified TiO_2 and commercial TiO_2 (Degussa P-25).

[1] A. Fujishima and K. Honda, *Nature* **238**, 37 (1972).

[2] H. Zhan, K. Chen and H. Tian, *Dyes Pigm.* **37**, 241 (1998).

[3] C. Sriwong, S. Wongnawa and O. Patarapaiboolchai, *Chem. Eng. J.* **191**, 210 (2012).

[4] H. Zhang, G. Chen and D.W. Bahnemann, *J. Mat. Chem.* **19**, 5089 (2009).

Induced few-electron GaAs Quantum Dots

L.A. Yeoh[a], A.M. See[a], O. Klochan[a], I. Farrer[b], D.A. Ritchie[b] and A.R. Hamilton[a]

[a] *School of Physics, University of New South Wales, Sydney 2052, Australia.*

[b] *Cavendish Laboratory, University of Cambridge, Cambridge, United Kingdom.*

Electrostatically defined, tunable quantum dots (QD) have been routinely fabricated from a two-dimensional electron gas (2DEG) in semiconductors such as GaAs [1] and have the potential to form the building blocks of a solid state quantum computer [2]. Such devices have been typically fabricated from modulation doped wafers. However the presence of dopants cause charge noise and temporal instability, as the dopants switch between ionized and de-ionized states [3,4]. To eliminate the need for dopants, the 2DEG can be electrostatically "induced" via a global metal top gate [5]. To operate the QD as a spin qubit, we need to create a small, few-electron QD to study the individual spin states. Such fine nanostructures require metal gate patterns in the sub-micron scale, plus a sharp, well defined, electrostatic potential [5]. Hence the 2DEG needs to be brought as close to the wafer surface as possible. Improvements in fabrication have allowed such induced devices to yield similar mobilities and densities at equivalent 2DEG depths from the wafer surface, as their modulation doped counterparts [6]. Recently, such techniques have allowed for the creation of stable, QDs containing hundreds of electrons [6,7].

Here we will present our work towards the fabrication and characterization of a few-electron QD, created from an induced GaAs/AlGaAs heterostructure. Our first devices exhibit excited states in the coulomb diamonds and contains tens of electrons.

[1] R. Hanson and D.D. Awschalom, *Nature* **453**, 1043 (2008).

[2] D. Loss and D.P. DiVincenzo, *Phys. Rev. A.* **57**, 120 (1998).

[3] M. Pioro-Ladrière *et al.*, *Phys. Rev. B* **72**, 115331 (2005).

[4] C. Buizert *et al.*, *Phys. Rev. Lett.* **101**, 226603 (2008).

[5] B.E. Kane *et al.*, *Appl. Phys. Lett.* **67**, 1262 (1995).

[6] W.Y. Mak *et al.*, *Appl. Phys. Lett.* **102**, 103507 (2013).

[7] A.M. See *et al.*, *Appl. Phys. Lett.* **96**, 112104 (2010).

SDW and AFM order in single crystal $EuFe_2As_2$ system under high-pressue using a new ceramic anvil high-pressure cell

N. Suresh[a], S.V. Chong[a], J. Tallon[a] and K. Kadowaki[b]

[a] *MacDiarmid Institute of Advanced Materials and Nanotechnology*

Victoria University of Wellington, New Zealand.

Callaghan Innovation Lower Hutt 5040 New Zealand.

[b] *Institute of Materials Science and Graduate School of Pure & Applied Sciences,*

University of Tsukuba - 1-1-1, Tennodai, Tsukuba, Ibaraki 305-8573, Japan.

Single crystals of $EuFe_2As_2$ (Eu122) doped with 0.6-phosphorus ($EuFe_2As_{1.4}P_{0.6}$) were grown using the FeAs flux technique. A newly designed high-pressure cell adapting ceramic anvils was used to probe the competition among spin-density wave (SDW), collapsed phase and superconductivity in Eu122. The magnetic moment at low temperatures was measured using a SQUID magnetometer with lead (Pb) as the pressure marker. The maximum pressure that can be attained with this new design is 5 GPa. This new cell was used in conjunction with dc magnetization measurements and we show that $EuFe_2As_{1.4}P_{0.6}$ undergoes a pressure-induced tetragonal-to-orthorhombic structural transition coinciding with antiferromagnetic ordering. We found the applied pressure and temperature at each of these transitions were similar to those reported in literature measured by resistivity and in other SQUID pressure cell designs giving us the confidence to employ this set-up to study other systems. Research collaborations using this high-pressure facility are invited.

Tribute to CSIRO Scientists

T.R. Finlayson[a]

[a] *School of Physics, University of Melbourne, Victoria 3010, Australia.*

The aim of this invited presentation is to pay tribute to the four CSIRO colleagues, Drs. John Dunlop, Tony Farmer, Gerry Haddad and Don Price, who lost their lives in the horrific crash of a Robinson R44 helicopter, near Panorama House, Bulli Tops, Wollongong, on 21st March, 2013. Two of these scientists, Dunlop and Price, had been most enthusiastic supporters of and regular contruibutors to this Annual Condensed Matter and Materials Conference, since its inception in 1977. The presentation will briefly summarise the scientific careers of all four colleagues. The assistance of Drs. Stephen Collocott and Tony Murphy, CSIRO, Lindfield, in providing some of the details concerning their colleagues for the preparation of this tribute presentation, is acknowledged.

Toward an Accurate Description of Rare Gas Phases

P. Schwerdtfeger[a], A. Hermann[a], E. Pahl[a] and J. Wiebke[a]

[a] *Centre for Theoretical Chemistry and Physics, The New Zealand Institute for Advanced Study, Massey University Auckland, Auckland, New Zealand.*

Rare gas solids provide an ideal testing ground for the accurate many-body treatment of electron correlation through a many-body decomposition of the interaction potential. Here we present complete basis set (CBS) limit calculations for the fcc lattices of solid neon and argon, using second- to fourth-order Møller-Plesset theory, MP2-4, and coupled-cluster calculations, CCSD(T), to describe electron correlation within a many-body expansion of the interaction potential up to third order. A correct description of the three-body Axilrod-Teller-Muto term for the solid state is only obtained from third-order on in the many-body expansion of the correlation energy, correcting the severe underestimation of long-range three-body effects at the MP2 level of theory. The dilemma that all two-body interaction potentials prefer the hcp over the fcc structure is discussed. The performance of the methods with increasing pressure is analyzed, showing that the convergence of the Møller-Plesset series deteriorates as the electronic band gap decreases, resulting in rather large deviations for the equation of state (pressure-volume dependence). The application to the accurate determination of melting temperatures at high pressures is discussed.

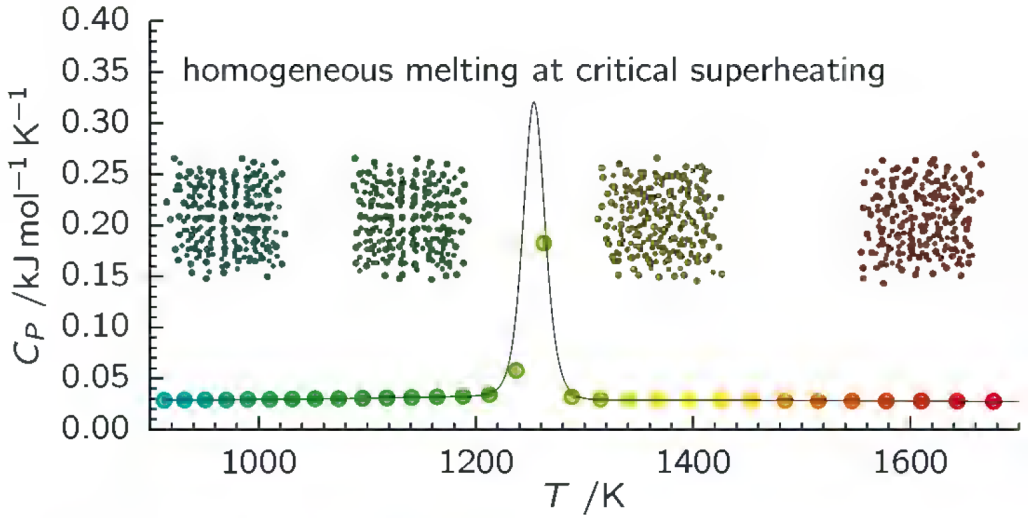

Figure 1. Temperature-dependence of the molar isobaric heat capacity C_P of argon at 10 GPa pressure. Also shown are snapshots of configurations of the Ar_{256} supercell below and above the homogeneous melting at critical superheating at a temperature of T^+ = 1254 K.
(from J. Wiebke, E. Pahl and P. Schwerdtfeger, *Angew. Chem.* **52**, 13202 (2013)).

Total State Designation for Electronic States of Periodic Systems

D. Andrae[a]

[a] *Institute of Chemistry and Biochemistry, Physical and Theoretical Chemistry, Freie Universität Berlin, Germany.*

The theory of electronic structure of solids has a large variety of tools at hand, from which it can choose to use the ones being (or seeming) most appropriate for a successful solution to a given problem. But the choice eventually made (wave-function-based or density-functional-based, level of treatment of electron correlation, etc.) sometimes appears to merely reflect the type of solid to be studied (molecular crystal, insulator, semiconductor, metal, etc.). Only little attention is given to the fact that a (much more) detailed description of the electronic state(s) of the total system (polymer, slab, crystal) plays, at best, only a minor role in many popular approaches to the problem. This is strange insofar as the clear identification and characterization of the electronic state(s) constitutes a sort of ``ultimate goal´´ of any quantum mechanical study of a system. An improvement of our theory of electronic structure in periodic systems with respect to total state characterization is highly necessary, also from a practical point of view. A better understanding of the possible total electronic states of a crystalline material may help a lot in understanding its behaviour in nanotechnological applications. It will also lead to a true density of (total) states, in contrast to the widely used density of (single particle) states.

Influence of Relativistic Effects on the Melting of Mercury

E. Pahl[a], F. Calvo[b] and P. Schwerdtfeger[a]

[a] *Centre for Theoretical Chemistry and Physics, INMS and NZIAS, Massey University Auckland, New Zealand.*

[b] *ILM, Université de Lyon and CNRS UMR 5306, France.*

Mercury, Hg, is the only elemental metal liquid at room temperature - the reasons for this phenomenon posed a long-standing puzzle in chemistry. Since the 80's the importance of relativistic effects in understanding the properties of heavier elements became clear: In the case of mercury, the valence (6*s*) electrons are stabilized due to relativity causing a very weak bonding in the mercury dimer and small clusters and it was speculated that also the low melting point of mercury at 234.32 K could so be explained.

By using parallel-tempering Monte-Carlo simulations we have now modelled the solid-liquid phase transition in mercury based on the so-called DIM (diatomics in molecules) interaction model. In this model, the complicated many-body effects in Hg are included approximately by expanding the Hamiltonian in a basis of the ground and the 12 lowest excited states of the Hg dimer [1]. A non-relativistic version of the DIM model was developed and both, the relativistic and non-relativistic models, were updated by using highly accurate, *ab initio* ground and excited potential curves of the Hg dimer [2,3].

The results showed that indeed relativistic effects, and more specifically scalar-relativistic relativistic ones, make Hg liquid at room temperature – without them mercury would melt more than 100°C higher than observed [4,5]!

[1] H. Kitamura, *Chem. Phys*. **325**, 207 (2006).

[2] F. Calvo, E. Pahl, P. Schwerdtfeger and F. Spiegelman, *J. Chem.Theory Comput.* **8**, 639 (2012).

[3] E. Pahl, D. Figgen, C. Thierfelder, K.A. Peterson, F. Calvo and P. Schwerdtfeger, *J. Chem. Phys.* **132**, 114301 (2010); E. Pahl, D. Figgen, A. Borschevsky, K.A. Peterson and P. Schwerdtfeger, *Theor. Chem. Acc.* **129**, 651 (2011).

[4] F. Calvo, E. Pahl, M.Wormit and P. Schwerdtfeger, *Angew. Chem. Int. Ed*. **52**, 7583 (2013).

[5] http://www.youtube.com/watch?v=NtnsHtYYKf0

Transport Models in Nanofluidics

G.R. Willmott[a,b]

[a] *Department of Physics, The University of Auckland, New Zealand.*

[b] *The MacDiarmid Institute for Advanced Materials and Nanotechnology, New Zealand.*

Nanofluidics, which involves fluid flows in and around submicron structures, has evolved from the established fields of microfluidics and nanotechnology. Nanofabrication provides the tools to build nanofluidic structures [1], and the field will be integral in efforts to understand complex biological interactions. Fluid flows are inherently laminar at small length scales, yet interesting and complex transport problems arise from a variety of potentially significant and concurrent effects – mechanisms, species and carriers, and geometries [2].

Here, nanofluidic transport will be discussed in the context of nanopore-based sensors. Such devices use 'resistive pulse sensing' to detect and analyse single nanoparticles, by examining the transient blockage of ionic current when the particle passes though the nanopore. Transport of both ions and nanoparticles are considered, while key mechanisms include electrophoresis, electro-osmosis, dielectrophoresis and pressure-driven flow. Molecular-scale nanopores are heavily studied for analysis of single molecules, particularly DNA, while sensors on the scale of ~100 nm are suitable for studying exosomes, emulsions and viruses. Overall transport dominance strongly depends upon experimental parameters [3].

Modelling approaches for molecular-scale transport are usually based on the space-charge model [2], which combines electrostatics with the Nernst-Planck and Navier-Stokes equations. For analysis of experiments using larger pores, a semi-analytical approach is probably more efficient [3]. There are applied research opportunities regarding dimensionless scaling, and validation of semi-empirical approaches. More fundamental nanofluidic challenges include understanding nanoscale wetting, disjoining pressure, and nanobubbles.

[1] C. Duan, W.Wang and Q. Xie, *Biomicrofluidics* **7**, 026501 (2013).

[2] R.B. Schoch, J. Han and P. Renaud, *Rev. Mod. Phys.* **80**, 839 (2008).

[3] G.R. Willmott, M.G. Fisk and J. Eldridge, *Biomicrofluidics* **7**, 064106 (2013).

Magnetic properties of rare-earth nitride heterostructures for MRAM devices

E.-M. Anton[a], B.J. Ruck[a], J.F. McNulty[a], F. Natali[a], S. Granville[b] and H.J. Trodahl[a]

[a] *The MacDiarmid Institute for Advanced Materials and Nanotechnology, School of Chemical and Physical Sciences, Victoria University of Wellington, Wellington 6140, New Zealand.*

[b] *The MacDiarmid Institute for Advanced Materials and Nanotechnology, Callaghan Innovation, Lower Hutt 5010, New Zealand.*

In recent years there is a growing demand for affordable and energy efficient memories, especially due to the drastically increased usage of mobile devices. New non-volatile memory (NVM) technologies therefore need to be developed, which keep the data safely stored without continuous power consumption. Promising emerging NVMs are magnetoresistive random access memories (MRAM), which are based on the difference in resistance between two stacked magnetic layers, depending if their magnetisations are aligned parallel or antiparallel. These magnetic tunnel junctions rely on a spin polarised current, a requirement for which the rare-earth nitrides (REN) seem ideal. Many RENs are ferromagnetic semiconductors which only conduct in the majority spin channel, giving rise to a highly spin polarised current and thus a large difference between the two resistance states. Moreover, the RENs show highly contrasting magnetic properties. SmN has a small magnetic moment and large coercive field exceeding 6 T, which makes it an ideal material for the reference layer, whereas GdN has a small coercive field of ~ 0.01 T enabling it to switch easily.

Thin film superlattices and bilayers of the two REN materials were made by physical vapour deposition and investigated by superconducting quantum interference device (SQUID) magnetometer, X-ray magnetic circular dichroism (XMCD) and polarised neutron reflectometry (PNR) to gain insights into their magnetic interlayer exchange. Whereas SQUID gives information about the integral magnetisation of the layer systems, XMCD can retrieve spin-, orbital- and element sensitive magnetic information, allowing to separate the magnetisation of the different layers. PNR is a depth resolved method, providing magnetic depth profiles across the constituent layers. The combination of these advanced experimental technologies provides insights into the magnetic interlayer exchange crucial to develop functional MRAM devices.

Magnetically driven electric polarization in frustrated magnetic oxide multiferroics

N. Narayanan[a,c], N. Reynolds[b], F. Li[a], A.M. Mulders[a], P. Rovillain[b,c], C. Ulrich[b,c], M. Bartkowiak[d], J. Hester[c], G. McIntyre[c] and W.D. Hutchison[a]

[a] *School of PEMS, UNSW Canberra, ACT, Australia.*

[b] *School of Physics, UNSW, Sydney, Australia.*

[c] *Bragg Institute, ANSTO, Sydney, Australia.*

[d] *HZB, Berlin, Germany.*

In multiferroics more than one ferroic order can coexist and in the present case we are interested in systems which exhibit simultaneous magnetic ordering and electric polarization (EP). Of particular interest are frustrated magnetic materials that exhibit an electric polarization that is strongly coupled to the magnetism [1]. Examples of such multiferroics are $RMnO_3$ (R= Tb, Dy), $Ni_3V_2O_8$, and $RbFe(MoO_4)_2$ [2-4]. This coupling can be utilized in applications such as magnetoelectric random access memory. Although technically relevant, the coupling mechanism between these two orders is complicated [1]. Whereas the magnetic ordering results from exchange interaction of unpaired spins, origins of EP coupled to the magnetic ordering depends on the interplay between lattice, orbital, spin and charge degrees of freedom. Several mechanisms such as the inverse Dzyaloshinskii-Moriya interaction, magnetostriction and coupling of the chirality to the crystal structure or a combination of them are currently discussed depending on the compound [2-5]. Additionally EP has ionic and electronic contributions. In the present work we investigate the coupling of magnetism to EP involving all three above mechanisms, in orthorhombic $DyMnO_3$ (DMO), $Cu_3Nb_2O_8$ and $Ba_3NiNb_2O_9$ with neutron powder diffraction (NPD), magnetization and heat capacity measurements focusing on the magnetic and multiferroic phase transitions. In order to investigate the role of the lattice distortion or equivalently the role of oxygen, isotope substitution of ^{16}O with ^{18}O was performed on DMO. All samples are prepared as single phases via the solid state route and NPD experiments are carried out at Wombat and at Echidna at OPAL.

[1] Y. Tokura *et al.*, *Adv. Mater*. **22**, 1554 (2010).

[2] R. Feyerherm *et al.*, *Phys. Rev. B* **73**, 180401 (R)(2006).

[3] M. Kenzelmann *et al.*, *Phys. Rev. Lett.* **95**, 087206 (2005), G. Lawes *et al.*, *Phys. Rev. Lett.* **95**, 087205 (2005).

[4] M. Kenzelmann *et al.*, *Phys. Rev. Lett.* **98**, 267205 (2007).

[5] R.D. Johnson *et al.*, *Phys. Rev. Lett.* **107**, 137205 (2011), J. Hwang *et al.*, *Phys. Rev. Lett.* **109**, 257205 (2012).

Exploring the Properties of Complex Layered Tin Cluster Compounds

M. Allison[a], S. Liu[b], C. Ling[b], G. Stewart[c] and T. Söhnel[a]

[a] *School of Chemical Sciences, University of Auckland, New Zealand.*

[b] *School of Chemistry, University of Sydney, NSW, Australia.*

[c] *School of PEMS, UNSW@AFDA, Canberra, Australia.*

Layered oxide structures have been observed to strongly show effects such ferroelectricity and giant magnetoresistance in semiconducting materials. Oxide materials containing Fe, Mn and Co have additionally been shown to exhibit novel multiferroic properties which could be extremely beneficial for future data storage devices. The parent compound for this presentation $Fe_4Si_2Sn_7O_{16}$ [1] provides a novel situation in oxide compounds. It can be described as a composite of intermetallic ($FeSn_6$) clusters and (FeO_6)/(SnO_6) oxide layers within the one structure. SiO_4 tetrahedra separate these layers which leads to electronic and magnetic isolation of the repeated layers by about 7 Å resulting in a nearly perfectly 2D oxide system comparable to a one layer thick oxide "thin film". In this study we have systematically replaced the iron positions of the oxide layer in the parent compound with divalent Mn in order to study the change in material properties. Refinements of the structures from Synchrotron and neutron powder diffraction patterns determined changes in lattice parameters which indicate that the MSn_6 octahedral layer in these materials may contain manganese instead of iron. ^{57}Fe-Mössbauer spectra (Fig. 1) seem to confirm a clear preference of Mn sitting in the oxide layers and Fe in the cluster layers. In this presentation we will show the current results into the effects this elemental substitution has on the crystal and magnetic structures of this family of compounds, additionally we will present some of the novel results from the spectroscopic and magnetic characterisation of these materials.

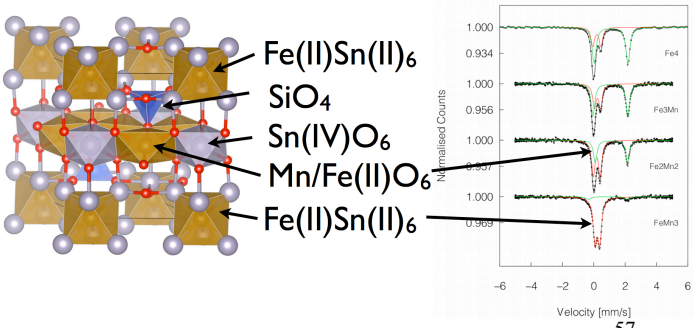

Figure 1. Crystal structure (left) and ^{57}Fe-Mössbauer spectra of $FeFe_{3-x}Mn_xSi_2Sn_7O_{16}$.

[1] T. Söhnel, P. Böttcher, W. Reichelt and F.E. Wagner, *Z. Anorg. Allg. Chem.* **624**, 708 (1998).

Low-temperature magnetic structure of $Ca_2Fe_2O_5$ determined by single-crystal neutron diffraction

J.E. Auckett[a], G.J. McIntyre[b], M. Avdeev[b] and C.D. Ling[a]

[a] *School of Chemistry, The University of Sydney, NSW 2006, Australia.*

[b] *Bragg Institute, ANSTO, NSW 2232, Australia.*

$Ca_2Fe_2O_5$ is a canted antiferromagnet (T_N = 720 K) which displays an anomalous elevation in its magnetic susceptibility for 60 K < T < 140 K. [1] Based on susceptibility measurements performed on oriented single crystals, Zhou *et al*. [2] proposed a reorientation of the antiferromagnetic (AFM) easy-axis from the crystallographic *a* axis to the *c* axis below 40 K, proceeding *via* a region of minimal magnetocrystalline anisotropy in the anomalous temperature interval.

In order to test this proposition, we have refined the atomic and magnetic structure of $Ca_2Fe_2O_5$ against high-quality neutron Laue diffraction data collected on floating-zone-grown single crystals between 10 K and 300 K. An *ad hoc* sample mount was designed to apply a small (~35 Oe) magnetic field to the sample, ensuring perfect compatibility with the magnetic susceptibility data, which were also collected in a small field. Our refinements against both zero-field and in-field diffraction data reproduce the G-type AFM structure of $Ca_2Fe_2O_5$ excellently at room temperature, including the known ferromagnetic canting. Careful examination of the refinement results reveals that the material is in fact best described by the room-temperature magnetic structure at all measured temperatures, though in the intermediate temperature interval (measured at T = 100 K) the spins may be less well-ordered due to competing sublattice interactions.

[1] A. Maljuk, J. Strempfer and C.T. Lin, *J. Cryst. Growth* **258**, 435 (2003).

[2] H.D. Zhou and J.B. Goodenough, *Solid State Sci.* **7**, 656 (2005).

Magnetoelectric coupling in isotopically subtituted $TbMn^{16/18}O_3$ and RMn_2O_5 (R = Tb, Ho, and Y) explored by Raman light scattering

P.J. Graham[a], P. Rovillain[a,b], A.M. Mulders[c], M. Yethiraj[b], D. Argyriou[d]
E. Pomjakushina[e], K. Conder[e], M. Kenzelmann[e] and C. Ulrich[a,b]

[a] *School of Physics, University of New South Wales, New South Wales 2052, Australia.*

[b] *The Bragg Institute, ANSTO, Lucas Heights, NSW 2234, Australia.*

[c] *School of PEMS, UNSW Canberra, Canberra, ACT 2600, Australia.*

[d] *European Spallation Source ESS AB, S-22100 Lund, Sweden.*

[e] *Paul Scherrer Institute, CH-5232 Villigen, Switzerland.*

Multiferroic materials demonstrate excellent potential for next-generation multifunctional devices, as they exhibit coexisting ferroelectric and magnetic orders. In magnetoelectric multiferroics, the existing coupling between both properties offers a unique possibility to manipulate ferroelectricity via magnetic order and vice versa opening unexpected new potential for high-density information storage and sensor applications. At present, the underlying physics of the magnetoelectric coupling is not fully understood, and competing theories propose conflicting experimental outcomes. By studying the lattice and magnetic excitations via Raman light scattering, we have obtained insight into the various coupling mechanism in multiferroic materials like $TbMnO_3$ and RMn_2O_5 (R = Tb, Ho, and Y).

Raman light scattering experiments were performed on $TbMn^{16/18}O_3$ oxygen-isotope-substituted single crystals. Pronounced anomalies in sign and strength of the phonon shifts at the magnetic phase transition at 43 K and the ferroelectric phase transition at 28 K indicate an interaction between the lattice and the magnetic and electric ordering, providing information about the nature of the competing magnetic interactions present in this compound.

Our Raman light scattering experiments on RMn_2O_5 (R = Tb, Ho, and Y) revealed opposite spin-phonon interactions for R = magnetic Tb and Ho, in contrast to non-magnetic Y. This offers a unique insight in the various competing spin exchange interactions, which lead to the highly frustrated spin structure and finally the multiferroic properties of RMn_2O_5. Using single crystal neutron diffraction at high magnetic fields (up to 11 T) we were able to determine a theoretically proposed but hitherto unobserved crystallographic phase transition, which naturally explains the origin of the ferroelectric polarization.

Stress Controlled Metal-to-Insulator Transitions in Thin Film Vanadium Oxides

J. Laverock[a], A.R.H. Preston[a], D. Newby, Jr.[a], K.E. Smith[a,b], S. Sallis[c], L.F.J. Piper[c], S. Kittiwatanakul[d], J. Lu[e], S.A. Wolf[d,e], M. Leandersson[f] and T. Balasubramanian[f]

[a] *Department of Physics, Boston University, Boston, Massachussetts,USA.*

[b] *School of Chemical Sciences, University of Auckland, Auckland, New Zealand.*

[c] *Department of Physics, Binghamton University, Binghamton, NY,USA.*

[d] *Department of Physics, University of Virginia, Charlottesville, VA, USA.*

[e] *Department of Materials Science and Engineering, University of Virginia, VA,USA.*

[f] *MAX-lab, Lund University, SE-221 00 Lund, Sweden.*

The metal-insulator transition (MIT) in VO_2 is of both fundamental and technical interest, the former due to important lingering questions about its origins, and the latter due to possible applications in electronic devices such as ultrafast optical switches. In bulk VO_2, a structural distortion accompanies the transition from the metallic (rutile) to the insulating (monoclinic) phase, which is known to impose a significant bottleneck on the timescale of the transition. Recently, the ability to control the transition temperature through chemical doping and/or nanoscale engineering has heralded renewed interest in the potential application of VO_2 as a novel functional material. Whereas the mechanism of the MIT in bulk VO_2 is now reasonably well understood, the situation is less clear with a large applied strain to the lattice. I will present the results of synchrotron radiation-excited photoemission, x-ray emission, and x-ray absorption spectroscopy studies of the MIT in strained VO_2 thin films. Our results reveal that the MIT may be driven towards a purely electronic transition, (i.e. one which does not rely on the Peierls dimerization), by the application of mechanical strain. Comparison with a moderately strained system, which does involve the lattice, demonstrates a crossover from Peierls-like to Mott-like transitions. Our observations have important implications for novel functional material engineering of VO_2, suggesting a route towards circumventing the structural bottleneck in the ultrafast timescale of the MIT.

Research supported in part by the U.S. Department of Energy under Grant No. DE-FG02-98ER45680.

Freudenbergite – a New Example of Electron Hopping

J.D. Cashion[a], A. Lashtabeg[b], E.R. Vance[c], D.H. Ryan[d] and J. Solano[e]

[a] *School of Physics, Monash University, Melbourne, Victoria 3800, Australia.*

[b] *Nanolytical, PO Box 21, The Gap, Brisbane, Qld 4061, Australia.*

[c] *Australian Nuclear Science and Technology Organisation, Menai, NSW 2234, Australia.*

[d] *Physics Department, McGill University, Montreal, Québec H3A 2T8, Canada.*

[e] *School of Chemistry, Monash University, Melbourne, Victoria 3800, Australia.*

We have recently [1] found that samples of freudenbergite with a mixed ferric-ferrous composition exhibit considerable electron hopping at room temperature as evidenced in ^{57}Fe Mössbauer spectra. Freudenbergite is most commonly ferric with composition $Na_2Fe^{3+}{}_2Ti_6O_{16}$, but can be ferrous, $Na_2Fe^{2+}Ti_7O_{16}$, with a complete solid solution possible between these end members. Since both iron and titanium can have two valences, it is of importance to understand whether the electron hopping is between neighbouring Fe^{2+} and Fe^{3+} ions or whether it involves titanium in the form

$$Fe^{2+} + Ti^{4+} \leftrightarrow Fe^{3+} + Ti^{3+}.$$

To try and distinguish between these possibilities, we will discuss the differences in the optical reflectance spectra between the black, electron hopping samples and the grey-green static samples. In addition, we will show new Mössbauer spectra for different freudenbergite compositions. Application of a magnetic field of 1.6 T did not change the proportion of the electron hopping contribution. The measured hyperfine field was enhanced above the applied field for both sites. Without the applied field, the ferrous contribution had to be fitted to two doublets, possibly representing the M1 and M2 sites, but with the applied field, they were able to be fitted as a single contribution. For the ferric sites, the M1 and M2 contributions were indistinguishable in both cases. On strongly heating a mixed valence sample, nearly half the iron was expelled as hematite, while the remainder was still contained as a titanate.

[1] J.D. Cashion, A. Lashtabeg, E.R. Vance and D.H. Ryan, *Hyperfine Interact.* (2013) DOI: 10.1007/s10751-013-0964-9.

Crystal and magnetic structure of Li_2MnSiO_4 and Li_2CoSiO_4 characterized by neutron diffraction measurement

Z. Mohamed[a,c], M. Avdeev[b] and C.D. Ling[a]

[a] *School of Chemistry, The University of Sydney, NSW 2006, Australia.*

[b] *Bragg Institute, Australian Nuclear Science and Technology Organisation, Lucas Heights, NSW 2234, Australia.*

[c] *Faculty of Applied Sciences, Universiti Teknologi MARA, 40450 Shah Alam, Malaysia.*

Lithium orthosilicates compounds Li_2MnSiO_4 and Li_2CoSiO_4 were synthesized by solid state reaction and characterized using X-ray powder diffraction, magnetic susceptibility measurement, heat capacity and neutron powder diffraction. The magnetic susceptibility measurement shows that Li_2MnSiO_4 and Li_2CoSiO_4 obey Curie Weiss behaviour at high temperature and undergo antiferromagnetic ordering below T_N = ~12 K and ~13 K respectively. The magnetic structures of both compound have been solved for the first time using low temperature neutron diffraction data. The results reveal that the magnetic structure of Li_2CoSiO_4 can be described as antiferromagnetic quasi-layers stacked along the *a*-axis with the magnetic moment ~2.92 μ_B aligned parallel to the *a*-axis. The magnetic structure of Li_2MnSiO_4 showed quite different behaviour compared to Li_2CoSiO_4. The origin of this complex magnetic structures will be discussed in terms of super-superexchange interactions among the transition metal ions, mediated by bridging SiO_4 tetrahedra.

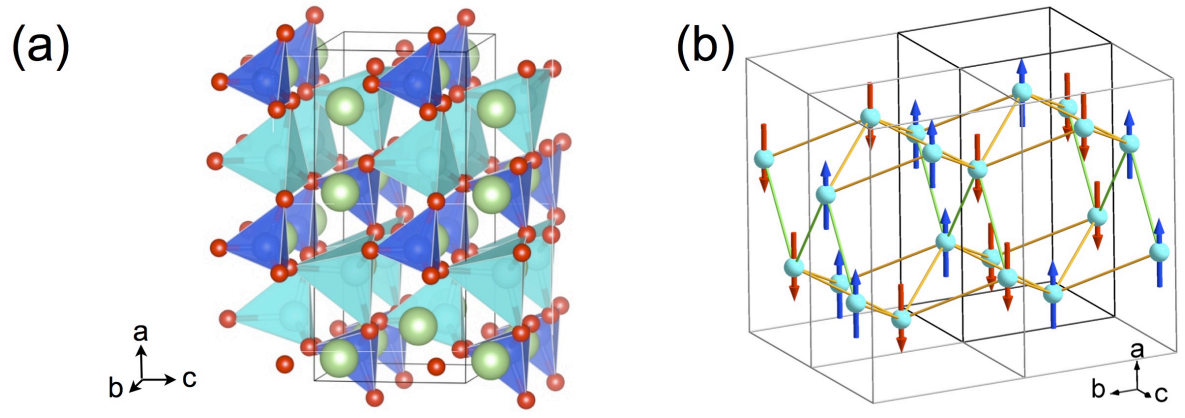

Figure 1. (a) Crystal and (b) Magnetic structure of Li_2CoSiO_4. Co atoms are cyan, Si are blue, Li are green and O are red.

[1] C. Masquelier and L. Croguennec, *Chem. Rev.* **113**, 6552 (2013).

[2] A. West and F. Glasser, *J. Solid State Chem.* **4**, 20 (1972).

Exotic Physics in Neutron Laue Diffraction

G.J. McIntyre[a]

[a] *Australian Nuclear Science and Technology Organisation, Lucas Heights NSW 2234, Australia.*

Neutron Laue diffraction has been reborn thanks largely to the success of X-ray Laue diffraction for protein crystallography at synchrotrons and to the development of efficient large-area image-plate detectors. The Laue technique with thermal neutrons is proving very successful for small-molecule crystallography on crystals frequently no larger than 0.1 mm^3, first on VIVALDI at the Institut Laue-Langevin in Grenoble, France [1], and now on KOALA on the OPAL reactor at ANSTO in Lucas Heights, Australia [2], and is opening neutron diffraction to fields of structural chemistry previously deemed impossible [3].

The high-resolution volumetric view of reciprocal space is particularly advantageous in the detection of phase changes, incommensurability and twinning, but does come at a price though: all scattering from the sample, inelastic as well as elastic, contributes to the observed Laue patterns. This can however reveal valuable physical information about the sample beyond the crystal structure, but careful analysis is required to extract the details in the two-dimensional projection intrinsic to Laue patterns.

Examples of exotic physics in neutron Laue diffraction experiments described here include:

- Rods of scattering from two-dimensional magnetic ordering [4]
- Observation of phonon scattering and determination of sound velocities
- Observation of quasi-Kossel lines in experiments with diamond-anvil cells
- Spin polarization of hydrogen nuclei to reduce the incoherent background in crystallographic studies of samples with high hydrogen content [5]

[1] G.J. McIntyre *et al.*, *Physica B* **385-386,** 1055-1058 (2006).

[2] N. Sharma *et al*., *J. Phys.: Conf. Ser*. **251,** 012028 (2010).

[3] A.J. Edwards, *Aust. J. Chem*. **64**, 869-872 (2011).

[4] E.M.L. Chung *et al.*, *J. Phys.: Condens. Matter* **16,** 7837-7852 (2004).

[5] F. Piegsa *et al.*, *J. Appl. Cryst*. **46,** 30-34 (2013).

Condensed phase studies at the THz/Far-IR Beamline at the Australian Synchrotron

D. Appadoo[a], C. Ennis[a] and R. Plathe[a]

[a] *The Australian Synchrotron, 800, Blackburn Rd, Clayton, VIC 3168, Australia.*

The THz/Far-IR beamline at the Australian Synchrotron is coupled to a Bruker IFS125HR FT spectrometer equipped with a variety of optical components which can cover the spectral range from 5 to 5000 cm^{-1}. Experiments from a variety of fields such as atmospheric and astrophysical science, geology, electrochemistry, nano-materials as well as biology have been successfully conducted at the beamline.

There is a range of instruments to accommodate the diverse requirements of the User community. For gas-phase experiments, the beamline is equipped with multiple-pass optics gas-cells: one of which can be coupled to a furnace to study reactive species, while another can be cooled to liquid nitrogen or helium temperatures to study aerosols and cold gases. Users also have access to a couple of cryostats (one > 79 K, the other > 6 K), a grazing incidence angle optical setup and a near-normal accessory to study condensed phase systems, thin films and surface interactions.

The synchrotron infrared light offers a S/N advantage over conventional thermal sources, but this advantage varies to a great degree upon the spectral range, sample size and resolution dictated by the application. In this paper, the capabilities and performance of the THz/Far-IR beamline at the Australian Synchrotron will be presented as well as some applications undertaken at the beamline, and future developments.

Status Report on SIKA – Taiwan's Cold Neutron Triple-Axis Spectrometer at OPAL

C.M. Wu[a], G. Deng[b] and J.S. Gardner[a]

[a] *National Synchrotron Radiation Research Center, Hsinchu 30076, Taiwan.*

[b] *Bragg Institute, ANSTO, Lucas Heights, NSW, Australia.*

We will report on the current status of SIKA, the triple-axis spectrometer with the view of the cold source from the reactor beam hall in OPAL, at ANSTO. SIKA is funded by the National Science Council of Taiwan and currently being commissioned by the National Synchrotron Radiation Research Center.

To provide the flexibility for scientific applications, SIKA's analyser can operate in a flat or in a multiplexing mode when coupled to the one-dimensional PSD consisting of 48 vertical position-sensitive wires, allowing the simultaneous data collection over a specified range in (Q, E). This analyser can also operate in a horizontal focusing mode that directs the scattered neutrons into a single-detector. The entire analyser-detector system as is packed into a single, well shielded secondary spectrometer housing which significantly reduces the background. As a state-of-the-art triple-axis spectrometer, SIKA is also equipped with a full automated sample stage and a series of collimations (both soller and radial). Neutron polarisation will be available for the incident and scattered beams through 3He polarisers.

[1] www.ansto.gov.au/research/bragg_institute/facilities/instruments/sika

[2] www.ansto.gov.au/discovering_ansto/anstos_research_reactor/opal_capabilities/cold_neutron_source

[3] www.ncnr.nist.gov/instruments/**bt7**_new/**BT7**Instrument.pdf

[4] W.G. Williams, Polarized Neutrons, Clarendon Press, Oxford (1988).

Polarised Neutrons for Materials Sciences Research at the Australian Nuclear Science and Technology Organisation (ANSTO)

W.T. Lee[a], A. Studer[a], K. Rule[a], S. Danilkin[a], D. Yu[a], R. Mole[a], S. Kennedy[a], E. Gilbert[a], K. Wood[a], F. Klose[a] and T. D'Adam[a]

[a] *Australian Nuclear Science and Technology Organisation, Lucas Heights, NSW, Australia.*

Polarised neutron scattering has been used extensively to study magnetism in materials. Diffraction allows us to resolve the distribution and orientation of the magnetic moments down to the atomic scale. Inelastic scattering studies the magnetic excitations. The complex magnetic structure in magnetic nanoparticles is a hot topic for Small Angle Neutron Scattering (SANS). Novel magnetic thin film and multilayer are the sujects of neutron reflectometry. The technique is also increasingly being used to significantly enhance the signal-to-noise ratio in SANS measurement of hydrogen-rich materials. At ANSTO, polarised neutron option is currently available on both the SANS instrument "Quokka" (incident beam) and the reflectometer "Platypus" (incident and scattered beam). Recent technological advance of polarised Helium-3 based neutron spin-filter technique has opened up the possibility of using polarised neutrons on a wider range of instruments. In addition to enhancing the capabilities of Quokka (both incident and scattered beam for hydrogen-rich material and magnetic nanoparticle studies) and Platypus (wide-angle analysis for e.g. patterned magnetic surface structure), we are installing and testing polarised neutron equipmetn on the diffractometer "Wombat" and inelastic-scattering instruments "Taipan", "Pelican" and "Sika". This new capability will become available for experiments from July 2014. Futhermore, a new supermirror polariser is being commissioned on Pelican for polarised inelastic scattering work. In this presentation, examples illustrating the technique and use of polarised neutron scattering and the current status of installation and test on instruments will be provided.

Approaching Metallic Hydrogen by Stealth: Via the High-Hydrides

N.W. Ashcroft[a]

[a] *Laboratory of Atomic and Solid State Physics, Cornell University, Ithaca, USA.*

A metallic phase of hydrogen has been experimentally detected under shock conditions. Underlying it is a familiar founding many-body problem of condensed matter and materials physics namely that of N spin-1/2 interacting electrons in a rigorously neutralizing homogeneous background; this yields the anti-ferromagnetic Wigner crystal at low density and a uniform paramagnetic electron fluid at high. A counterpart problem described by exactly the same physics arises for protons where, in addition to a change in all signs, the mass of these Fermions is increased over those of the electrons by a factor 1836. If these two macroscopic systems are taken to co-occupy a common volume V, and all mutual Coulomb interactions now included, the quantum problem of the first element (hydrogen), then ensues. It can therefore be established as two coupled Fermion problems and its states exhibit a rich array of orderings as temperature and density are progressively increased. A prominent state is the metallic phase of hydrogen occurring at high compression and which is present, for example, in our giant planets. However, the problem can also be extended to include the addition of a second or third element, and if in relatively small proportions this leads to the high-hydrides. Their materials properties are also rich and in structural terms they include the possibility of arrangements arising where the quantum mechanics of the protons are quite central; the consequences may be described as *quantum dis-proportionation*. Further, the arguments suggesting the possibility of superconductivity at high temperatures in metallic hydrogen (via the standard phonon pairing mechanism) have their close parallels in the high-hydrides. Additionally if the polarizabilities of the ions of the added second or third elements are high there is also the possibility of further enhancement via quantized waves of polarization. In this way materials can be developed which are predominantly hydrogen but which may achieve metallicity at pressures lower than required for pure hydrogen.

Research supported by the US National Science Foundation.

Exploring Jupiter's icy moons with old techniques and big facilities – new insights on sulfuric acid hydrates

H.E. Maynard-Casely[a], M. Avdeev[a], H.E.A. Brand[b] and K.S. Wallwork[a]

[a] *Australian Nuclear Science and Technology Organisation, Lucas Heights NSW 2234, Australia.*

[b] *Australian Synchrotron, 800 Blackburn Road, Clayton, VIC 3168, Australia.*

Sulfuric acid hydrates have been proposed to be abundant on the surface of Europa [1], and hence would be important planetary-forming materials for this moon and its companions Ganymede and Callisto. Understanding of the surface features and subsurface of these moons could be advanced by firmer knowledge of the icy materials that comprise them [2], insight into which can be drawn from firmer knowledge of physical properties and phase behaviour of the candidate materials. We wish to present results from a study that started with the question 'What form of sulfuric acid hydrate would form on the surface of Europa?', with this study undertaken with *in situ* powder diffraction at Australian Synchrotron and ANSTO. We have used the Powder Diffraction beamline at Australian synchrotron [3] and the Echidna (High-resolution neutron powder diffraction) instrument of the Australian Nuclear Science and Technology Organization, [4] to obtain a number of new insights into the crystalline phases formed from H_2SO_4/H_2O mixtures.

These instruments have enabled the discovery a new water-rich sulfuric acid hydrate form [5], improved structural characterisation of existing forms [6] and charting of the phase diagram of this fundamental binary system [7]. This has revealed exciting potential for understanding more about the surface of Europa from space, perhaps even providing a window into its past.

[1] R.W. Carlson *et al.*, *Science*, **286**, 97 (1999).
[2] A.D. Fortes *et al.*, *Space Sci. Rev.*, **153**, 185 (2010).
[3] K.S. Wallwork *et al., AIP Conf. Proc.*, **879**, 879 (2007).
[4] Liss, K.D., *et al., Phys. B – Cond. Mat.*, **385**, 1010 (2006).
[5] H.E. Maynard-Casely *et al., J. Geophys Res: P*, **118**, 1895 (2013).
[6] H.E. Maynard-Casely *et al., J. App.Cryst.*, **45**, 1198 (2012).
[7] H.E. Maynard-Casely *et al., Icarus* (In Review).

Large room temperature magnetoresistance in nanogranular materials

J. Leveneur[a], G.V.M. Williams[b], J. Kennedy[a,b], T. Prakash[a] and P.P. Murmu[a]

[a] *National Isotope Centre, GNS Science, PO Box 31312, Lower Hutt 5010, New Zealand.*

[b] *The MacDiarmid Institute for Advanced Materials and Nanotechnology, SCPS, Victoria University, PO Box 600, Wellington 6140, New Zealand.*

Magnetoresistance and spin transport have raised a lot of interest in the past decades as they allow for the miniaturisation of high sensitivity magnetic field sensors and new electronic devices [1]. Magnetoresistance can occur in nanogranular materials and have different origins. For instance, spin tunnelling magnetoresistance happens when two ferromagnetic nanoparticles with some degree of electronic spin polarisation are separated by a thin insulator layer. This leads to a negative magnetoresistance that saturates for high magnetic fields. Lorentz-force like and geometric mechanisms lead to positive magnetoresistances and can show no saturation for magnetic fields as high as 9 T [2,3]. However, the magnetoresistance behaviour is often complex and can involve more than one mechanism as well as depending strongly on the investigated systems. Therefore, there is an interest in developing further magnetoresistive nanomaterials in order to improve our understanding of the underlying mechanisms.

In this report we present the results from structural, magnetic and magnetotransport measurements on several nanogranular systems. They were made by low energy ion implantation and electron beam annealing, arc-discharge, and chemical methods. Ferromagnetism and superparamagnetism were observed. The resultant magnetoresistance mechanisms with be discussed that include spin tunnelling magnetoresistance and a Lorentz force like magnetoresistance arising from the current injection region.

[1] I. Žutić, J. Fabian and S. Das Sarma, *Rev. Mod. Phys.* **76**, 323 (2004).

[2] F. Xiu, Y. Wang, K. Wong, Y. Zhou, X. Kou, J. Zou, and K.L. Wang, *Nanotechnology* **21**, 55602 (2010).

[3] J. Leveneur, J. Kennedy, G.V.M. Williams, J. Metson, and A. Markwitz, *Appl. Phys. Lett.* **98**, 053111 (2011).

Magnetic order in gadolinium manganite probed by ^{155}Gd-Mössbauer spectroscopy

G.A. Stewart[a] and G. Wortmann[b]

[a] *School of Physical, Environmental and Mathematical Sciences, UNSW Canberra, Australian Defence Force Academy, PO Box 7916, Canberra BC 2610, Australia.*

[b] *Department of Physics, University of Paderborn, Paderborn 33098, Germany.*

The orthorhombic manganites $RMnO_3$ (R = Gd, Tb, Dy) remain of considerable research interest because of their multiferroic behaviour. From an experimental point of view, $GdMnO_3$ differs from the others in that Gd is an extremely strong absorber of neutrons and is not amenable to neutron diffraction investigations of its magnetic structure. Nevertheless, from bulk single crystal magnetization [1] and x-ray diffraction measurements [2], we know that the Mn moments first undergo a transition to an incommensurate (sinusoidal collinear) arrangement at T_{IC} = 42 K. Below T_{CA} = 20 K, they then lock into a canted A-type antiferromagnetic (AFM) structure with weak ferromagnetism (FM) in the b-direction (Pnma notation). It was also concluded that the Gd moments order magnetically in their own right at T_{Gd} = 6 - 7 K [1]. More recently, x-ray magnetic resonant scattering (XMRS) was used to probe the local moment at the Gd site [2]. It was confirmed that the Gd moments order at T_{Gd} ≈ 7 K with a possible further modification of the magnetic structure at about T* = 4 - 5 K.

In this present work, ^{155}Gd-Mössbauer spectroscopy is used to probe the magnetic hyperfine field at the ^{155}Gd nucleus. The magnetic exchange field increases markedly at T_{Gd} and the Gd^{3+} moment at 1.8 K is evidently close to its saturation value of 7 μ_B. A simple point charge model estimate of the lattice electric field gradient generates likely alignments of the Gd moment. These are then compared with predictions based on the earlier magnetisation and XRMS data [1,3].

[1] A.B. Hemberger, *Phys. Rev. B* **40**, 024414 (2004).

[2] T. Arima, T. Goto, Y. Yamasaki, S. Miyasaka, K. Ishii, M. Tsubota, T. Inami, Y. Murakami and Y. Tokura, *Phys. Rev. B* **72**, 100102(R) (2005).

[3] R. Feyerherm, E. Dudzik, A.U.B. Wolter, S. Valencia, O. Prokhnenko, A. Maljuk, S. Landsgesell, N. Aliouane, L. Bouchenoire, S. Brown and D.N. Argyriou, *Phys. Rev. B* **79**, 134426 (2009).

Enigma of Resonant Inelastic X-ray Scattering (RIXS) data for cuprates

O.P. Sushkov[a]

[a] *School of Physics, University of New South Wales, New South Wales 2052, Australia.*

There have been a dramatic progress in RIXS techniques over the pastdecade. RIXS data for cuprate superconductors became available during pasttwo years. The data map magnetic excitations in the energy range larger than 100meV and for all possible doings, from undoped to overdoped.

The magnetic excitations are completely unexpected and contradict to allexisting theoretical models. The contradiction is especially strong in theoverdoped regime which previously was thought to be close to the Normal Fermi Liquid. I will overview the RIXS data and explain what is striking in the data from the theoretical point of view.

Upper critical and irreversible fields of polycrystalline $CeFeAsO_{1-x}F_x$ superconductors

S.V. Chong[a], G.V.M. Williams[b] and S. Sambale[a,b]

[a] *MacDiarmid Institute for Advanced Materials and Nanotechnology, Callaghan Innovation Research Ltd., P.O. Box 31310, Lower Hutt 5040, New Zealand.*

[b] *MacDiarmid Institute for Advanced Materials and Nanotechnology, School of Chemical and Physical Sciences, Victoria University of Wellington, P.O. Box 600, Wellington, New Zealand.*

We have investigated the upper critical field (H_{c2}), irreversible field (H_{irr}) and critical current density (J_c) of polycrystalline samples of Ce oxypnictide at different doping levels (x = 0.13 to 0.25). H_{c2} was obtained from temperature dependent resistivity measurements with increasing applied magnetic field. Critical field values as high as 150 Tesla were observed with a decreasing trend as the doping level shifts from a slightly under-doped state to the highly over-doped region. The irreversible fields of as-prepared polycrystalline samples were lower in this superconductor compared with other rare-earth oxypnictides, with values below 3 Tesla at 20 K. However, H_{irr} in the magnetic-field aligned samples with the c-axis parallel to the applied magnetic field show a much higher H_{irr} when compared with non-aligned samples. Furthermore, H_{irr} and the coherence length, $\xi(0)$ were found to increase with increasing doping. The origin of irreversibility was studied by determining the exponent 'n' extracted from plots of $\log_{10}(H_{irr})$ versus $\log_{10}(1-T/T_c)^n$. We found that H_{irr} follows a 3D vortex lattice-melting model similar to the other low anisotropic iron-based superconductors. Preliminary J_c measurements from field-loop magnetization measurements show intragrain self-field J_c values as high as 10^6 A/cm^2, which is consistent with that previously found in underdoped (x = 0.10) Ce-oxypnictide [1].

[1] S.V. Chong, T. Mochiji, S. Sato and K. Kadowaki, *J. Phys. Soc. Japan: Suppl. C* **77**, 27 (2008).

Phonons in a highly-correlated electron system: the heavy-fermion superconductor $CeCu_2Si_2$

M. Loewenhaupt[a], S. Danilkin[b], L. Capogna[c], A. Schneidewind[d], O. Stockert[e] and K. Hradil[f]

[a] *Institut für Festkörperphysik, Technische Universität Dresden, 01062 Dresden, Germany.*

[b] *Bragg Institute, ANSTO, Kirrawee DC, NSW 2232, Australia.*

[c] *Institut Laue-Langevin, 38042 Grenoble Cedex 9, France.*

[d] *Jülich Center for Neutron Science at FRM II, 85747 Garching, Germany.*

[e] *Max-Planck-Institut für Chemische Physik fester Stoffe, 01186 Dresden, Germany.*

[f] *Röntgenzentrum, TU Wien, 1060 Wien, Austria.*

$CeCu_2Si_2$ crystallizes in the tetragonal $ThCr_2Si_2$-type structure with 5 atoms in the primitive unit cell. It exhibits non-conventional superconductivity driven by low-energy magnetic excitations [1]. The Ce^{3+} Hund's rule J=5/2 ground state is split by the action of the crystalline electric field into 3 doublets, with two excited doublets forming a quasi-quartet at around 30 meV [2]. Except for Raman data [3] no information about the lattice dynamics was available up to date. We therefore performed inelastic neutron scattering at low temperatures (3 K and 10 K) on a large single crystal on the thermal triple-axis spectrometers PUMA (FRM II) and TAIPAN (OPAL) to determine the phonon dispersion relations in the [001/110] plane. The measured dispersion curves will be compared with ab-initio DFT calculations. In addition we could refine the crystal field level scheme resulting in the observation that the excited quasi-quartet actually consists of two considerably broadened doublets situated at around 28 meV and 35 meV, respectively.

[1] O. Stockert, J. Arndt, E. Faulhaber, C. Geibel, H. S. Jeevan, S. Kirchner, M. Loewenhaupt, K. Schmalzl, W. Schmidt, Q. Si and F. Steglich, *Nature Physics* **7**, 119 (2011).

[2] E.A. Goremychkin and R. Osborn, *Phys. Rev. B* **47**, 14280 (1993).

[3] S.L. Cooper, M.V. Klein, Z. Fisk and J. L. Smith, *Phys. Rev. B* **34**, 6235 (1986).

The thermodynamics of high-Tc superconductors

J. Tallon[a]

[a] *Robinson Research Institute, Victoria University of Wellington, P.O. Box 31310, Lower Hutt 5040, New Zealand.*

Thermodynamics presents a powerful theoretical tool which imposes strong constraints on spectroscopic behaviour independent of microscopic mechanism. This is particularly the case for superconductors. This talk will focus on high-temperature superconductors and will illustrate how: (i) thermodynamics can uncover normal-state behaviour that would occur if superconductivity could be suppressed, (ii) the crucial effects of impurity scattering on suppressing superfluid density and transition temperature can be fully accounted for, again with no recourse to microscopic mechanism, (iii) energy gaps in the density of states can be extracted, and (iv) the most important property for applications, critical current density, can be specified as a function of temperature and doping.

ABSTRACTS

Poster Presentations

First–principle study of palladium-defect pairing in doped Si

A.A. Abiona[a,*] and H. Timmers[a]

[a] *School of Physical, Environmental and Mathematical Sciences, The University of New South Wales, Canberra Campus, ACT 2602, Canberra, Australia.*

The electric field gradient (EFG) measured by hyperfine interaction techniques, e.g. time-differential perturbed angular correlation (TDPAC), provides relevant information about the interaction of probe atoms like ^{100}Pd/^{100}Rh with other defects. TDPAC study of palladium (Pd) in doped Si identified two possible Pd-defect pairings. Pd-vacancy pairing was observed in n-type Si irrespective of the dopant (P, As and Sb) type while Pd-B pairing was observed in B-doped p-type silicon [1, 2]. In Ge, however, TDPAC measurements confirmed that Pd pairs with vacancy in both n- and p-type dopants (Sb and Ga) [3]. The question that arises is why is Pd pairing with dopant in p-type Si but with vacancy in p-type Ge?

TDPAC data interpretation and assigning of a particular defect configuration to the EFG of the defect complex is a very difficult task. This paper aims at complementing the understanding of the pairing of Pd with defects in silicon using Density Functional Theory (DFT). The DFT calculations confirmed the observed palladium-defect pairing in both the n- and p-type Si. However, the Pd atom is located on bond-centred site in Si instead of on the substitutional site as observed in n-type Si. Based on the calculations, we deduce that Pd occupies the interstitial site to pair with B in B-doped Si because of the small atomic size of B relative to its host material Si.

[1] R. Dogra *et al.*, *Hyperfine Interact.* **177,** 33 (207).

[2] R. Dogra *et al.*, *J. Electron. Mater.* **38,** 623 (2009).

[3] A.A. Abiona, W. Kemp and H. Timmers, *Hyperfine Interact.* **221**, 65-72 (2012).

* *On leave from Centre for Energy Research and Development, Obafemi Awolowo University, Ile-Ife, Nigeria.*

M/TiO_2 Photocatalysts (M=Au, Pd, Pt and Au-Pt) for H_2 Production from Ethanol-Water Mixtures

Z.H.N. Al-Azri[a,b] and G.I.N. Waterhouse[a,b]

[a] *School of Chemical Sciences, The University of Auckland, Auckland, New Zealand.*

[b] *The MacDiarmid Institute for Advanced Materials and Nanotechnology, New Zealand.*

In this study, the activity of M/TiO_2 photocatalysts (M = Au, Pd, Pt and bimetallic Au-Pt) for hydrogen (H_2) production from ethanol-water mixtures (80 vol.% CH_3CH_2OH) under UV irradiation was investigated and compared. Metal loadings were in the range 0-4 wt.%. Nanocrystalline TiO_2 (Evonik P25, S_{BET} = 50 m^2g^{-1}) was used as the support phase. Results demonstrate that the photocatalytic activity of M/TiO_2 photocatalysts for H_2 production from aqueous ethanol solutions depends on many factors, including (i) the metal co-catalyst; (ii) the metal loading on the TiO_2 support; (iii) the oxidation state of the noble metal, and (iv) the strength of the metal-support interaction (MSI) [1,2]. Pd/TiO_2 photocatalysts exhibited the highest activity for H_2 production, with the optimum loading being ~0.5 wt.% (H_2 production rate of 49 mmol g^{-1} h^{-1}). For Pt/TiO_2 and Au/TiO_2 photocatalysts, the optimum metal loadings were 1 wt.% and 2 wt.%, respectively, which afforded similar H_2 production rates (33-35 mmol g^{-1} h^{-1}). Bimetallic $Au-Pt/TiO_2$ photocatalysts showed lower H_2 production activity compared to either Au/TiO_2 or Pt/TiO_2 photocatalysts, indicating that no synergy exists between the co-loaded metals under the applied test conditions. TEM data showed that the Pd and Pt cocatalysts were highly dispersed over the TiO_2 support, with an average particle size less than 2 nm. For Au/TiO_2, the MSI was weaker and thus the average metal nanoparticle size was larger (6 ± 2 nm) and the metal nanoparticle more spherical in shape. XPS analyses confirmed the presence of zero valent metal on the surface of the photocatalysts. The noble metal co-catalysts function as an electron sinks to suppress electron-hole pair recombination in TiO_2 (confirmed through photoluminescence measurements) as well as provide active centres for photocatalytic H_2 generation.

[1] M.A. Nadeem, M. Murdoch, G.I.N. Waterhouse, J.B. Metson, M.A. Keane, J. Llorca and H. Idriss, *J. Photochem. Photobiol. A–Chem.* **216**, 2-3 (2010).

[2] V. Jovic, Z. Al-Azri; W-T. Chen, D. Sun-Waterhouse, H. Idriss, G.I.N. Waterhouse, *Top. Catal.* **56**, 12 (2013).

Spin-reorientation in DyGa

R.A. Susilo[a], J.M. Cadogan[a], R. Cobas[a], S. Muñoz-Pérez[a] and M. Avdeev[b]

[a] *School of Physical, Environmental and Mathematical Sciences, UNSW Canberra at the Australian Defence Force Academy, Canberra, ACT, BC2610, Australia.*

[b] *Bragg Institute, ANSTO, PMB 1, Menai, NSW 2234, Australia.*

The RGa compounds crystallize in the orthorhombic CrB-type structure (*Cmcm* space-group), which can be viewed as a stacking of trigonal prisms along the crystallographic a-axis with rare earth atoms at the corners and the gallium atoms nearly at the centres. They order ferromagnetically with a Curie temperature ranging from a high of ~187 K in GdGa to a low of 15 K for TmGa.

DyGa is a ferromagnet with a Curie temperature (T_C) of 115(2) K. Based on single-crystal susceptibility measurements by Shohata [1], the easy direction of magnetic order was found to be along the c-axis. Recently, Zhang *et al.* [2] reported a weak shoulder at ~25 K in their magnetization data, which might correspond to a spin-reorientation . In this report, we present our neutron diffraction results to investigate the magnetic ordering of DyGa. Despite the substantial neutron absorption by the Dy (50 at.% of the sample), refinement of our neutron diffraction patterns confirms the c-axis order below T_C. Furthermore, upon cooling below 25 K we observe a canting of the Dy moments away from the c-axis towards the a-axis. At 3 K, the Dy moment is 9.8(2) μ_B and the Dy magnetic moments point in the direction θ = 22(2)° with respect to the crystallographic *c*-axis.

[1] N. Shohata, *J. Phys. Soc. Japan* **42,** 1873 (1977).

[2] X.Q. Zheng, J. Chen, J. Shen, H. Zhang, Z.Y. Xu, W.W. Gao, J.F. Wu, F.X. Hu, J.R. Sun and B.G. Shen, *J. Appl. Phys.* **111,** 07A917 (2012).

90° Magnetic Coupling in a NiFe/FeMn/biased NiFe Spin Valve Investigated by Polarised Neutron Reflectometry

S.J. Callori[a,b], T. Zhu[c] and F. Klose[a]

[a] *School of Physics, University of New South Wales, Sydney 2052, Australia.*

[b] *Bragg Institute, Australian Nuclear Science and Technology Organisation, Lucas Heights NSW 2234, Australia.*

[c] *Institute of Physics, Chinese Academy of Sciences, Beijing 100190, China.*

We have used the PLATYPUS reflectometer at ANSTO to perform polarised neutron reflectometry in order to investigate 90° magnetic coupling in a $Ni_{81}Fe_{19}/Fe_{50}Mn_{50}$/biased $Ni_{81}Fe_{19}$ spin valve system. Spin valves play an important role in current and developing technological systems, such as spintronics devices or magnetoresistive sensors. For the later usage, perpendicular coupling in a spin valve structure leads to a desired linear, reversible resistance response to an applied magnetic field.

The spin valve presented here consists of both free and exchange biased ferromagnetic $Ni_{81}Fe_{19}$ layers, the later of which is pinned by an antiferromagnetic $Ir_{25}Mn_{75}$ layer at low applied magnetic fields. The free $Ni_{81}Fe_{19}$ may be magnetically reversed under low fields, and standard magnetometry measurements on similar systems have suggested perpendicular orientation of the free and biased magnetisations at zero field [1]. Magnetometry measurements, however, are only capable of providing information about the magnetisation within a sample along the direction of the applied field. In contrast, polarised neutron reflectometry (PNR) is capable of resolving the in-plane magnetisation vectors both along and perpendicular to the applied magnetic field as function of layer depth. Here, PNR was used to obtain magnetic vector depth profiles of the spin valve at several applied fields, including low fields near the switching point of the free $Ni_{81}Fe_{19}$ layer. At these fields a large spin-flip signal was observed in the free layer, indicating magnetisation aligned perpendicular to the external field applied along the pinned layer magnetisation. Both the non-spin flip and spin-flip signals were also tracked around the free layer hysteresis loops and can be used to map the evolution of the free $Ni_{81}Fe_{19}$ layer during magnetic reversal.

[1] T. Liu, T. Zhu, J.W. Cai and L. Sun, *J. Appl. Phys.* **109**, 094504 (2011).

Synthesis and Characterisation of 3DOM ZIF-8 Thin-Films for Optical Gas Sensing Applications

H.K. Chahal[a], G.M. Miskelly[a] and G.I.N. Waterhouse[a]

[a] *School of Chemical Sciences, The University of Auckland, Auckland, New Zealand.*

By combining the inherent microporosity and high surface area of metal organic frameworks (MOFs) with the tuneable optical properties of photonic crystals, new and improved optical sensors could potentially be developed. This study describes the successful fabrication of three-dimensionally ordered macroporous (3DOM) ZIF-8 photonic crystal thin-films using the colloidal crystal templating technique. Colloidal crystal thin films comprising mondisperse carboxylate-terminated polystyrene (PS-COOH) colloids of diameter ~300 nm arranged on a face centred cubic lattice were first prepared. ZIF-8 nanoparticles were then grown in the interstitial voids of the colloidal crystal films, by immersion of the template in an aqueous solution containing Zn^{2+} and 2-methylimidazole (MeIM). Finally, the polymer template was removed by chemical etching in dimethylformamide (DMF) yielding iridescent 3DOM ZIF-8 photonic crystal films with high specific surface area (1767 m^2 g^{-1}). The optical properties of the 3DOM ZIF-8 films could be tuned by changing the diameter of the PS-COOH colloids used to prepare the templates. The photonic band gap (PBG) along the [111] direction red-shifted reversibly on exposure to alcohol vapours, suggesting these materials could be useful in gas sensing applications.

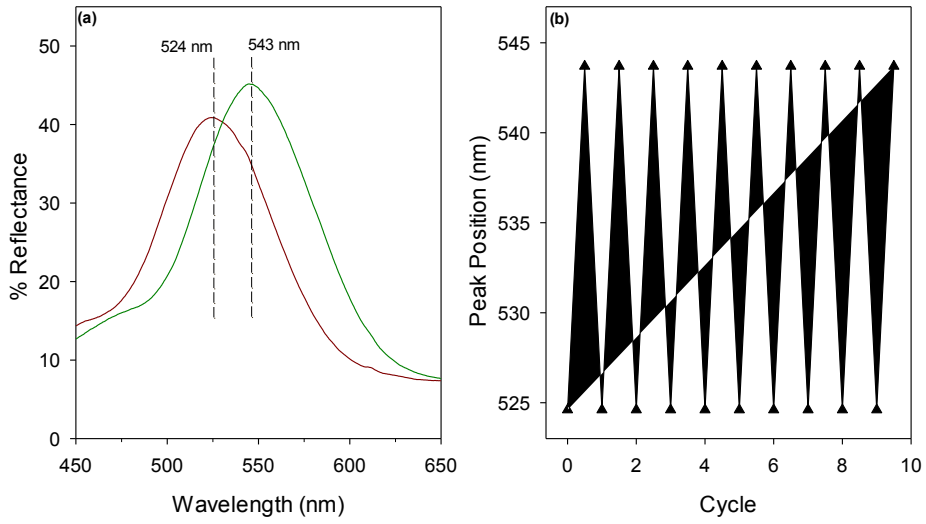

Figure 1. UV-Vis reflectance spectra of (a) 3DOM ZIF-8 thin film before and after exposure to saturated ethanol vapour. The PBG position is red-shifted upon ethanol sorption (b) Plots showing the PBG shift over repeat cycles of ethanol vapour and nitrogen gas exposure.

Novel M-Pt/C (M = Ru, Sn, RuSn) Electrodes for Direct Alcohol Fuel Cells

M. H. Chan[a] and G.I.N. Waterhouse[a]

[a] *School of Chemical Sciences, The University of Auckland, New Zealand.*

Direct methanol fuel cells (DMFCs) have attracted considerable attention as power sources due to their simplicity and high energy conversion efficiency. Strong economic and environmental pressures exist to develop efficient DEFCs since ethanol is renewable biofuel. This project is aimed at fabrication of novel M-Pt/C anode materials for DMFCs and DEFCs. Ru, Sn and Pt nanoparticles (total metl loading typically 5-20 wt.%) were deposited on 3-dimensionally ordered macroporous carbons fabricated by the colloidal crystal template technique, and the performance of the resulting M-Pt/C (M = Ru, Sn or both) anode materials systematically evaluated through electrochemical studies of ethanol oxidation in acidic media. XPS, XRD and TEM analyses confirmed the presence of metallic Pt, Ru and Sn on graphite like surface of the carbon support (BET area 800 m^2 g^{-1} in the absence of metal). Cyclic voltametry studies of methanol and ethanol oxidation in acidic media show the Pt/C materials fabricated are excellent electrocatalysts, with the electrocatalytic activity for alcohol oxidation increasing linearly with Pt loading in the range 0-15 wt.%. The electrocatalytic activity could be further enhanced through the introduction of Ru (1-2 wt. %) and Sn (1-2 wt. %) as promoters, whilst keeping the total metal content fixed at 10 wt.%. Electrocatalyst activity for methanol and ethanol oxidation decreased in the order RuSn-Pt/C > Ru-Pt/C > Sn-Pt/C > Pt/C. Pt can also be easily poisoned by CO formed from the electrooxidation of alcohols, but the presence of Sn and Ru on the electrocatalyst surface facilitate the oxidation of CO to CO_2, which explains the high electrocatalytic activity realised in the trimetallic RuSn-Pt/C system.

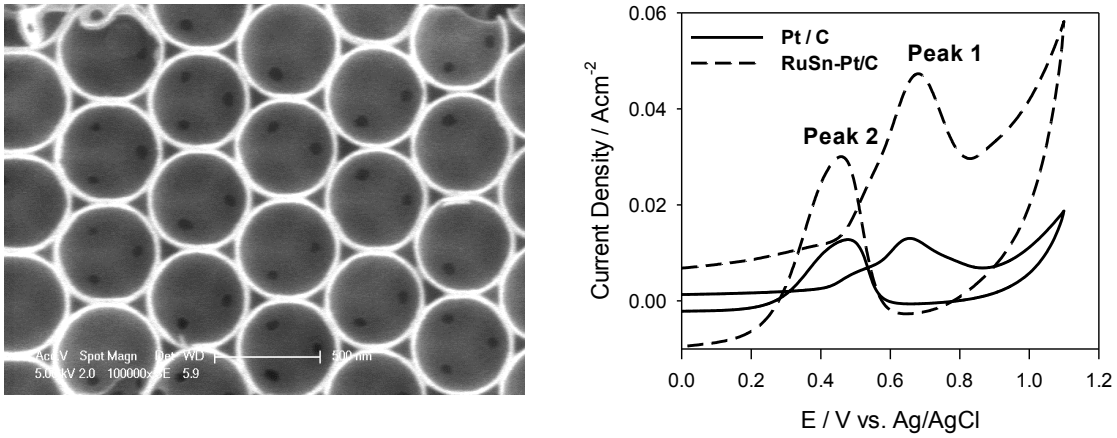

Figure 1. SEM of 3DOM Carbon (left) and CV for CH_3OH oxidation in acidic media (right).

Ni/TiO_2 – A low cost photocatalyst system for H_2 Production from Biofuels

W.-T. Chen[a] and G.I.N. Waterhouse[a]

[a] *School of Chemical Sciences, The University of Auckland, New Zealand.*

Ni/TiO_2 photocatalysts (Ni loadings 0-4 wt.%) were prepared by the complex precipitation method [1], H_2 reduced at 500 ^oC, characterised and evaluated for H_2 production from ethanol-water mixtures under UV excitation. Degussa P25 TiO_2 (85 wt.% anatase, 15 wt.% rutile) was used as the support phase. TGA, XRD, UV-Vis and XPS measurements provided evidence for the presence of metallic Ni nanoparticles on the surface of the photocatalysts, though the Ni nanoparticles were very small (< 2nm) and highly dispersed over the oxide support and thus difficult to observe by TEM. The Ni/TiO_2 photocatalysts were very active for H_2 production from ethanol-water mixtures under UV excitation, with the optimal Ni loading being ~0.5 wt.% (H_2 production rate = 33.4 mmol g^{-1} h^{-1}). High H_2 production rates were achieved over a wide range of ethanol concentrations. The 0.5 wt.% Ni/TiO_2 photocatalyst displayed superior photocatalytic activity to a standard reference photocatalyst, 2 wt.% Au/TiO_2, at ethanol concentrations between 1-30 vol.%, which may be due to the higher dispersion of the active metal co-catalyst realised in the Ni/TiO_2 system. Results suggest that Ni/TiO_2 is a promising low cost alternative to noble metal-based photocatalysts for solar H_2 production from biofuels.

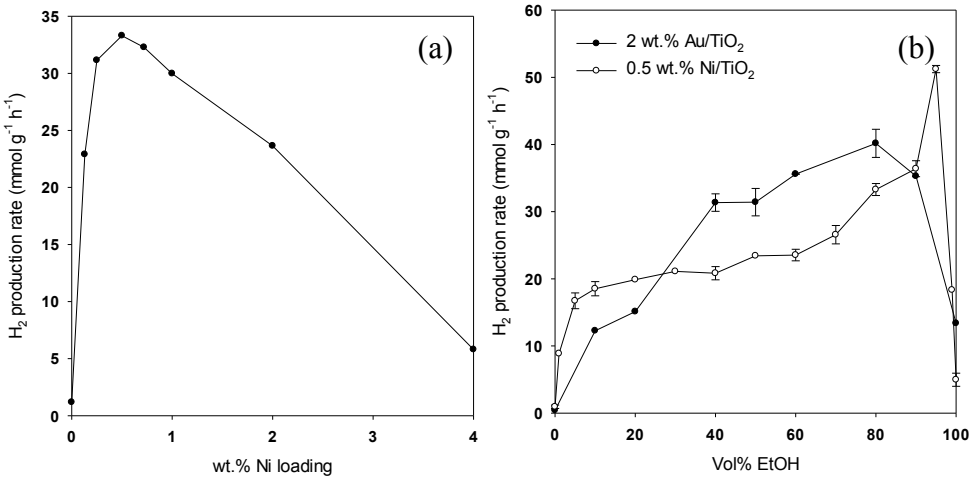

Figure 1. (a) H_2 production rate versus Ni loading for various Ni/TiO_2 photocatalysts in ethanol-water mixtures (80 vol.%) under UV excitation (b) H_2 production rates versus ethanol concentration for 0.5 wt.% Ni/TiO_2 photocatalyst and 2 wt.% Au/TiO_2 photocatalyst under UV excitation.

[1] L.S. Yoong, F.K Chong and B.K. Binay, *Energy* **34**, 1652 (2009).

Enriching the properties of Mo-oxide layered hybrids with electron-rich zigzag fused aromatic spacer molecules

I. u-din[a,b], S.V. Chong[b], S.G. Telfer[a], G.B. Jameson[a], M.R. Waterland[a] and J.L. Tallon[b]

[a] *MacDiarmid Institute for Advanced Materials and Nanotechnology, Institute of Fundamental Sciences, Massey University, Private Bag 11222 Palmerston North 4442, New Zealand.*

[b] *MacDiarmid Institute for Advanced Materials and Nanotechnology, Callaghan Innovation Research Ltd., P.O. Box 31310, Lower Hutt 5040, New Zealand.*

For the first time 3,8-phenanthroline, a zigzag fusion of 3 benzene rings, has been employed as a bridging ligand to develop a system of layered organic-inorganic hybrid materials. The resulting materials exhibit two (2-D) and three dimensional (3-D) covalently bonded hybrid frameworks constructed from single and bimetallic inorganic oxide layers interlinked by organic ligands. This opens up possibilities for developing new materials by introducing different magnetic ions within the inorganic layers and the incorporation of other hetero-polycylic aromatic organic spacers in-search for improved magnetic properties and even superconductivity in these hybrid materials [1]. Here we report the synthesis and properties of 2-D (**I**) MoO_3-(3,8-phenanthroline)$_{0.5}$ and (**II**) MoO_3-(3,8-phenanthroline)$_{0.3+\delta}$, and 3-D (**III**) $CuMoO_4$-(3,8-phenanthroline)$_{0.5}$ hybrids. Raman measurements correlate very well to the structural data and illustrate that how small changes in crystal structure can have significant effects on vibrational characteristics of the hybrid network. Compound **II** with ~0.33 phenanthrolines appears to be self-doped compared with **I**, while the insertion of Cu^{2+} ions within the inorganic layers in **III** seems to induce antiferromagnetic behaviour in the otherwise diamagnetic material. We also observed a heat capacity peak in zero field at around 8 K and diamagnetic (magnetization) transitions at ~12 K under very low applied magnetic field in **III**, which might be associated to magnetic orders caused by the different oxidation states of Cu or the compound is superconducting with a very low upper critical field.

[1] S.V. Chong and J.L. Tallon, "*Novel layered organic/inorganic hybrid materials*", New Zealand Provisional Patent # 615066 (4 September 2013).

Inorganic/Organic Composites for X-ray Imaging

N. Winch[a] and A. Edgar[a]

[a] *School of Chemical and Physical Sciences, Victoria University, Welllington, New Zealand.*

X-ray imaging is widely used in medicine, dentistry, security, and materials inspection. Traditionally, imaging has been done using a photographic film – phosphor screen combination, but over the past two decades, this has been progressively replaced by various imaging plate technologies. One such technology is that of storage phosphors, where incident x-rays falling on a storage-phosphor imaging-plate generate electrons and holes, some of which are locally trapped. Recombination is stimulated by incident red light, and the resulting blue recombination emission I(x,y), which is proportional to the incident X-ray intensity, is recorded across the plate so as to extract an X-ray image of any object placed in the x-ray beam.

Currently, the highest performance storage phosphor is CsBr, doped with europium, but as made the material is completely inactive. It must be first thermally processed in the presence of water vapour so as to generate a high concentration of the active recombination centre, whose detailed structure [1,2] is still a matter of some debate, but which appears to involve a Eu^{2+} - H_2O atomic centre. However, whilst the material has an outstanding X-ray sensitivity, the spatial resolution remains inferior compared to other rival techniques due to light scattering of the stimulating and emitted light from the powdered CsBr grains in the plate. We have earlier described how a higher resolution, transparent, non-scattering form can be made by pressing [3] , and how it can be used with a simple image read-out process [4]. In this paper, we describe an alternative process in which the CsBr is chemically modified so as to refractive-index match an organic polymer binder. The materials science design and thermal and spectrocsopic properties of the composite are discussed and the performance of the resulting organic/inorganic composite prototype imaging plates is presented.

[1] H. F. Vrielink, F. Loncke *et al.*, *Phys. Rev. B*, **83,** 054102 (2011).

[2] G. Appleby, H. von Seggern *et al., J. Appl. Phys.* **109**, 013507 (2011).

[3] N.M. Winch and A. Edgar, *Phys. Stat. Solidi A* **209**, 2427 (2012).

[4] N.M. Winch and A. Edgar, *Nucl. Instrum. Meth. A* **654**, 308 (2011).

Mechanical Properties of Tungsten Copper Composites: Direct Measurement by Neutron Diffraction

P.J. Mignone[a,b], T.R. Finlayson[a,b], S. Kabra[c], S-Y. Zhang[c], G.V. Franks[a,b] and D.P. Riley[b,d]

[a]*Department of Chemical and Biomolecular Engineering, University of Melbourne, Vic., 3010, Australia.*

[b]*Defence Materials Technology Centre, Hawthorn, Vic., 3122, Australia.*

[c]*CCLRC Rutherford Appleton Laboratory, Chilton, Didcot OX11 0QX, England.*

[d]*Australian Nuclear Science and Technology Organisation, Lucas Heights, N.S.W., 2234, Australia.*

The composite W-10 wt%Cu (19.35% by volume, assuming neglegible porosity) has been studied using the ENGIN-X beamline at the ISIS pulsed neutron source at the Rutherford Appleton Laboratory. An as-machined, compression sample was initially measured in order to check for the presence of residual stresses in the composite, using a mixed powder sample of the same elemental weight fractions as the "zero stress" comparison. Then a series of mechanical tests were carried out on the composite for applied compressive loads up to 250 MPa at both room temperature and 100°C and compared with similar tests carried out on pure tungsten and copper samples.

Residual stress values of -280 MPa (for the tungsten matrix) and 480 MPa (for the copper particulate phase) were measured for the as-machined sample. This is a surprising result, given that the yield stress for copper is typically less than 100 MPa but is not inconsistent with residual stresses reported in the literature for W-Cu composites [1]. The mechanical properties for the composite have also been determined from the results of these in-situ, mechancial tests and compared with finite element calculations based on microstructural models for the composite material [2].

[1] T. Wieder, A. Neubrand, H. Fuess and T. Pirling, *J. Mater. Sci. Letts.* **18**, 1135 (1999).

[2] P.J. Mignone, M. Wang, T.R. Finlayson, D.P. Riley and G.V. Franks, *Mater. Sci. Eng. A* (2013) (in press).

Novel SERS substrates for the Identification of Adulterants in Milk

P.-H. Hsieh[a], D. Sun-Waterhouse[a] and G.I.N. Waterhouse[a]

[a] *School of Chemical Sciences, The University of Auckland, New Zealand.*

Surface enhanced Raman spectroscopy (SERS) is a powerful analytical technique that attracts interest in chemistry and biology for the detection of low concentration analytes. SERS enhancement factors as high as ~10^{10}-10^{11} have been reported for highly optimised Au and Ag substrates [1], however the low general reproducibility of SERS substrates is an obstacle to the SERS technique's widespread use in routine quantitative analyses. The development of stable and sensitive SERS active substrates is a priority. This research explores the fabricationa and viability of novel SERS substrates, comprising Au nanoparticles immobilised on 3-dimensionally ordered macroporous (3DOM) $Si_{1-x}Ti_xO_2$ supports. Here we present preliminary data relating to the fabrication and optical characterisation of such SERS substrates. Results show that Au nanoparticles of various size (predominantly < 10 nm) may be successfully deposited on 3DOM $Si_{1-x}Ti_xO_2$ supports at high loadings (up to 70 wt.% Au). The Au localised surface plasmon resonance and photonic bandgap along the [111] direction in the 3DOM supports red-shifted linearly with increasing solvent refractive index, which means that in addition to acting as SERS substrates these materials can also be used for solvent refractive index sensing. Thus, the described materials have potential as multi-functional optical sensing elements. Current work is being directed towards evaluation of the SERS activities of the Au/3DOM $Si_{1-x}Ti_xO_2$ substrates in milk-related systems.

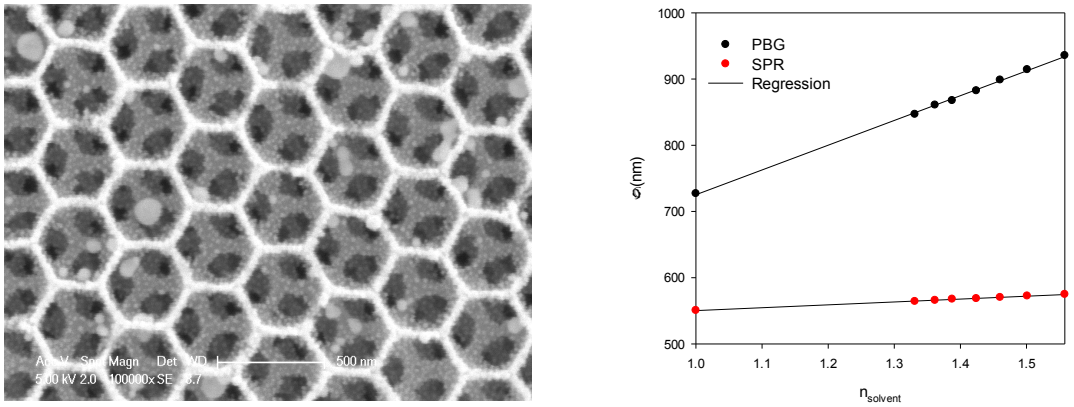

Figure 1. Au/3DOM $Si_{1-x}Ti_xO_2$ substrate (left) and Au LSPR and PBG shift versus solvent refractive index (right).

[1] B. Sharma, R.R. Frontiera, A.-I. Henry, E. Ringe and R.P. Van Duyne, *Mat. Today* **15**, 16 (2012).

ESR studies of Magnetocaloric $PrMn_{2-x}Fe_xGe_2$

Q.Y. Ren[a], W.D. Hutchison[a], J.L. Wang[b,c] and S.J. Campbell[a]

[a] *School of Physical, Environmental and Mathematical Sciences, The University of New South Wales, Canberra, ACT 2600, Australia.*

[b] *Institute for Superconductivity and Electronic Materials, University of Wollongong, Wollongong, NSW 2522, Australia.*

[c] *Bragg Institute, Australian Nuclear Science and Technology Organisation, Lucas Heights, NSW 2234, Australia.*

In a recent paper, we investigated the magnetic structures, phase transitions and magnetocaloric entropy of $PrMn_{1.6}Fe_{0.4}Ge_2$ by a combination of bulk magnetometry, ^{57}Fe Mössbauer spectroscopy and electron spin resonance (ESR) over the temperature range 5-300 K [1]. This work followed on from a broader study of the $PrMn_{2-x}Fe_xGe_2$ family of compounds [2], in which it was found that with decreasing temperature from the paramagnetic region, three magnetic phase transitions have been detected for $PrMn_{1.6}Fe_{0.4}Ge_2$. The transition temperatures and related magnetic structures (using the notation of [3]) the magnetic structures are [1]: (i) paramagnetism to intralayer antiferromagnetism (AFl) at T_N^{intra}=370 K; (ii) AFl to canted ferromagnetism (Fmc) at T_C^{inter}~230 K, and (iii) a third transition around T_C^{Pr}~30 K with ferromagnetic ordering of the Pr sublattice resulting in the combined magnetic region (Fmc+F(Pr)).

Here the ESR, focusing on the Pr^{3+} 4f magnetic moment and undertaken in the vicinity of the lowest transition temperature, is the subject of further analysis in order to correlate the observed resonant line/s and changes in g-factors with the phases mentioned above. In particular an aim is to link the increase in g factor of the Pr^{3+} ion (from g = 0.85 in the region above T_C^{Pr}~30 K to g ~ 2.5 at 8 K) with the bulk moments measured via DC magnetisation.

[1] W.D. Hutchison, J.L. Wang and S.J. Campbell, *Hyperfine Interact.* **221**, 35 (2012).

[2] J.L. Wang, S.J. Campbell, A J Studer, M Avdeev, M Hofmann, M Hoelzel and S X Dou, *J. Appl. Phys.* **104**, 103911 (2008).

[3] G. Venturini, R. Welter, E. Ressouche and B. Malaman, *J. Magn. Magn. Mater*. **150**, 197 (1995).

Investigation of the order parameter of Pr in the filled skutterudite $PrRu_4P_{12}$ by soft resonant x-ray diffraction

F. Li[a], A.M. Mulders[a], W.D. Hutchison[a], M. Garganourakis[b], Y. Tanaka[c], K. Nishimura[d] and H. Sato[e]

[a] *School of Physical, Environmental and Mathematical Sciences, The University of New South Wales, Canberra, ACT, 2600, Australia.*

[b] *Swiss Light Source, Paul Scherrer Institut, CH-5232 Villigen PSI, Switzerland.*

[c] *RIKEN SPring-8 Center, Harima Institute, Sayo, Hyogo 679-5148, Japan.*

[d] *Graduate School of Science and Engineering, University of Toyama, Toyama 930-8555, Japan.*

[e] *Department of Physics, Tokyo Metropolitan University, Hachioji, Tokyo 192-0397, Japan.*

The filled skutterudite $PrRu_4P_{12}$ which shows a metal-insulator (MI) transition at 62.3 K has attracted some attention recently since the origin of the MI transition is not yet well understood [1-6]. Given that no MI transition is observed in $LaRu_4P_{12}$ [7] implies that the Pr 4f electrons have an integral role. In this study the order parameter associated with the Pr 4f shells in $PrRu_4P_{12}$ is investigated via soft resonant x-ray diffraction in combination with x-ray absorption spectroscopy at the Pr $M_{4,5}$ edges, utilising the dipolar transition $3d \rightarrow 4f$. A resonance enhancement of the (100) superlattice reflection at the Pr $M_{4,5}$ edges signalling the order parameter of the Pr ions was observed below T_{MI} and underwent a steady increase upon temperature decreasing. The experimental spectra and subsequent analysis rule out the existence of magnetic, charge or orbital order as well as any Pr lattice displacement however imply that the resonant diffraction signal arises in essence from the two different crystal field environments of the Pr 4f electrons.

[1] C. Sekine, T. Uchiumi and I. Shirotani, *Phys. Rev. Lett.* **79**, 3218 (1997).
[2] C.H. Lee, H. Matsuhata. A. Yamamoto, T. Ohta, K. Ueno, C. Sekine, I. Shirotani and T. Hirayama, *J. Phys.: Condens. Matter* **13** L45 (2001).
[3] C. Sekine, T. Inaba, M. Yokoyama, H. Amitsuka and T. Sakakibara, *Physica B* **281-282** 303 (2000).
[4] C.H. Lee, H. Oyanagi, C. Sekine, I. Shirotani and M. Ishii, *Phys. Rev. B* **60** 13253 (1999).
[5] K. Ishii *et al., J. Magn. Magn. Mat.* **310** e178 (2007).
[6] S. Kong, W. Zhang and D. Shi, *New J. Phys.* **10** 093020 (2008).
[7] S.R. Saha, H. Sugawara, Y. Aoki, H. Sato, Y. Inada, H. Shishido, R. Settai, Y. Onuki and H. Harima, *Phys. Rev. B* **71** 132502 (2005).

The magnetic properties of $Nd_2Sn_2O_7$

P. Imperia[a], R.J. Aldus[a], K.C. Rule[a] and A. Studer[a]

[a] *ANSTO, The Bragg Institute, Australia.*

In this paper we will discuss the magnetic properties of the pyrochlore $Nd_2Sn_2O_7$ as measured with the neutron scattering instruments Wombat and Taipan at the Bragg Institute neutron scattering facility. The measurements were conducted on a polycrystalline sample in zero magnetic field and 10 Tesla. The sample, loaded in OFHC copper can, was mounted into a dilution insert and measured between 340 mK and 50 K. The results indicated that the material doesn't spontaneously magnetically order. However, upon application of the magnetic field, the sample is easily polarised. Achieving ultra-low temperature with a powder samples is a difficult task. Here we will discuss common strategies used to improve conductivity in the mK range and the implication for this particular study. The equipment available at the neutron scattering instruments of Bragg Institute for measurements in high magnetic fields and low temperature will be also illustrated.

Structure and Magnetism Studies of $Cu_{1-x}Co_xSb_2O_6$ Solid Solution

H.-B. Kang[a], C. Ling[b] and T. Söhnel[a]

[a] *The University of Auckland, School of Chemical Sciences, Private Bag 92019, Auckland, New Zealand.*

[b] *The University of Sydney, School of Chemistry, NSW 2006, Sydney, Australia.*

$CuSb_2O_6$ is the most widely studied structure in the ternary Cu-Sb-O system. The structure and magnetism of $CuSb_2O_6$ have been studied intensively revealed due to the discovery of high T_c copper oxides. Doping of Co into $CuSb_2O_6$ is designed to investigate two factors. Firstly, it seems not possible to have a direct phase transition from a tetragonal trirutlie modification to a monoclinic modification; subsequently at least an orthorhombic modification should exist between the two modifications. Secondly, it is very interesting how the magnetic behavior changes from 1D magnet ($CuSb_2O_6$) to 2D magnet ($CoSb_2O_6$) by replacing the transition metal on the A site of the trirutile structure.

$CuSb_2O_6$ shows a phase transition from tetragonal trirutile structure to a monoclinic distorted structure at around 100 °C to 130 °C due to the Jahn-Teller distortion of Cu^{2+} (d^9-system) [1]. The magnetic behavior of $CuSb_2O_6$ is considered as S=1/2 one-dimensional Heisenberg antiferromagnets (HAF) with strong anisotropy in the square Cu-sublattice above 20 K [2]. $CoSb_2O_6$ crystallizes in the tetragonal trirutile structure (Fig.1) showing a two-dimensional HAF behavior [3].

Co doping on the A site of $CuSb_2O_6$ helps to investigate how the structural phase turns from the monoclinic modification into the tetragonal trirutile modification and we could observe a possible orthorhombic modification between the two phases by Synchrotron X-ray powder diffraction. Assuming that $CuSb_2O_6$ adopts the tetragonal trirutile structure based on $CoSb_2O_6$ above 130 °C, a complete solid solution should be revealed. However, high synchrotron powder measurements at 200 °C and even at 500 °C indicate that this is not the case. A possible orthorhombic modification can be found from all $Cu_{1-x}Co_xSb_2O_6$ solid solutions except $CoSb_2O_6$ at 200 °C. Two different structures can be found between $CuSb_2O_6$ and $Cu_{0.7}Co_{0.3}Sb_2O_6$ on one side and $Cu_{0.7}Co_{0.3}Sb_2O_6$ and $CoSb_2O_6$ on the other side at 500 °C. It could be considered that $CuSb_2O_6$ is still distorted even at 500 °C.

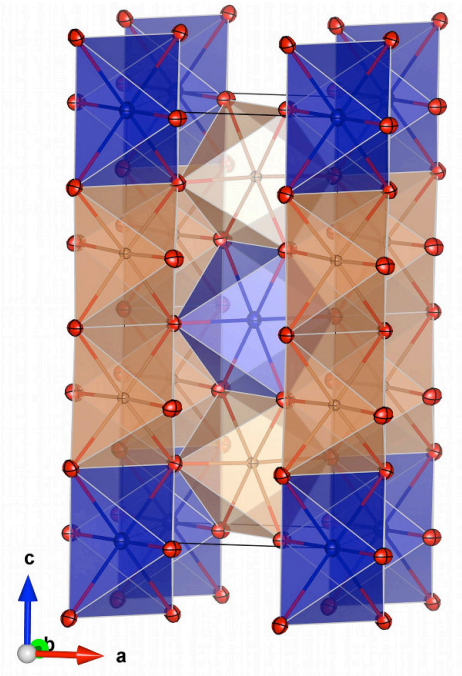

Figure 1. Crystal structure of $CoSb_2O_6$ refined on single crystal neutron data.

$CuSb_2O_6$ exhibits a S = ½ one dimensional Heisenberg antiferromagnet (HAF) with strong anisotropy in the square Cu-sublattice above 20 K [2] whereas $CoSb_2O_6$ exhibits two dimensional HAF [3]. According to the magnetic susceptibilities of $Cu_{1-x}Co_xSb_2O_6$, it is possible to investigate that the magnetic behavior of all compounds except $CuSb_2O_6$ are similar to $CoSb_2O_6$. It seems like the magnetic behavior of $CuSb_2O_6$ can be turned into the 2D magnet behavior with a very small amounts of Co doping.

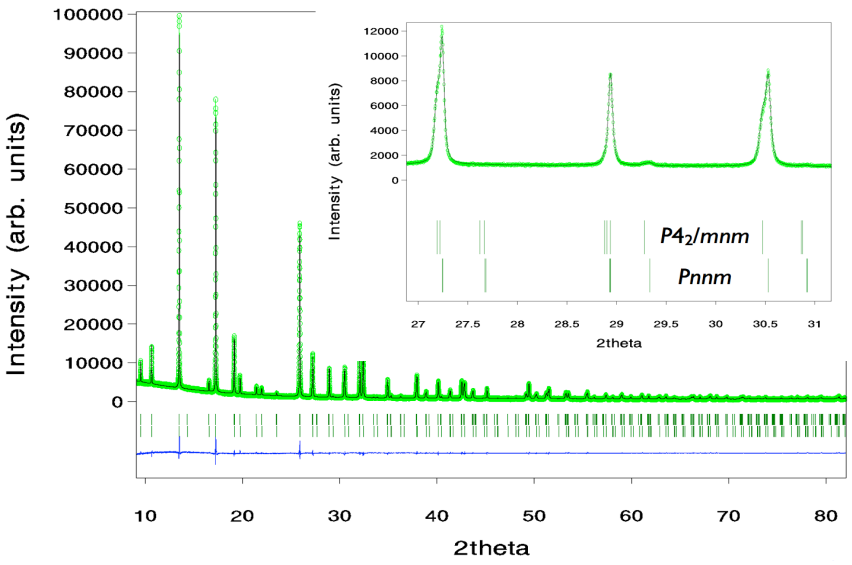

Figure 2. The Rietveld refinement of X-ray synchrotron data of $Cu_{0.7}Co_{0.3}Sb_2O_6$

[1] J.G. Bednorz and K.A. Müller, *Z. Phys. B*. **64**, 189 (1986).

[2] A.V. Prokofiev, F. Ritter, W. Assmus, B.J. Gibson and R.K. Kremer, *J. Cryst. Growth*. **247**, 457 (2003).

[3] J. N. Reimers, J. E. Greedan C. V. Stager, and R. Kremer, *J. Solid State Chem*. **83**, 20 (1989).

Magnon mediated superconducting pairing in the vicinity of magnetic quantum critical point

Y. Kharkov[a] and O.P. Sushkov [a]

[a] *School of Physics, University of New South Wales, New South Wales 2052, Australia.*

It has been recently established, both theoretically and experimentally, that cuprate superconductors have magnetic quantum critical point at about 10% doping. In the present work we consider a simplified theoretical model which allows to address a generic problem how magnetic quantum criticality influences superconducting pairing. We demonstrate that the paring is significantly enhanced in the vicinity of the critical point.

Ferromagnetism of Co,Eu Co-doped ZnO and 5%-Co doped TiO_2 Magnetic Semiconductors

O.J. Lee[a], X. Luo[a], W.T. Lee[b], V. Lauter[c], G. Triani[b], S. Li[a] and J.B. Yi[a]

[a] *University of New South Wales, Kensington, NSW, Australia.*

[b] *Australian Nuclear Science and Technology Organisation, Lucas Heights, NSW, Australia.*

[c] *Oak Ridge National Laboratory, Oak Ridge, TN, USA.*

Diluted magnetic semiconductor has attracted wide interest due to its potential applications in spintronics devices. Oxide semiconductor based diluted magnetic semiconductors has been investigated in detail for possible ferromagnetism above room temperature. However, most of the diluted magnetic semiconductors show very weak ferromagnetism. The magnetic moment is originated from the doped magnetic element, such as Fe, Co, Ni. Rare-earth element, which shows strong spin-orbit coupling, may enhance the magnetic anisotropy of the diluted magnetic semiconductors, thus enhances the ferromagnetism. In this work, we used both Co and Eu to co-dope ZnO and deposited Co doped TiO_2 thin films in order to achieve a diluted room-temperature magnetic semiconductor with strong ferromagnetism. 4%Co and 4%Eu or 6% Eu were used for the doping by implantation in ZnO and 5%Co-TiO_2 film were deposited on $LaAlO_3$ substrate under different oxygen partial pressures from 10^{-4} to 10^{-6} torr. For the ZnO-based thin films, XRD analysis indicates there is no secondary or impurity phase. Magnetic measurement by SQUID shows room temperature ferromagnetism. Polarized neutron reflectometry (PNR) analysis illustrates that ZnO film is 100 nm in thickness and the magnetic layers is around 30 nm, which is in consistent with the penetration depth of Co and Eu implantation, indicating the magnetic moment is due to the Co and Eu codoping. 4%Co, 4%Eu codoped ZnO film has a saturation magnetization of 3.57 emu/cm^3, while 4%Co, 6%Eu codoped ZnO film has a saturation magnetization of 9.62 emu/cm^3, indicating the significant enhancement of saturation magnetization by more rare earth element doping. For the TiO-based thin films, XRD analysis show epitaxial growth and that the films have anatase phases. TEM confirms the single crystal like microstructure. EDX mapping indicates that Co is uniformly distributed in the TiO_2 matrix, suggesting effective doping of Co dopant. Magnetic measurement shows that film deposited under lower oxygen partial pressure has a larger saturation magnetization. PNR shows that the magnetization is uniformly distributed along the film thickness. The magnetization for the film deposited under an oxygen partial pressure of 10^{-6} torr is about 4.2 emu/cm^3, which is much smaller than that measured by SQUID (30 emu/cm^3). This suggests a magnetic dead layer on the film surface.

Temperature dependence of structural parameters of the layered magnetic glass $Fe_{0.5}Ni_{0.5}PS_3$

D.J. Goossens[a], W.T. Lee[b] and A.J. Studer[b]

[a] *Australian National University, Canberra, ACT, Australia.*

[b] *Australian Nuclear Science and Technology Organisation, Lucas Heights, NSW, Australia.*

The layered magnetic materials of the MPS_3 family (M=2+ metal) show a wide range of behaviours. Recently, magnetic glassiness, with a relaxation time of the order of an hour, was observed in $Fe_{0.5}Ni_{0.5}PS_3$ [1]. The relaxation depends on sample history, both thermal and applied magnetic field. Here some aspects of the behaviour of the magnetic and crystal structure with temperature and field are explored using the Wombat powder diffractometer at ANSTO (Figure 1). Diffuse scattering can be seen to decrease as temperature falls and to fall sharply at the magnetic transition, and at different scattering vector Q to the magnetic Bragg peaks. This suggests a short-range ordered magnetic structure with different spin-spin correlations to the long-range ordered structure.

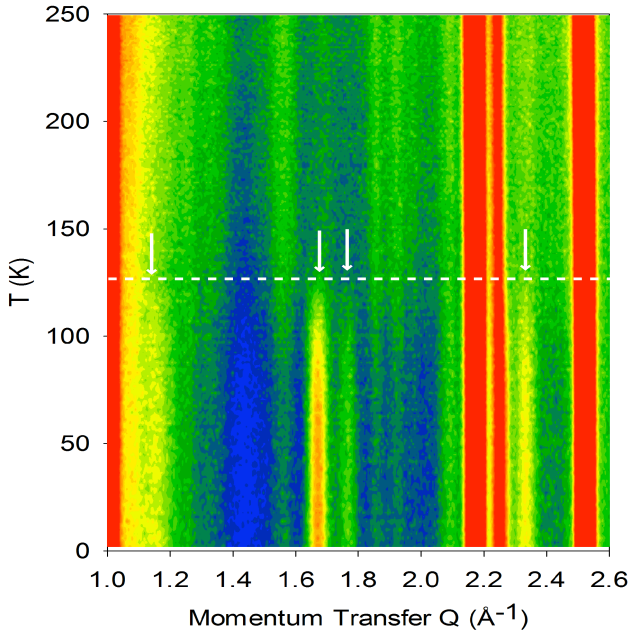

Figure 1. Temperature-dependent neutron scattering from $Fe_{0.5}Ni_{0.5}PS_3$. White arrows indicate magnetic Bragg reflections that vanish at TN, noted by the dotted line.

[1] D.J. Goossens, S. Brazier-Hollins, D.R. James, W.D. Hutchison and J.R. Hester, *J. Magn. Magn. Mater.* **334**, 82 (2013).

Generalization of the Onsager quantization condition for spin-orbit coupled systems

T. Li[a] and O.P. Sushkov [a]

[a] *School of Physics, University of New South Wales, New South Wales 2052, Australia.*

The oscillating resistivity of metals in magnetic field was explained by Onsager as a manifestation of quantum interference. Assuming that there are no coupled internal degrees of freedom, a charged particle will accumulate a phase when moving through a full loop in space, and this phase appears in the semi-classical expression for the energy spectrum. We present the extension of the semiclassical theory to spin systems in which both the orbital dynamic and internal dynamics are present, which implies that particle will acquire a total rotation in the internal space over a full loop. We demonstrate that for spin-½ systems, this allows the precessional dynamic of spin to be recovered from magnetic oscillations, and compare results of our theory with recent experiment.

Characterization of the carboxyl groups in graphene oxide

C. Liang[a], G. Xu[a] and J. Jin[a]

[a] *School of Chemical Sciences, University of Auckland, Auckland 1010, New Zealand.*

The graphite oxide and graphene oxide (GO) have attracted researcher's interest sustainably after it was first synthesized by Brodie in 1859 due to its outstanding chemical, physical and biological properties as well as served for precursor of chemically converted graphene. The new material has been sparked and largely focuses on optoelectronics transistors, bio-devices, energy storage devices and polymer nanocomposites. Although graphene oxide has been utilised and investigated for more than a century, the accurate structure of graphene oxide remains unclear and elusive. The structure analysis of graphene oxide has been one of the difficult problems in the field of carbon material sciences. One reason is that graphene oxide has a variety of compositions depending on the different synthetic methods and conditions, although it is simply composed of C, H and O. Another reason is that considering the huge size of graphitic platelets, current analysis techniques are not able to distinguish the accurate chemical groups and configuration in graphene oxide sheet. That often leads researchers to draw different conclusions even upon similar spectra results. Among the different chemical groups in graphene oxide, carboxyl groups are very critical and useful due to its unique properties. Carboxyl groups reflect the acidity[1], are relevant to solubility and stability[2] as well as a lot of chemical functionalization involving that[3]. Further understanding the properties of carboxyl group in graphene oxide can be very critical and useful for future research. Herein, we try to show the reactivity and density of carboxyl groups in surface and periphery of graphene oxide by using titration, UV, FTIR and solid state NMR.

[1] A.M. Dimiev, L.B. Alemany and J.M. Tour, *ACS Nano* **7**, 576 (2012).

[2] D. Li *et al.*, *Nature Nanotech.* **3**, 101 (2008).

[3] Z.-B. Liu *et al.*, *J. Phys. Chem. B* **113**, 9681 (2009).

Designing new $n = 2$ Sillen-Aurivillius phases by lattice-matched substitutions in the halide and $[Bi_2O_2]^{2+}$ layer

S. Liu[a], P.E.R Blanchard[a], M. Avdeev[b], B.J. Kennedy[a] and C.D. Ling[a]

[a] *School of Chemistry, The University of Sydney, New South Wales 2006, Australia.*

[b] *The Bragg Institute, ANSTO, PMB 1, Menai 2234, Australia.*

The chemical and structural flexibility of the perovskite structure, which makes it so ubiquitous in nature and useful in a range of technological applications, extends to layered variants such as Ruddlesden-Popper, Dion- Jacobson and Aurivillius phases. Multi-layered variants such as the Sillen-Aurivillius phases are related to Aurivillius phases by the insertion of an additional halide layer between every second $[Bi_2O_2]^{2+}$ layer [1].

Sillen-Aurivillius phases exist in various combinations of *n* number of perovskite layers and *m* halide layers. We have synthesised a new $n = 2$, $m = 1$ Sillen-Aurivillius compound $Bi_3Sr_2Nb_2O_{11}Br$ [2] based on $Bi_3Pb_2Nb_2O_{11}Cl$ [3] by simultaneously replacing Pb^{2+} with Sr^{2+} and Cl^- with Br^-. Rietveld refinements against X-ray and neutron powder diffraction data revealed a significant relative compression in the stacking axis, in contrary to the belief of inserting a significantly larger halide layer in the new compound. We could not stabilise other combinations such as $Bi_3Sr_2Nb_2O_{11}Cl$ and $Bi_3Pb_2Nb_2O_{11}Br$ due to inter-layer mismatch.

Sr^{2+} doping reduces the impact of the stereochemically active $6s^2$ lone pair found on Bi^{3+}/Pb^{2+} site, resulting in a contraction of the stacking axis by 1.22 % and an expansion of the *a-b* plane by 0.25 %, improving inter-layer compatibility with Br^-. XANES analysis shows that the ferroelectric distortion of the *B*-site cation is less apparent in $Bi_3Sr_2Nb_2O_{11}Br$ compared to $Bi_3Pb_2Nb_2O_{11}Cl$. Variable-temperature neutron diffraction data show no evidence for a ferroelectric distortion.

[1] B. Aurivillius, *Chem. Scrip.* **23**, 143 (1984).

[2] S. Liu, P.E.R. Blanchard, M. Avdeev, B.J. Kennedy and C.D. Ling, *J. Solid State Chem.* **205**, 165 (2013).

[3] A. M. Kusainova, P. Lightfoot, W. Z. Zhou, S. Y. Stefanovich, A. V. Mosunov and V. A. Dolgikh, *Chem. Mater.* **13**, 4731 (2001).

Thermoelectric Properties of Polycrystalline Gadolinium Nitride

T. Maity[a], H.J. Trodahl[a], B.J. Ruck[a], H. Warring[a] and F. Natali[a]

[a] *The MacDiarmid Institute for Advanced Materials and Nanotechnology,*
School of Chemical and Physical Sciences,
Victoria University of Wellington, PO Box 600, Wellington 6140, New Zealand.

For decades, magnetic and semi-conducting elements have taken the centre stage in developments of the field of electronics. Recent attention has largely shifted towards producing devices using the electronic spin as well as charge degree of freedom. By manipulating these two properties, spintronics has great promise to avail devices with very high speeds, minimal power usage and added functionality. Ferromagnetic rare earth nitrides (RENs) have promising future in spintronics devices. Though our overall understanding of these materials has improved over the last decade, some fundamental questions about their conducting state are yet to be answered.

Gadolinium nitride (GdN) has been widely studied REN to understand its ferromagnetic-ordering and electronic structure. A significant amount of research has been carried out on its magnetic, transport and optical properties but thermopower is yet to be investigated. Thermopower is a strong energy dependent transport phenomena, hence it provides critical insight of the material's electronic properties and other excitations (e.g phonon and magnon drag) with variable range of temperature and magnetic field. In this paper we present the first experimental investigation of the thermopower of polycrystalline gadolinium nitride, measured using an experimental set-up designed for measuring the temperature dependent thermopower of thin films inside a bath cryostat. Our initial reasult shows a negative thermopower, as expected because of the negative charge carriers, and strong temperature dependence. At low temperatures we observe a peak near the ferromagnetic transition temperature which is clearly correlated with ferromagnetic-ordering. The results will be interpreated in terms of the normal diffusion theropower and phonon/magnon drag contributions.

Reflectometry as a tool for studying dye molecule orientation in dye-sensitised solar cells (DSCs)

J. McCree-Grey[a,b] and J.M. Cole[a]

[a] *Cavendish Laboratory, University of Cambridge, UK.*

[b] *Bragg Institute, ANSTO, Sydney, Australia.*

With world energy demand set to double by 2050,[1] it is imperative that clean, efficient and cost-effective alternatives to fossil fuels are developed. Dye-sensitised Solar Cells (DSCs) are a positive step towards a low-cost, mass-producible source of photovoltaic power, with laboratory devices now capable of reaching efficiencies of up to 15%.[2]

Typical DSCs consist of a dye-sensitised semiconductor surrounded by a redox electrolyte and sandwhiched between two transparent, conductive substrates. The dye is the principle light adsorber, injecting photo-excited electrons into the semiconductor conduction band and giving rise to the cells electrical characteristics. The electron injection is enabled by the dye's physical and electrostatic interaction with the semiconductor surface and the nature of this interaction can have a major impact on the cell's performance.

Many dye species have been trialled in DSCs in efforts to improve these characteristics, however, the fundamental properties of dye orientation and molecular packing on the semiconductor surface remain widely unknown. X-ray reflectometry (XRR) has already been successfully applied to this field of DSCs[3] but application of reflectometry to a fully-functioning DSC has still yet to be realised. This presentation will discuss results obtained using X-ray reflectometry to study the dye-orientations and packing densities for a number of different dye systems. Further discussion on the development of procedures to then apply neutron reflectometry to study a fully functioning dye-sensitised solar cell will then be examined.

[1] International Energy Agency *Energy Technology Perspectives 2008 – Scenarios and Strategies to 2050* OECD/IEA (2008).

[2] M. Lui, M. B. Johnston and H. J. Snaith, *Nature* **501**, 395 (2013).

[3] M. J. Griffith, M. James, G. Triani, P. Wagner, G. G. Wallace and D. L. Officer, *Langmuir* **27**, 12944 (2011).

Fabrication, Optical and Photocatalytic Properties of TiO_2 Colloidal Crystals

S.E. Park[a] and G.I.N. Waterhouse[a]

[a] *School of Chemical Sciences, The University of Auckland, New Zealand.*

This study describes the successful fabrication and optical characterisation of TiO_2 colloidal crystals, comprising monodisperse TiO_2 colloids with diameters in the range 400-1100 nm arranged on a face-centered cubic lattice. Batches of monodisperse TiO_2 colloids of different diameters were first fabricated by the dodecylamine-catalysed hydrolysis of titanium tetraisopropoxide (TTIP) in a methanol/acetonitrile/water solvent mixture. By varying the H_2O:TTIP ratio, TiO_2 colloids of different diameter were obtained. Gravitational sedimentation of the TiO_2 colloids dispersed in ethanol yielded well-ordered TiO_2 colloidal crystals (Figure 1). XRD, TEM and FT-IR analyses showed the as-prepared TiO_2 colloids to be amorphous and containing significant amounts of dodecylamine. Direct calcination of the as-prepared colloids (or colloidal crystals) at 500^{o}C yielded dense, low surface area (10 m^2g^{-1}) monodisperse anatase TiO_2 colloids. Hydrothermal treatement of the as-prepared colloids, followed by calcination at 500^{o}C, yielded monodisperse mesoporous, high surface area (80-100 m^2g^{-1}) anatase TiO_2 colloids. Calcination of the anatase TiO_2 colloids at 700^{o}C yielded monodisperse rutile TiO_2 colloids. The optical properties of the TiO_2 colloidal crystals were consistent with a modified Bragg's law expression which considers refraction and diffraction of light in the TiO_2 colloidal crystals. Decoration of the mesoporous, high surface area anatase TiO_2 colloids with Au or Pd nanoparticles (yielded Au/TiO_2 and Pd/TiO_2 photocatalysts with excellent activities for H_2 production from ethanol-water mixtures under UV excitation.

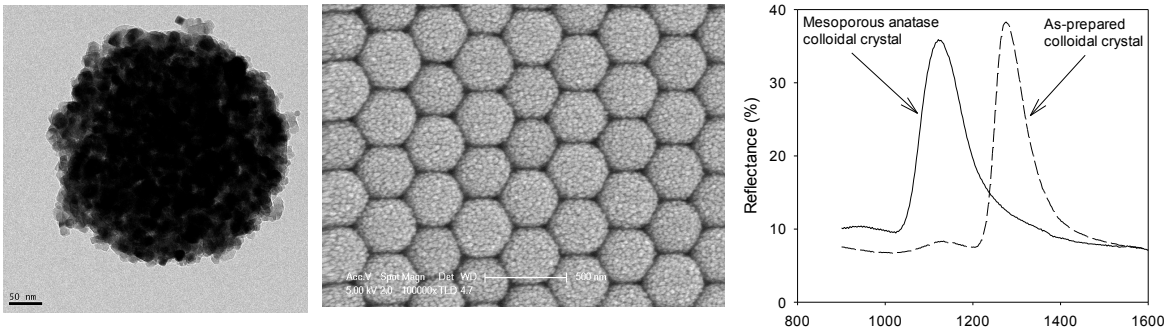

Figure 1: (left) TEM image for a mesoporous anatase TiO_2 colloidal crystal prepared at H_2O:TTIP=10; (centre) SEM image of fcc(111) plane of the corresponding TiO_2 colloidal crystal; (right) UV-Vis spectrum for the TiO_2 colloidal crystal showing a photonic band gap along the [111] direction at nm.

Alkali metal and alkaline earth metal oxide materials for high temperature CO_2 absorption and desorption studies

A.F. Pavan[a] and C.D. Ling[a]

[a] *School of Chemistry, University of Sydney, NSW 2050, Australia.*

Novel ceramic materials that are able to absorb CO_2 at high temperatures (>500^{O}C) have gained wide attention in recent years regarding their stability over a large number of cycles over a range of high temperatures [1,2]. Such ceramics have been considered for use in combustion chambers and in the smoke stacks of power plants where combustion gases, containing a mix primarily of CO_2 and N_2, exist at high temperature. Compared to other CO_2 sequestration technologies, these ceramics have both advantages (eg. can be fit to existing power plants) and disadvantages (eg. limited kinetics) [3].

My research involves the synthesis and CO_2 absorption studies of ceramics; specifically, alkali metal and alkaline earth metal oxides. Examples of materials already known to show significant CO_2 absorption include Li_5AlO_4 [4], $Li_6Zr_2O_7$[5], Na_2ZrO_3[6] and $Ba_4Sb_2O_9$[7]. The aim is to investigate the phase formations and structural evolution of these metal oxides under CO_2 conditions over the temperature range 873–1173 K.

Previous work has focused on the identification of phases *ex situ* and studies of their practical absorption capacity and kinetics. My work aims to understand both how the process works and how the structural evolution of the phases affects the CO_2 sorption of the materials over time *in-situ* [8].

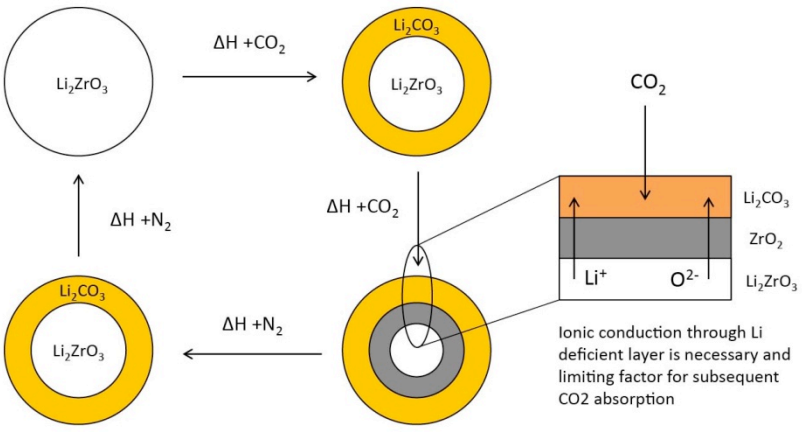

[1] B.N. Nair, R.P. Burwood, V.J. Goh, Nakagawa and K.T. Yamaguchi, *Prog. Mater. Sci.*, **54**, 511 (2009).

[2] S. Choi, J.H. Drese and C.W. Jones, *Chem.Sus.Chem.* **2**, 796 (2009).

[3] E. Favre, *J. Membr. Sci.* **294**, 50 (2007).

[4] L. Tatiana, Ávalos-Rendón and H. Pfeiffer, *Energy Fuels **26**,* 3110 (2012).

[5] S. Wang, C. An and Q.H. Zhang, *J. Mater. Chem. A. **1**,* 3540 (2013).

[6] L. Martínez-Cruz and H. Pfeiffer, *J. Phys. Chem. C* **116***,* 9675 (2012).

[7] M.T.Dunstan, A.F. Pavan, V.V. Kharton, M. Avdeev, J.A. Kimpton, V.A. Kolotygin, E.V. Tsipis and C.D. Ling, *Solid State Ionics,* **235**, 1 (2013).

[8] S.J. Friedmann, *Elements*, **3**, 179 (2007).

Characterisation of permalloy and magnetite nanopowders

T. Prakash[a,b], G.V.M. Williams[a], J. Kennedy[a,b], P.P. Murmu[b], J. Leveneur[b], S.V. Chong[c], P. Couture[a,b] and S. Rubanov[d]

[a] *The MacDiarmid Institute for Advanced Materials and Nanotechnology, SCPS, Victoria University of Wellington, PO Box 600, Wellington 6140, New Zealand.*

[b] *National Isotope Centre, GNS Science, PO Box 31312, Lower Hutt 5010, New Zealand.*

[c] *Callaghan Innovation Research Limited, PO Box 31310, Lower Hutt 5010, New Zealand.*

[d] *University of Melbourne, Inst Bio21, Melbourne, Victoria 3010, Australia.*

Magnetic nanoparticles are being actively researched because of the potential applications that include magnetic storage [1] and magnetic sensors [2]. Very small nanoparticles can be superparamagnetic where there is no hysteresis [3]. This can be advantageous in magnetic sensor applications and can allow for very small magnetic fields to be measured. They can also display a magnetoresistance [4], which can be used in magnetic sensing applications.

In this report we present the results from structural, Raman, magnetic, and magnetoresistance measurements on magnetic nanopowders made by arc-discharge and chemical methods. We show that permalloy and magnetite nanopowders can be made by arc-discharge and they contain a fraction of nanoparticles with dimensions below the superparamagnetic limit. We discuss changes to the arc-discharge setup that can lead to a higher fraction of superparamagnetic nanoparticles. The results are compared with similar measurements on magnetite made by a chemical method.

[1] G.F. Goya, T.S. Berquo and F.C. Fonseca, *J. Appl. Phys.* **94**, 3250 (2003).

[2] J. Daughton, J. Brown, E. Chen, R. Beech, A. Pohm, and W. Kude, *IEEE Transactions on Magnetics* **30**, 4608 (1994).

[3] N.A. Spaldin, *Magnetic Materials, Fundamentals and Device Applications* (Cambridge University Press, Cambridge, England, 2003).

[4] J. Leveneur, J. Kennedy, G.V.M. Williams, J. Metson, and A. Markwitz, *Appl. Phys. Lett.* **98**, 053111 (2011).

Molecular Dynamics Simulations of Thermal Condutivity of UO_2, $PuCrO_3$ and $PuAlO_3$

M.J. Qin[a], E.Y. Kuo[a], M. Robinson[b], N.A. Marks[b], G.R. Lumpkin[a] and S.C. Middleburgh[a]

[a] *Institute of Materials Engineering, Australian Nuclear Science and Technology Organisation, New Illawarra Road, Lucas Heights, Australia.*

[b] *Nanochemistry Research Institute, Curtin University, Perth, Western Australia.*

The thermal conductivities of the $PuCrO_3$ and $PuAlO_3$ precipitates in UO_2 fuel have been calculated using non-equilibrium molecular dynamics simulations. The $PuCrO_3$ phase showed a markedly lower thermal conductivity than UO_2, which will impact the microstructure, fission product distribution and gas release properties of UO_2-based fuels. The $PuAlO_3$, in both its orthorhombic and rhombohedral structures, showed greater thermal conductivity in comparison to $PuCrO_3$, lower than UO_2 at low temperatures but higher at elevated temperatures. Additions of Al with Cr to doped fuels is therefore likely to have a beneficial impact on the thermal conductivity of the fuel as opposed to solely doping with Cr.

Influence of Plasma Impurities on the Effective Performance of Fusion Relevant Materials

D.P. Riley[a], M. Guenette[a], A. Deslandes[a], S. C. Middleburgh, G. Lumpkin[a], L. Thomsen[b] and C. Corr[c]

[a] *Institute of Materials Engineering, ANSTO, NSW, Australia.*

[b] *Australian Synchtron, SXR, Victoria, Australia.*

[c] *Research School of Physics & Engineering, ANU, ACT, Australia.*

The development of a sustainable source of power derived from fusion energy is presently constrained by the limited number of materials capable of operating under such extreme conditions. Plasma facing components within magnetically confined fusion reactors must withstand extremes of temperature and loads, while maintaining a high tolerance to radiation damage from energetic particles or neutrons. More specifically, factors of sputtering yield, thermal conduction, electrical conduction and retention of fuel can all degrade the performance of the reactor and hence detrimentally lower the efficiency. In aiming to improve our understanding of materials capable of operating within the fusion environment, it is essential to establish how present generation materials become degraded.

Use of ion beam accelerators and linear plasma devices simulate the respective impact of energetic neutron damage (14.1 MeV) and plasma erosion (H^+, D^+, He^+) within a magnetically confined fusion environment. Methods of characterising changes in the local structure and chemistry of surface and near surface regions of fusion relevant materials quantify material degradation resulting from the uptake of plasma impurities. While complementary density functional theory (DFT) simulations have identified possible mechanisms for degradation of material performance. An overview of material evaluation methods will also be presented.

Novel Magnetic Properties of Rare-Earth Nitrides

B.J. Ruck[a]

[a] *The MacDiarmid Institute for Advanced Materials and Nanotechnology, School of Chemical and Physical Sciences, Victoria University of Wellington, Wellington, New Zealand.*

Most members of the rare-earth nitride series have been recognised as ferromagnetic for over 40 years, though there are some for which that has been confirmed only recently. Their electronic states have been less well characterised, with even basic questions such as whether they are metals or semiconductors adequately addressed only after recent advances in thin film fabrication. Several are now recognised as intrinsic ferromagnetic semiconductors. Here I will describe studies of the magnetic properties of several rare-earth nitrides based on magnetometry and x-ray magnetic circular dichroism, supported by transport measurements to elucidate the interplay between the electronic structure and the magnetic ordering. I will focus in particular on GdN (with zero orbital angular momentum), SmN (with almost zero net magnetic moment), and EuN. The magnetic transition temperature of GdN is independent of the carrier concentration over a large range, which we explain within a model based on magnetic polarons [1]. EuN should not be magnetic at all owing to the Hund's rule ground state of the Eu^{3+} ion with $J = 0$, but we have found that EuN films prepared with a substantial concentration of nitrogen vacancies are ferromagnetic with transition tempertaure exceeding 100 K [2]. The magnetic moments originate from Eu^{2+} ions within the films, although both the 2+ and the 3+ ions show magnetic polarisation.

[1] Do Le Binh, B.J. Ruck, F. Natali, H. Warring, H.J. Trodahl, E.-M. Anton, C. Meyer, L. Ranno, F. Wilhelm and A. Rogalev, *Phys. Rev. Lett.* **111**, 167206 (2013).

[2] F. Natali, B.J. Ruck, H. J. Trodahl, Do Le Binh, S. Vezian, B. Damilano, Y. Cordier, F. Semond and C. Meyer, *Phys. Rev. B* **87**, 035202 (2013).

^{75}As NMR of underdoped $CeFeAsO_{0.93}F_{0.07}$

S. Sambale[a,b,c], D. Rybicki[c], G.V.M. Williams[a] and S.V. Chong[b]

[a] *School of Chemical and Physical Science, Victoria University of Wellington, Wellington 6011, New Zealand.*

[b] *Callaghan Innovation, Lower Hutt, New Zealand.*

[c] *Faculty of Physics and Earth Science, Institute for Experimental Physics II, University of Leipzig, Leipzig, Germany.*

We report the results from a ^{75}As NMR study of underdoped $CeFeAsO_{1-x}F_x$ with x=0.07 that should be at the critical point between a spin density wave that occurs for x<0.07 and superconductivity that occurs for x>0.07. Contrary to the previous study on an overdoped and superconducting sample with x=0.20 [1], we find that there is only one As site, which suggests the absence of electronic phase sepration. The temperature dependent shift of the central transition is consistent with hyperfine coupling from magnetic Ce to As, which was also observed for x=0.20. Additional, we found an even higher ^{75}As spin-lattice relaxation rate in x=0.07 when compared with x=0.20 that suggests an even stronger coupling to Ce. Our low temperature ^{75}As NMR spectra for x=0.07 show a splitting of the central line that is also observed in a sample with x=0. The splitting is due to a spin density wave and indicates that the sample is magnetically spatially inhomogeneous.

[1] D. Rybicki, T. Meissner, G.V.M. Williams, S.V.Chong, M. Lux and J.Haase, *J. Phys.: Condens. Matter*. **25**, 315701 (2013).

Influence of Oxygen on the Performance of Organic Field Effect Transistors

L. Kehrer[a], A. Gassmann[a], C. Melzer[a] and H. von Seggern[a]

[a] *Electronic Materials Department, Institute of Materials Science, Technische Universität Darmstadt, Alarich-Weiss-Straße 2, 64287 Darmstadt, Germany.*

Functional stability of organic electronic devices such as organic field-effect transistors is still a great challenge for everyday use and a long way from being solved. The instability discussed here results from an oxygen defect, which is crucial for logic elements. In a logic circuit the OFETs are often held in the off-state, thus under depletion, where they change their properties and therewith the properties of the complete electronic circuit. In the present talk we report on the temporal behavior of oxygen based light- and field-induced defects in state-of-the-art poly(3-hexylthiophene), P3HT field-effect transistors. Experimentally a substantial shift of the threshold voltage and an increase in the off-current by three orders of magnitude has been reported when illuminating top-gate P3HT based field-effect transistors with visible light under forward gate bias [1]. Three time constants have been found at room temperature: two for the detrapping of electrons released from oxygen defects and one for the elimination of the oxygen defect itself. A set of rate equations will be shown to describe the behavior of the temporal development of the threshold voltage and the off-current of a P3HT transistor whilst the traps are optically filled as well as during the subsequent detrapping of electrons from the oxygen defects. In addition, the activation energies of the detrapping are determined.

[1] L.A. Kehrer, S. Winter, R. Fischer, C. Melzer and H. von Seggern, *Synth. Metals* **161**, 2558 (2012).

Solar Hydrogen Production using Au/TiO_2 Photocatalysts

R. Shahlori[a] and G.I.N. Waterhouse[a]

[a] *School of Chemical Sciences, The University of Auckland, Auckland, New Zealand.*

Semiconductor photocatalysis is one of the most promising future technologies for H_2 production. In this study, a series of Au/TiO_2 photocatalysts (Au loadings of 0.75, 1.5 or 3.0 wt.%) were fabricated using Degussa P25 TiO_2 as the support phase, and then subjected to detailed characterisation by TEM (Figure 1), XRD, XPS, photoluminescence, UV-Vis spectrometry and H_2 production tests (Figure 2). Results show that all the Au/TiO_2 photocatalysts comprised Au nanoparticles of average size 4-6 nm uniformly distributed over the TiO_2 support. Deposition of Au nanoparticles dramatically enhanced the photocatalytic activity of P25 TiO_2 for H_2 production from alcohol-water mixtures under UV irradiation, with the optimum Au loading being 1.5 wt.%. The Au nanoparticles serve as cathodic sites by accepting electrons photoexcited in TiO_2, and then transferring them to water or aqueous protons to generate H_2. The rate of H_2 production over the 1.5 wt.% Au/TiO_2 photocatalyst was stongly dependent on the nature of the alcohol used as a sacrificial hole scavenger in the H_2 productions tests (Figure 2). Eleven different alcohol-water systems were tested, with diols (1,2-ethane diol and 1,2-butane diol) and triols (glycerol) being superior hole scavengers compared to primary, secondary or tertiary mono alcohols. The high hydrogen production rates achieved in this study suggests that Au/TiO_2 photocatalysts are promising candidates for solar H_2 production from water and biofuels at UV fluxes comparable to those in sunlight.

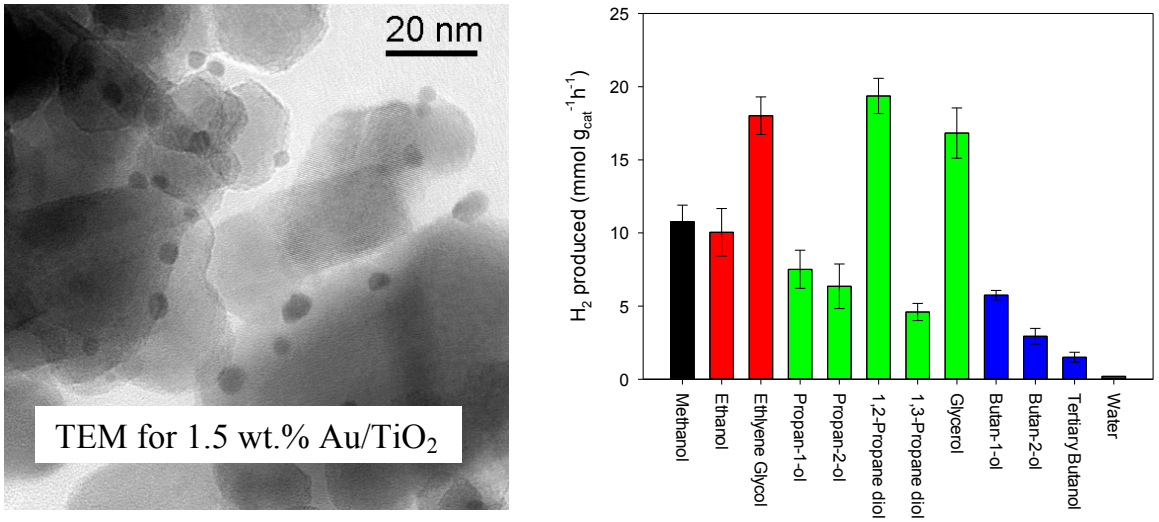

Figure 1. H_2 production rates for 1.5 wt.% Au/TiO_2 photocatalyst in different alcohol-water mixtures (10 vol.% alcohol, UV flux 4 mW cm^{-2}).

Electrical tuning of the hole Zeeman spin splitting in (100) Quantum wells

A. Srinivasan[a], I. Farrer[b], D.A. Ritchie[b] and A.R. Hamilton[a]

[a] *School of Physics, University of New South Wales, NSW 2052, Australia.*

[b] *Cavendish Laboratory, University of Cambridge, Cambridge CB3 0HE, United Kingdom.*

The Spin-orbit (SO) interaction has attracted great research interest of late, due to its potential application in spintronic devices, which aim to achieve all-electrical control of spin [1]. Quantum confined holes in GaAs heterostructures provide a rich playground for controlling and studying spin, due to the strong SO coupling in the valence band [2]. In particular, these systems allow electrical tuning of SO induced B=0 (Rashba) spin-splitting via the application of gate-biases [3].

Despite the great interest in these systems, a detailed understanding of the spin-orbit interaction and its effects on the spin of holes is far from complete. In particular there is very limited experimental or theroetical work available on the effect of the Rashba interaction on the *g*-factor of quantum confined holes. In this work, we invesitgate this using a two-dimensional hole system confined to a 15nm quantum well in a (100) GaAs heterostructure. The holes are further confined to a one dimensional (1D) channel using surface gates, and overall top and back gates allow us to control the degree of structural inversion asymmetry and hence alter the strength of the Rashba interaction. The use of a 1D channel allows a direct spectroscopic measurement of the Zeeman spin splitting as a function of magnetic field, which is not possible in a 2D system [4, 5]. Our measurements show that the electric field across the quantum well can be used to tune the *g*-factor. Perhaps surprisingly, we find that increasing the Rashba strength suppresses the measured *g*-factors. Our results demonstrate modification of the *g*-factor via the spin-orbit interaction, which could be of value in spintronics applications.

[1] S. Datta and B. Das, *Appl. Phys. Lett.* **56**, 665 (1990).

[2] R. Winkler, *Spin–Orbit Coupling Effects in Two-Dimensional Electron and Hole Systems* (Berlin: Springer, 2003).

[3] S.J. Papdakis *et al.*, *Science*. **283**, 2056 (1999).

[4] J. C. H. Chen *et al.*, *New J. Phys.* **12**, 033043 (2010).

[5] A. Srinivasan *et al.*, *Nano Lett.* **13,** 148 (2013).

Identifying further inelastic neutron crystal field transitions in $ErNiAl_4$

G.A. Stewart[a], W.D. Hutchison[a], Z. Yamani[b], J.M. Cadogan[a] and D.H. Ryan[c]

[a] *School of Physical, Environmental and Mathematical Sciences, UNSW Canberra, Australian Defence Force Academy, PO Box 7916, Canberra BC 2610, Australia.*

[b] *Canadian Neutron Beam Centre, National Research Council, Chalk River, Ontario, ON K0J 1J0, Canada.*

[c] *Physics Department, McGill University, Montreal, Quebec, H3A 2T8, Canada.*

The orthorhombic, intermetallic series $RNiAl_4$ (R = rare earth) exhibits interesting magnetic behaviour [1], including the potential for low temperature, inverse, magnetic cooling [2]. Given that the $RNiAl_4$ magnetism is associated solely with the R sub-lattice and is influenced strongly by the local crystal field (CF) interaction at the R-site, it is important that the CF interaction be characterised. However, the R site's local, orthorhombic (C_{2v}) symmetry requires nine CF parameters to be determined. Early CF characterization attempts reported in the literature were based on the observed bulk, single-crystal, magnetic anisotropy but ignored the important rank 6 terms [3, 4].Our first inelastic neutron scattering (INS) measurements were performed on Er^{3+} (J = 15/2) in $ErNiAl_4$ at the Helmholtz Zentrum Berlin's NEAT time-of-flight instrument. Despite the limited incident neutron energy range, well-defined transitions were observed for the first three (3, 7.4 and 11.4 meV) of the 7 excited Kramers doublets. A semi-empirical approach was applied in a first effort to interpret these data in terms of a full CF Hamiltonian [5].

We report here on our more recent, on-going, INS measurements that exploit the thermal energies and polarisation neutron capability of the Triple Axis Spectrometer (C5) facility at the Canadian Neutron Beam Centre in Chalk River. In addition to the low energy transitions observed at HZB there already appear to be further peaks at 15.5, 21 and 42 meV.

[1] W.D. Hutchison, D.J. Goossens, K. Nishimura, K. Mori, Y. Isikawa and A.J. Studer, *J. Magn. Magn. Mater.* **301**, 352 (2006).

[2] L. Li, K. Nishimura and W.D. Hutchison, *Solid State Commun*. **149**, 932 (2009).

[3] T. Mizushima *et al*., *J. Phys. Soc. Japan* **68**, 637 (1999).

[4] T. Mizushima *et al*., *J. Phys. Soc. Japan* **65**, 146 (1996).

[5] B. Saensunon, G.A. Stewart, P.C.M. Gubbens, W.D. Hutchison and A. Buchsteiner, *J. Phys.: Condens. Matter* **21**, 124215 (2009); Corrigendum *J. Phys.: Cond. Matter* **22**, 029801 (2010).

Thin-Film Thermopower Measurement System Open for Business

J.G. Storey[a] and N. Suresh[a,b]

[a] *Superconductivity & Energy Group, Callaghan Innovation, Lower Hutt, New Zealand.*

[b] *MacDiarmid Institute, Victoria University of Wellington, New Zealand.*

Thermopower is a measure of the magnitude of the voltage generated across a material in response to an applied temperature gradient. Besides their obvious use in determining the suitability of a new material for energy-harvesting applications, thermoelectric power measurements provide a wealth of information on the nature and behaviour of the charge carriers in materials [1].

We have constructed a system for measuring the thermopower of thin-film samples at temperatures from 7 to 300 K. The system is based around a closed-cycle cryogen-free vacuum cryostat and is controlled by a Java-based software package written in-house. The presentation will cover a description of the system, including example data obtained from second-generation high-temperature superconductor wires, as well as a discussion of the merits of using Java as an alternative to LabVIEW. New collaborations are welcome.

[1] J.G. Storey, J.L. Tallon and G.V.M. Williams, *Europhysics Letters* **102**, 37006 (2013).

Phase transition enhanced thermoelectric performance in Cu_2Se

H. Liu[a,b], X. Shi[a], W. Zhang[a], L. Chen[a] and S. Danilkin[c]

[a]*Shanghai Institute of Ceramics,Chinese Academy of Sciences,Shanghai 200050, China.*

[b]*University of Chinese Academy of Sciences, Beijing 100049, China.*

[c]*The Bragg Institute, Australian Nuclear Science and Technology Organisation, NSW 2322, Australia.*

Worldwide efforts to searching for good thermoelectric materials are frequently focusing on normal phases in crystalline semiconductors. The material's thermoelectric performance is described the parameter of figure of merit, zT, which is around unity around room temperature and above 1.5 at high temperatures. In the Cu_2Se with anti-fluorite structure above 400K, Se atoms form a rigid face-centred cubic lattice, while the copper ions are highly disordered or moving around the tetrahedral voids with liquid-like mobility, resulting in an extraordinarily low lattice thermal conductivity, which enables zT up to 1.5 at 1,000K [1]. Here, we report significantly enhanced thermoelectric performance during the phase transitions in Cu_2Se and iodine doped Cu_2Se. It is showed that the critical electron and phonon scattering greatly improve the thermopower and strongly reduce the thermal coductivity, leading to the improvement in the figure of merit more than 3-7 times compared to the normal phases, and achieving zT value of 2.3 at 400K [2]. This mechanism pave a new way to increase the figure of merit of thermoelectric materials, and expend the utility of thermoelectrics in electronic cooling industry.

[1] H. Liu, et al. *Nature Mater.* **11**, 422 (2012).

[2] H. Liu, et al. *Adv. Mater.* (Published online, DOI: 10.1002/adma.201302660, 2013).

Characterisation of self-supporting submicron-thick graphitic carbon foils with reflection spectroscopy

H. Timmers[a,b,c], C. Jansing[b], M. Tesch[b], M. Gilbert[b], A.G. Muirhead[c], A. Gaupp[d,b] and H.-Ch. Mertins[b]

[a] *School of Physical, Environmental and Mathematical Sciences, University of New South Wales, Canberra, ACT 2600, Australia.*

[b] *University of Applied Sciences, Münster, Fachbereich Physikalische Technik, Stegerwaldstraße 39, D-48565 Steinfurt, Germany.*

[c] *Department of Nuclear Physics, Research School of Physics and Engineering, Australian National University, Canberra, ACT 0200, Australia.*

[d] *HZB, Albert-Einstein-Straße 15, D-12489 Berlin, Germany.*

Some electrostatic ion accelerators, radioactive ion beam facilities, proton synchrotrons and accelerator mass spectrometers rely on submicron-thin, self-supporting graphitic carbon foils that change the charge state of swift heavy ions. This is achieved by 'stripping' electrons off the ion by transmitting it through the foil [1]. In order to be effective, these ‘stripper’ foils may need to be as thin as 20 nm to allow for optimum ion beam focusing. If such foils were single-crystalline graphite, a 20 nm thickness would correspond to about 300 atomic layers.

The fundamental challenge in making carbon stripper foils is to achieve stability against ion irradiation at minimum foil thickness. Under heavy ion beam irradiation the foils tend to thicken in the beam spot, experience mechanical tension and can suddenly disintegrate. Such failure interrupts ion beam operation and is not desirable. Recent developments of new types of deposition technologies have produced new types of foils. Some new types of foils perform significantly better under ion bombardment compared to others [2]. These differences may be due to the foil microstructures, which have been suggested to be polycrystalline graphite or to contain single-walled carbon nanotubes.

In this work reflection spectroscopy with polarised light in the visible and soft x-ray range [3] is applied to characterise different types of self-supporting, submicron-thick graphitic carbon foils. Anticipated results may identify electronic and corresponding structural differences of the various types of foils that are employed for electron stripping and inform studies on other types of graphitic carbon. Preliminary results will be presented and discussed.

[1] G. Dollinger and P. Maier-Komor, *Nucl. Instr. Meth. in Phys. Res.* **A 257**, 64 (1987).

[2] A.G. Muirhead and J.K. Heighway, *Nucl. Instr. Meth. in Phys. Res.* **A 655**, 61 (2011).

[3] H.-Ch. Mertins *et al.*, *Phys. Rev.* **B 70**, 235106 (2004).

X-ray Dose Dependence and Spectral Hole-Burning Properties of Ball Milled Nanocrystalline $Ba_{0.5}Sr_{0.5}FCl_{0.5}Br_{0.5}:Sm^{3+}$

X.Wang[a] and H. Riesen[a]

[a] *School of Physical, Environmental and Mathematical Sciences, University of New South Wales, Canberra, ACT 2600, Australia.*

Nanocrystalline $Ba_{0.5}Sr_{0.5}FCl_{0.5}Br_{0.5}$ doped with Sm^{3+} ions was prepared by a facile ball milling mehod at room temperature. Upon X-ray irradiation the Sm^{3+} is converted to Sm^{2+} [1-3]. The integrated photoluminescence intensities of the characteristic Sm^{3+} transition at around 594 nm and Sm^{2+} transition at around 687 nm were measured with excitation wavelengths of 401 nm and 415 nm, respectively. The sample was irradiated for a range of different times in a powder X-ray diffractometer and the X-ray dose dependence of both Sm^{3+} and Sm^{2+} transition was measured. Spectral hole-burning properties of the resulting Sm^{2+} were investigated in the $^7F_0$-$^5D_0$ transition. The mechanochemical process facilitates the synthesis of a proper solid solution and hence the inhomogeneous width of the Sm^{2+} transition is significntly increased. Ball-milled samples may have some potential in frequency domain optical data storage.

[1] H. Riesen and W.A. Kaczmarek, *Inorg. Chem.* **46**, 7235 (2007).

[2] H. Riesen, W.A. Kaczmarek, *Radiation storage phosphor & application, International PCT Application*, WO 2006063409-A1, (2008).

[3] Z. Liu, M.A. Stevens-Kalceff and H. Riesen, *J. Phys. Chem. C* **116**, 8322 (2012).

Characterising Graphene Nanoribbons using Raman Microscopy

M.R. Waterland[a], H. Dykstra[a] and A.J. Way[a]

[a] *Institute of Fundamental Sciences, Massey University, Palmerston North, New Zealand.*

Berry *et al.* recently reported a novel method for the production of graphene nanoribbons [1]. In this method graphite is mechanically fractured (using a diamond-knife equipped microtome) into nanoribbons with nanometre widths and the graphite ribbons are exfoliated with surfactants. This method produces large quantities of high purity graphene nanoribbons (*i.e.* no chemical side-products).

Edge structure (*i.e.* zig zag vs armchair) of graphene nanoribbons largely controls their electronic properties but the ability to control the edge structure during mechanical fracturing is an unknown parameter. Polarised Raman spectroscopy can characterise graphene edge structure and provides a valuable tool for investigating the edge structure of graphene nanoribbons.

We are applying low-frequency polarised Raman microscopy to the analysis of graphene nanoribbons, produced using the Berry method, in this work. We present preliminary results on graphite and graphene nanoribbons. Computational studies are also being used to establish correlations between spectral features and graphene nanoribbon edge structure. We will also present some preliminary computational studies that examine the changes in vibrational mode frequencies and intensities between models for zig zag edges and arm chair edges.

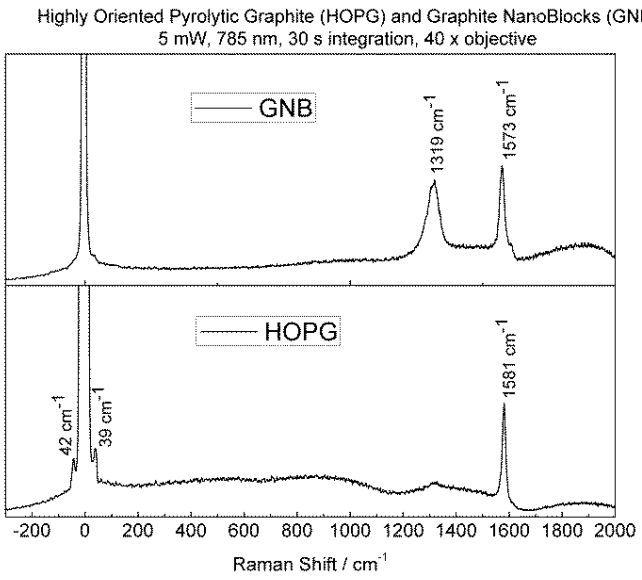

[1] N. Mohanty, D. Moore, Z. Xu, T.S. Sreeprasad, A. Nagaraja, A.A. Rodriguez and V. Berry, *Nature Comms.* **3**, 844 (2012).

Structural Investigation of Tungsten Bronze Type Relaxor Ferroelectrics

T.A. Whittle[a] and S. Schmid[a]

[a] *School of Chemistry, The University of Sydney, NSW 2006, Australia.*

Tungsten bronze type compounds have been shown to display a variety of industrially relevant properties including optical and electronic properties [1,2]. Primary among these properties is ferroelectricity [3,4]. Ferroelectric materials are ubiquitous in technological applications, from everyday consumer electronics to sophisticated technical instruments. Traditional ferroelectric materials are limited by the temperature range at which they can operate effectively. In contrast, relaxor ferroelectric materials show comparable properties over a much larger temperature range. Additionally, relaxor ferroelectric properties can be tuned by the frequency of an applied electric field, this allows for greater material selectivity for a desired application.

There is a fundamental relationship between the structure of these compounds and the properties they possess [5]. As such a comprehensive analysis of the crystal structure of relaxor ferroelectric materials is essential to explaining the observed properties and ultimately predicting the relationship between chemistry and properties.

The focus of this work is the complementary use of synchrotron X-ray and neutron diffraction for the structural analysis of tungsten bronze type relaxor ferroelectric materials. Of particular interest is the location of morphotropic phase boundaries (MPBs) such as that observed for PZT. MPBs are regions of dramatically enhanced properties due to a mixing of ferroelectric states [6,7].

In this presentation relaxor ferroelectric tungsten bronze type materials in the $Ba_xSr_{3-x}Ti_{1-y}Zr_yNb_4O_{15}$ quaternary phase system will be discussed. The structures of the four end members of this system have been previously reported. However, no investigations utilising synchrotron X-ray diffraction have been performed and little utilising neutrons. $Sr_3ZrNb_4O_{15}$ is only mentioned once in the literature [8], contrary to $Sr_3TiNb_4O_{15}$ which has had three alternate structural models reported [9-11]. The majority of the phase space of this system remains explored and the location of phase transitions is unreported in the literature.

Structural models resulting from Rietveld refinements [12] for members of this quaternary system will be presented, shedding light on new lead free relaxor ferroelectric materials.

[1] L. Z. Xiao, K. Li, R. M. Asif,Q. L. Xiao and M. C. Xiang, *J. Appl. Phys.* **114**, 124102/1 (2013).

[2] B. N. Parida, R. D. Piyush, R. Padhee and R. N. P. Choudhary, *J. Phys. Chem. Solids* **73**, 713 (2012).

[3] D.-W. Fu, H.-L. Cai, Y. Liu, Q. Ye, W. Zhang, Y. Zhang, X.-Y. Chen, G. Giovannetti, M. Capone, J. Li and R.-G. Xiong, *Science* **339**, 425 (2013).

[4] J. Kreisel, M. Alexe and P. A. Thomas, *Nat. Mater.* **11**, 260 (2012).

[5] P. S. Halasyamani and K. R. Poeppelmeier, *Chem. Mater.* **10**, 2753 (1998).

[6] M. Ahart, M. Somayazulu, R. E. Cohen, P. Ganesh, P. Dera, H.-K. Mao, R. J. Hemley, Y. Ren, P. Liermann and Z. Wu, *Nature* **451**, 545 (2008).

[7] D. Pandey, A. K. Singh and S. Baik, *Acta Crystallogr. A* **64**, 192 (2008).

[8] V. G. Kryshtop, R. U. Devlikanova and E. G. Fesenko, *Inorg. Mater.* **15**, 1777 (1979).

[9] F. W. Ainger, W. P. Brickley and G. V. Smith, *Proc. Brit. Ceram. Soc.* **18**, 221 (1970).

[10] R. R. Neurgaonkar, J. G. Nelson and J. R. Oliver, *Mater. Res. Bull.* **27**, 677 (1992).

[11] E. O. Chi, A. Gandini, K. M. Ok, L. Zhang and P. S. Halasyamani, *Chem. Mater.* **16**, 3616 (2004).

[12] H. Rietveld, *J. Appl. Crystallogr.* **2**, 65 (1969).

Neutron powder diffraction and Synchrotron PD and XAS studies of $Cu_{5-x}Mn_xSbO_6$ and $Cu_5Sb_{1-x}Mo_xO_6$

D.J. Wilson[a] and T. Söhnel[a]

[a] *School of Chemical Sciences, The University of Auckland, Auckland, New Zealand.*

Cu_5SbO_6 is a mixed valence copper compound that crystallises in a modified Delafossite structure type ($CuFeO_2$), with two distinct modifications [1-3]. The high temperature modification is of particular interest due to ferromagnetic-antiferromagnetic short range ordering of Cu^{2+} pairs in the structure. Compounds like $CuFeO_2$ crystallising in the Delafossite structure are one of the few groups of compounds showing the rare property of multiferroic behaviour.

In order to influence the magnetic properties of Cu_5SbO_6, magnetically active transition metals were doped into the structure. Manganese and molybdenum were doped into the structure separately and in conjunction. Synchrotron and neutron powder diffraction techniques were conducted in order to determine the incorporation of the doping metal. In addition to powder diffraction techniques, X-ray absorption spectroscopy was used to probe the oxidation state/s of the incorporated metal [4]. Magnetic susceptibility measurements of the doped Cu_5SbO_6 were performed in order to compare with Cu_5SbO_6.

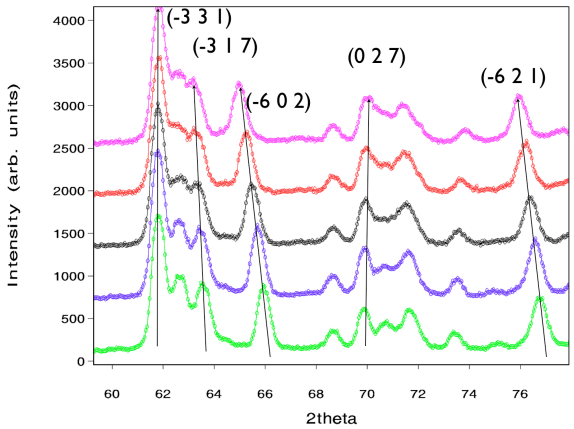

Figure 1. Shifts of the reflection peaks in the NPD patterns of the high temperature modification of $Cu_{5-x}Mn_xSbO_6$.

[1] E. Rey, BScHons Thesis, The University of Auckland (2010).

[2] E. Rey, P. Z. Si and T. Söhnel, *Proceedings of the 35th Annual Condensed Matter and Materials Meeting*, WaggaWagga, Australia, Canberra, Australian Institute of Physics, 22-25. ISBN: 978-0-646-55969-8 (2011). arXiv:1107.3617v1 [cond-mat.mtrl-sci].

[3] E. Climent-Pascual, P. Norby, N. H. Anderson, P. W. Stephens, H. W. Zandbergen, J. Larsen and R. J. Cava, *Inorg. Chem*, **51** 557 (2012).

[4] D.J. Wilson, BScHons Thesis, The University of Auckland (2013).

A novel approach to synthesis of highly reduced graphene oxide

G. Xu[a], C. Liang[a], J. Zhang[a], H. Kang[a] and J. Jin[a]

[a] *School of Chemical Science, The University of Auckland, New Zealand.*

Since graphene was firstly isolated by Geim's group from UK, graphene has expeditiously become a new super star in the view of nanotechnology and material science [1]. Chemically reduced graphene oxide has been viewed as one of the novel methods for preparation of graphenes in large yields. In order to synthesis reduced graphene oxide, various reducing agents have been proposed to reduce graphene oxide, including hydrazine, ascorbic acid, proteins, carbon monoxide, NaOH, ethanol, $NaNH_3$, aluminium powder, hydriodic acid, glucose et. Metal hydrides including a group of powerful reducing reagents have frequently been used in organic synthesis. Until now, sodium borohydride ($NaBH_4$) and lithium aluminium hydride (LAH) [2] have already been applied in GO reduction successfully. Super Hydride is an extraordinarily super-strong nucleophilic reductant available for unselectively reducing carboxylic acid, carbonyl, ester and epoxy groups to hydroxyl groups, even a lot more powerful and cleaner than $NaBH_4$ and lithium aluminium hydride. Here, for the first time, we propose a method using super hydride as a new reducing reagent on graphene oxide, and with the comparison of the reduction capacity towards that of LAH and $NaBH_4$, which have been commonly employed in similar application. We have used a series of analytical techniques including UV-Vis, FTIR, Raman spectroscopy, elemental analysis, XRD, XPS, TGA and AFM characterization to confirm that super hydride is far more powerful and efficient in converting oxygen functional carbon moieties as the reduction towards graphene oxides. Furthermore, our research demonstrates a new advantageous solution processing method that forwards one step towards applicability of the "tool box" in organic chemistry reducing reagents for production of reduced graphene oxides in high quality.

[1] A.K. Geim and K.S. Novoselov, *Nat. Mater.* **6**, 183 (2007).

[2] A. Ambrosi *et al.*, *Chem. Mater.* **24**, 2012 2292 (2012).